FIXED WING UAV TARGET GEOLOCATION ESTIMATION FROM CAMERA IMAGES

SABIT KANAT İHA'LAR İÇİN KAMERA BAZLI HEDEF KONUM KESTİRİMİ

ALİ KESKİN

ASSOC. PROF. DR. BİLSAY SÜMER

Supervisor

Submitted to

Graduate School of Science and Engineering of Hacettepe University

As a Partial Fulfillment to the Requirements

For the Award of the Degree of Master

In Mechanical Engineering

2021

To my wife…

ABSTRACT

FIXED WING UAV TARGET GEOLOCATION ESTIMATION FROM CAMERA IMAGES

ALİ KESKİN

Master of Science, Department of Mechanical Engineering

Supervisor: Assoc. Prof. Dr. Bilsay SÜMER

September 2021, 102 pages

In this thesis, a target geolocation measurement model for a fixed wing unmanned aerial vehicle which equipped with an image processing system and standard sensors has been created. The measurement model begins to calculate the position of the relevant stationary target when the moment the target of interest is selected in the image. The Extended Kalman filter, which uses the pixel position of the target in the image plane, position, and angular position of the aircraft, is developed for the measurement model. Different from previous studies, the deviation of camera placement angles has been taken into account in the designed filter. In the flight tests, the target position was calculated with an accuracy of 5 meters, from a distance around 400 meters, in a time interval of 15-20 seconds. Also, camera placement angle errors were calculated with a precision of 1 degree. In addition, a loitering maneuver control algorithm has been designed that uses the pixel position of the target on the image plane. This control algorithm holds the target in the camera field of view and desired distance between UAV and target. Unlike the common loitering control algorithms such as waypoint navigation, this loitering maneuver control algorithm is designed independently from any GPS measurement. Hence, it will work regardless of

GPS, as long as the angular positions of the aircraft are measured correctly. The control algorithm is designed as modular, so it can be used in any fixed-wing aircraft which has an image processing system and standard sensors. It can be easily implemented as an outer loop for roll attitude controllers.

Keywords: Target geolocation, Image based GPS denied loitering, Image based target line of sight estimation

ÖZET

SABİT KANAT İHA'LAR İÇİN KAMERA GÖRÜNTÜLERİNDEN HEDEF KONUM KESTİRİMİ

ALİ KESKİN

Yüksek Lisans, Makina Mühendisliği Bölümü

Tez Danışmanı: Doç. Dr. Bilsay SÜMER

Eylül 2021, 102 sayfa

Bu tez çalışmasında görüntü işleme sistemine sahip ve standart algılayıcılarla donatılmış sabit kanatlı bir insansız hava aracı için ilgili hedefin coğrafi konumunu hesaplayan ölçüm modeli oluşturulmuştur. Ölçüm modeli, görüntüde ilgilenilen hedefin seçildiği andan itibaren ilgili sabit hedefin konumunu hesaplamaya başlar. Ölçüm modeli için hedefin görüntü düzlemindeki piksel konumunu ve hava aracının konumunu, hızını ve açısal pozisyonunu kullanan genişletilmiş Kalman filtresi kullanılmıştır. Tasarlanan filtre de önceki çalışmalardan farklı olarak kamera yerleşim açılarının sapması dikkate alınmıştır. Uçuş testlerinde yaklaşık 400 metre uzaklıktan, 15 - 20 saniye süre aralığında, 5 metre hassasiyetinde hedef konumu hesaplanmıştır. Ayrıca, kamera yerleşim açı hataları da 1 derece hassasiyetinde hesaplanmıştır. Ek olarak, hedefin görüntü düzleminde bulunan piksel konumunu referans alan ve hava aracının hedef etrafında dolanmasını sağlayan kontrol algoritması tasarlanmıştır. Bu kontrol algoritması, hedefi kamera görüş alanında tutar ve İHA ile hedef arasındaki mesafeyi kontrol eder. Tasarlanan bu algoritma, nokta navigasyonu gibi mevcut manevralardan farklı olarak herhangi bir GPS ölçümüne ihtiyaç duymamaktadır. Dolayısı ile bu algoritma GPS'den bağımsız olarak

hava aracının açısal pozisyon bilgileri doğru ölçüldüğü sürece çalışacaktır. Kontrol algoritması modüler olarak tasarlanmıştır ve bu sayede görüntü işleme sistemine ve standart algılayıcılara sahip bir sabit kanat hava aracında kullanılabilir. Yuvarlanma açısı kontrolcüleri için bir dış döngü olarak kolaylıkla uygulanabilir.

Anahtar Kelimeler: Hedef konum kestirimi, Görüntü bazlı GPS'den bağımsız hedef etrafında dolanma manevrası, Görüntü bazlı hedef görüş hattı hesaplama

ACKNOWLEDGMENTS

TABLE OF CONTENTS

LIST OF FIGURES

LIST OF TABLES

SYMBOLS AND ABBREVIATIONS

Symbols

ϕ, θ, ψ	Euler angles (roll, pitch, yaw)
ϕ_g, θ_g, ψ_g	Gimbal Euler angles (roll, pitch, yaw)
ϕ_{ref}	Reference roll angle
χ	Track angle
$\dot{\chi}, \dot{\psi}$	Track and heading angle rate
V_g	Ground speed in the horizontal plane
V_a	Airspeed in the horizontal plane
V_w, ψ_w	Wind speed and direction angle w.r.t North
R	Turn radius
θ_{lat}	Latitude in the ECEF frame
θ_{lat}	Longitude in the ECEF frame
h	Altitude in the ECEF frame
h_{AGL}	Ground level altitude
ϵ_x, ϵ_y	Pixel coordinates in the image plane
$\hat{\epsilon}_x, \hat{\epsilon}_y$	Normalized pixel coordinates in the image plane
fov_H, fov_V	Horizontal and vertical field of view angles of the image sensor
k_i	Radial distortion parameters
f	Focal length in pixels
F	Distance between target and camera frame origin in pixels
$\mathbb{L}$	Distance between target and camera frame origin in metrics
P	Conversation gain from pixel units to metrics.
p_i	Tangential distortion parameters

$\mathcal{F}^E$	ECEF coordinate frame
$\mathcal{F}^V$	Vehicle carried coordinate frame
$\mathcal{F}^B$	Body fixed coordinate frame
$\mathcal{F}^G$	Gimbal coordinate frame
$\mathcal{F}^C$	Camera coordinate frame
$\mathcal{F}^I$	Image coordinate frame
X^A, Y^A, Z^A	X-Y-Z axis of coordinate frame of A
R_A^B	Rotation matrix from coordinate frame A to B
ψ_{LOS}, θ_{LOS}	Azimuth and elevation angles
$\psi_{LOS,pos}, \theta_{LOS,pos}$	Azimuth and elevation angles that are estimated from the position
$\Delta\psi_{LOS}, \Delta\theta_{LOS}$	Azimuth and elevation angle biases
$P_{objx}, P_{objy}, P_{objz}$	Target position in local NED frame
$P_{uavx}, P_{uavy}, P_{uavz}$	UAV position in local NED frame
$V_{uavx}, V_{uavy}, V_{uavz}$	UAV speed in local NED frame

Abbreviations

DTED	Digital Terrain Elevation Data
ECEF	Earth Centered Earth Fixed
EKF	Extended Kalman filter
FOV	Filed of View
GPS	Global Positioning System
GNS	Global Navigation Satellite Systems
IMU	Inertial Measurement Unit
ISR	Intelligence, surveillance, and reconnaissance
LM	Loitering Munition

LOS	Line of Sight
RLS	Recursive Least Squares
RTK	Real Time Kinematics
UAV	Unmanned Air Vehicle
UAS	Unmanned Air System

1. INTRODUCTION

1.1 Unmanned Air Vehicles

Unmanned Air Vehicles (UAV) are autonomously or remotely controlled flying vehicles without an onboard crew or pilot, and the whole system that contains necessary equipment such as UAVs, ground control station landing, and launching mechanism is called as Unmanned Air System (UAS) [1]. UASs are widely used in civil applications as well as military applications. Since UASs are controlled remotely, they are an ideal choice rather than manned systems for dull, dirty, and dangerous missions [2]. Therefore, in military applications, UASs have commonly been used in intelligence, surveillance, and reconnaissance (ISR) missions. In addition, usage UASs with lethal payload for military applications is increasing. These UASs, which are also known as "kamikaze / suicide drones" are called loitering munitions (LM). Figure 1-1 shows examples of ISR and LM UAVs.

Figure 1-1: Top Left to right, Togan [3] and Kargu [4] rotary wing UAV, bottom Alpagu [5] fixed wing UAV.

1.2 Motivation and Objective

In recent years application areas of UAS's are growing due to the development of other disciplines. Especially due to improvements in vision processing, image sensors have become the main and standard sensor for UASs. One of the aims to widening UAS's application areas is to decrease external control. In other words, increasing the autonomy of UAS increases its application areas. Therefore, knowing the location of a point of interest becomes essential to increase UAV's autonomy. By using target location, UAS performs more tasks autonomously or more optimally. However, the target position is not always available, especially in unknown territories. Thanks to the sensors of UAV, using target location in the camera, UAV's attitude, and positions, the target position is estimated. Figure 1-2 shows a general flow chart of the target position estimation process. Camera images are taken by the vision system, point of interest is continuously tracked and estimated its pixel location. Then pixel locations are combined with UAV inertial measurements to obtain the Line of Sight (LOS) vector and target position.
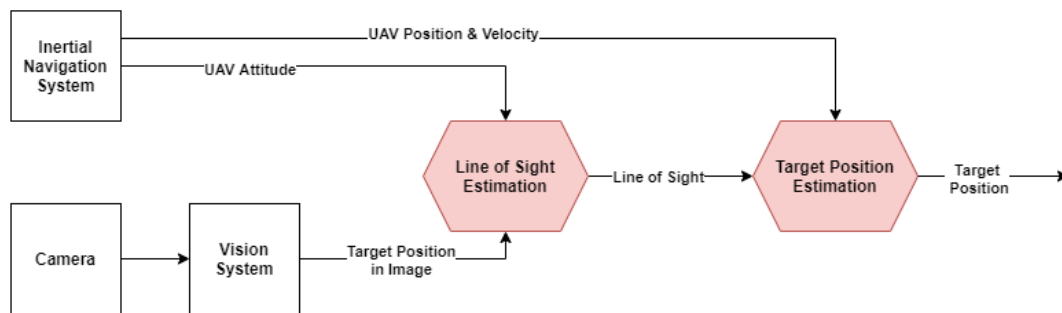
Figure 1-2: Target position estimation flowchart

Knowing the target position is handy for LM and ISR missions. For example, Figure 1-3 shows the target-approach maneuvers of Switchblade UAS [6] in one of its patents [7]. This patent is about maneuver with a gimballed camera without losing target in camera images. In Figure 1-3, the left figure shows maneuver with two fixed cameras, one is side-looking, and the other is front looking. In this case, during this maneuver, the target is lost that is losing target in a field of view (FOV) of the camera, so that gimballed camera is used. The maneuver is re-designed, as shown in the right figure. However, for the fixed camera situation, even if the target lost event is inevitable, this maneuver is performed fully autonomously by using the target location. While UAV loiters around the target, the

target position is estimated by combining image and inertial sensor measurements of UAS. Then using this estimated target location, the target-approach maneuver is done. After the loss event is finished, when the target is in the FOV of the front camera, using target location, target position in the image is estimated and transferred to the vision system to start target tracking in the image. So that, UAV is guided by a vision system in diving into the target phase. Also, for the gimballed case, the target-approach maneuver is done more optimal way using the target location. Knowledge of target location is useful for many other missions. For example, in the case of forest fire, fire location is estimated and reported. Location of illegal activities in borders is reported. Also, estimated stationary target positions may be used to locate UAV in GNSS denied situations.
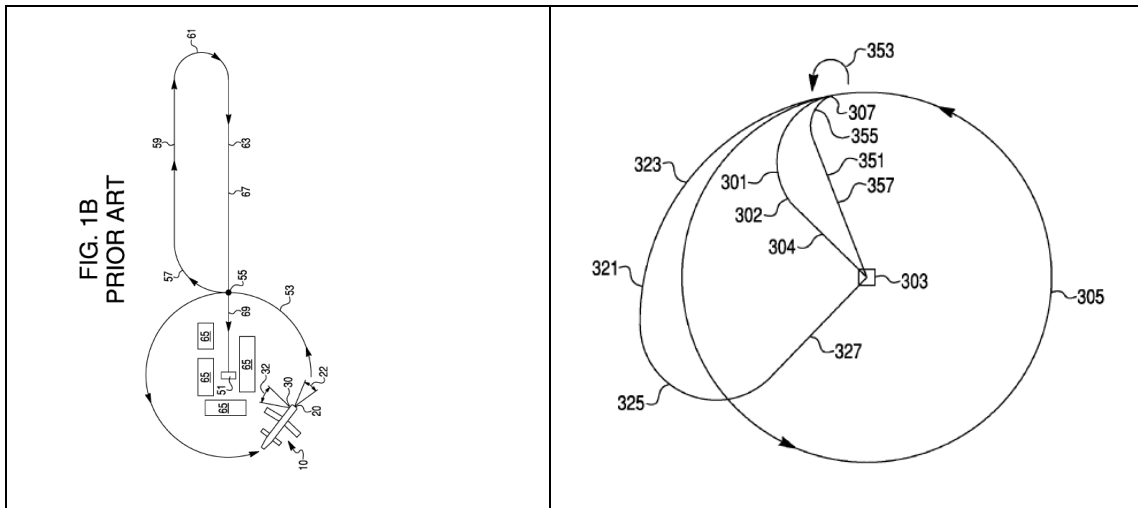
Figure 1-3: Switchblade target-approach maneuvers. The left figure shows maneuver with a fixed camera, and the right shows maneuver with a gimballed camera [7]

Target position estimation accuracy depends on target and UAV positions. This dependency is called as precision of dilution [8]. Estimation accuracy is increased by designing a proper flight path. Generally, flight paths are designed by using the target position. Still, UAV can maneuver around target by using target positions in image, UAV sensors, camera parameters, and orientation. Thanks to the image sensor, UAV can loiter around target without using Global Navigation Satellite System (GNSS) measurements.

One of the objectives of the thesis is to design a control system such that UAV autonomously tracks the desired target, independent from GNSS data. Another objective is an investigation of target geolocation methods and analyzing their performances.

1.3 Necessary Sub-Systems and Sensors

In this section, required subsystems and sensors that are used in this work are mentioned.

1.3.1   Inertial Measurement Unit (IMU)

Inertial measurement unit (IMU) combines accelerometers and gyroscopes. Accelerometers and gyroscopes are both placed perpendicular to three axes so that IMU measures accelerations and rotational rates at three principal axes [9]. In addition, some of IMUs consist of a barometric pressure sensor and compass to increase the degree of freedom of the measurement. Figure 1-4 shows commercial IMUs with a different degree of freedoms.

Figure 1-4: IMU [10]

1.3.2   Global Navigation Satellite System (GNSS)

Satellites, ground control stations, and receivers are parts of GNSS. Satellites orbit around Earth and continuously transfer signals. These signals are captured by the receiver's antenna. Based on the time difference between satellite and receiver, the distance between satellites is estimated [9]. Distance from four or more satellites enables to determine the position of the receiver.

1.3.3   Inertial Navigation System (INS)

INS uses outputs of inertial sensors to compute navigation state data such as attitude, position, and velocity [9]. GNSS generally aids them in estimating more precise positions.

1.3.4   Vision System

The vision system tracks objects which are selected by a user in camera images. Also, the vision system returns their pixel locations. Following a desired moving object in real-time, image sequences are called object tracking. Kanade Lucas Tomasi (KLT) algorithm is one of the simple and effective technique [11]. KLT algorithm finds feature points from a region of interest to track it in images. A good feature is defined as "*feature to be good if it can be tracked well*" [12]. Figure 1-5 shows successive sequential target tracking.

Figure 1-5: Vision system successive target tracking [5]

1.3.5   Air Data System

Air data system measures total and static pressures then it converts these pressure values into airspeed and barometric altitude [13]. The system contains pitot and static pressure

sensors. Also, it may include 5-hole or 7-hole pitot tube probe or alpha-beta vane to measure aerodynamic flow angles. This system is not required for target geolocation, but it is essential for controlling UAV longitudinal motion (altitude and airspeed) for GNSS denied situations.

1.4 BACKGROUND

In this section, the technical basics that are used in this thesis are described.

1.4.1 UAV Attitude (Euler Angles)

Angular position (attitude) of UAV is described with three angles [14]. These three angles are roll (ϕ), pitch (θ) and yaw or heading (ψ) angles that are called as Euler angles.

Roll Angle

Roll defines rotation around the front to back axis of the UAV. With this movement, the wings move up and down asynchronously. Left wing upwards and right wing down is defined as positive roll angle. Figure 1-6 and Figure 1-7 show positive roll angle.
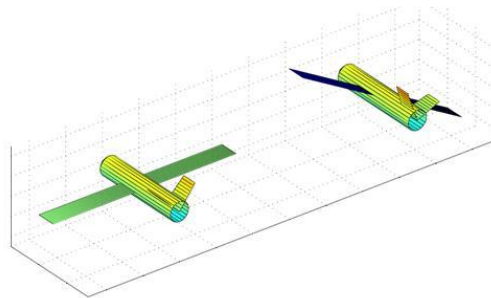
Figure 1-6: Top diagonal view of a UAV with a positive roll angle [15]
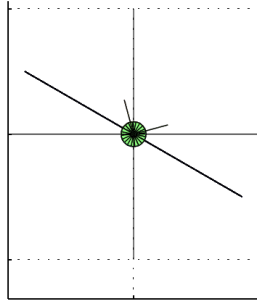
Figure 1-7: Rear view of a UAV with positive roll angle [15]

Pitch Angle

Pitch angle is rotation around the side-to-side axis of the UAV. With this rotation, the nose of the UAV moves up and down around the center of gravity. While UAV nose up movement is defined as positive pitch, the nose-down movement is defined as negative pitch. Figure 1-8 and Figure 1-9 shows positive pitch motion.
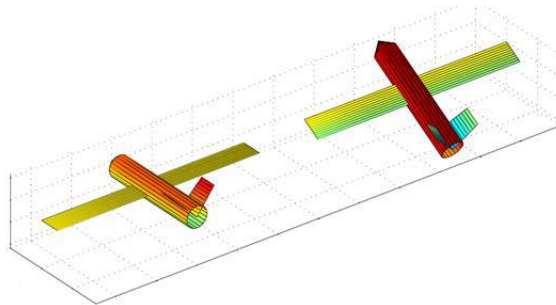
Figure 1-8: Top diagonal view of a UAV with a positive pitch angle [15]
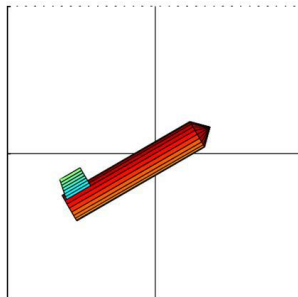
Figure 1-9: Right-side view of a UAV with a positive pitch angle [15]

Yaw Angle

Yaw angle is rotation around the vertical axis of the UAV. Defines right and left motion of nose of UAV in the horizontal plane. Right nose movement is defined as positive, and left nose movement is negative. Figure 1-10 and Figure 1-11 show positive yaw motion.
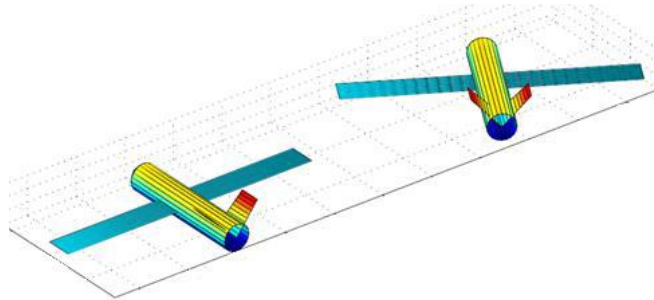
Figure 1-10: Top diagonal view of a UAV with a positive yaw angle [15]
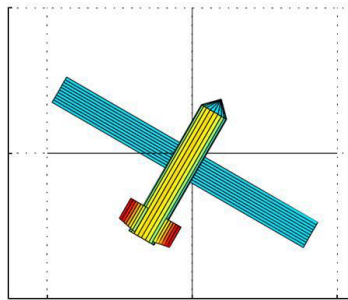
Figure 1-11: Top view of a UAV with positive yaw angle [15]

1.4.2   Coordinate Frames

Since velocity, position, and orientation (if represented as a rotation vector) are all vectors, they require a reference frame to define them. There are different types of coordinate frames. Generally, cartesian or circular frames are used in aviation. The coordinate frame is defined by its origin and perpendicular unit axes. Depending on the application, different coordinate frames can be used [16]. In the following sections, coordinate frames that are used in this work are described.

Earth Centered Earth Fixed Coordinate Frame (ECEF)

Earth centered means that origin of ECEF frame ($\mathcal{F}^E$) is on the center of mass of the Earth. Earth fixed implies that this frame rotates with Earth. X (X^E) and Y (Y^E) axes are on the equatorial plane, X^E axis directs to Greenwich meridian, Z (Z^E) axis on the spin axis of Earth and Ye axis is perpendicular to both X^E and Z^E axes [13]. ECEF frame is mostly used as an inertial frame that is a non-accelerating and non-rotation frame. Generally, geodetic coordinate system that is a polar coordinate system is used to define a position in this frame [16]. In geodetic frame Earth is considered as ellipsoid and latitude (θ_{lat}), longitude (θ_{lon}) and altitude (h) are used to describe position in ECEF frame.
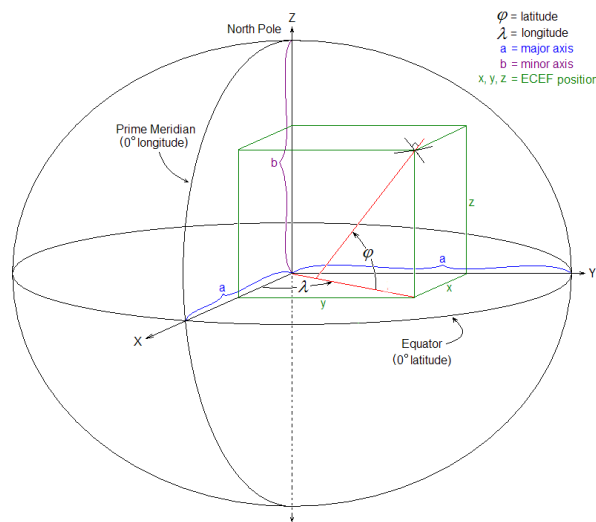
Figure 1-12: ECEF and NED frames

North-East-Down (NED) Coordinate Frame

NED is a right-handed cartesian coordinate frame. As its name suggests, its axes are oriented North, East, and Down, respectively. It is used as a reference frame to describe the attitude of UAVs. Its origin is in the center of mass of UAV, and it is called vehicle carried coordinate frame ($\mathcal{F}^V$).

9
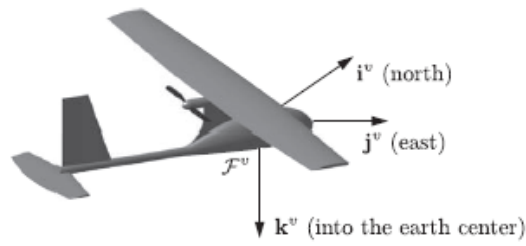
Figure 1-13: Vehicle carried coordinate frame [17]

NED frame origin can be places desired location in space. So that, it can be used as an inertial frame to simplify equations and called a local geographic frame [18].
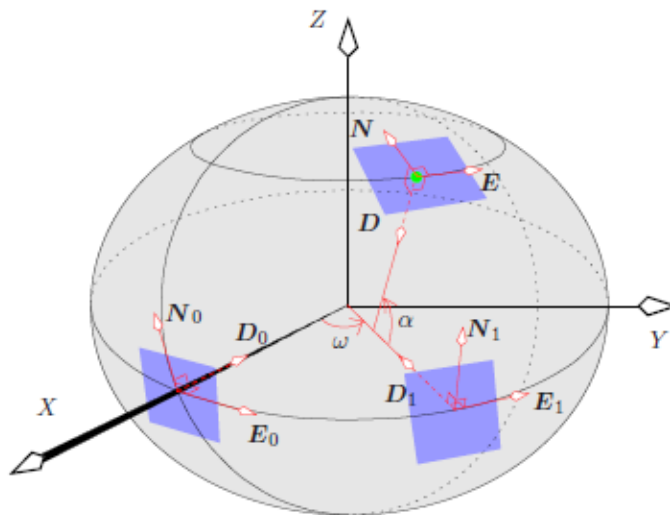
Figure 1-14: Local NED coordinate frames at different locations [18]

Body Fixed Coordinate Frame

Body fixed frame ($\mathcal{F}^B$), shown in Figure 1-15, is a right-handed cartesian coordinate frame. This frame is fixed to the body of an object and rotates and moves with it, and its origin is in the center of mass of the object. As seen from the figure, X (X^B) axis points nose of UAV, Y (Y^B) axis is in the right-wing direction and Z (Z^B) axis points downward. Inertial sensor measurements are described in this frame [13].

10
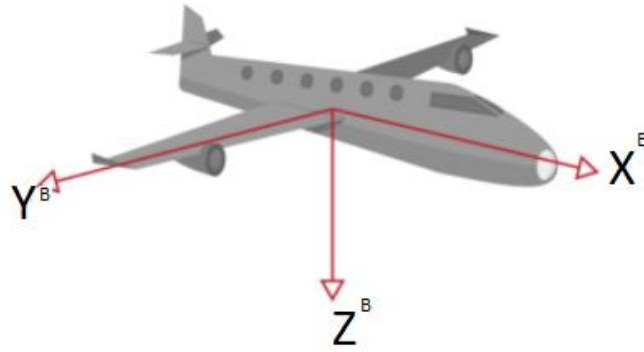
Figure 1-15: Body coordinate frame [16]

Gimbal Coordinate Frame

Gimbal coordinate frame ($\mathcal{F}^G$) is used to represent angular position of the gimbal with respect to the body coordinate frame. It can be assumed that the origin of this frame is in the center of mass of the UAV since the dimensions of small UAVs are short. Gimbal azimuth (ψ_{gimbal}), gimbal elevation (θ_{gimbal}) and gimbal roll (ϕ_{gimbal}) angles are Euler angles of this frame (3-2-1 rotation) with respect to the body frame. Generally, gimbals rotate around two axes so that gimbal roll can be neglected. Figure 1-16 and Figure 1-17 shows UAV with gimbal azimuth and gimbal elevation angles.
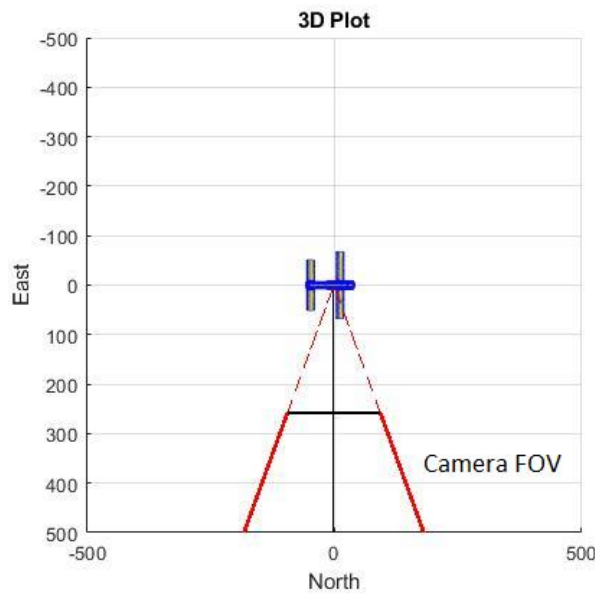
Figure 1-16: Top view of UAV with 90-degrees gimbal azimuth angle
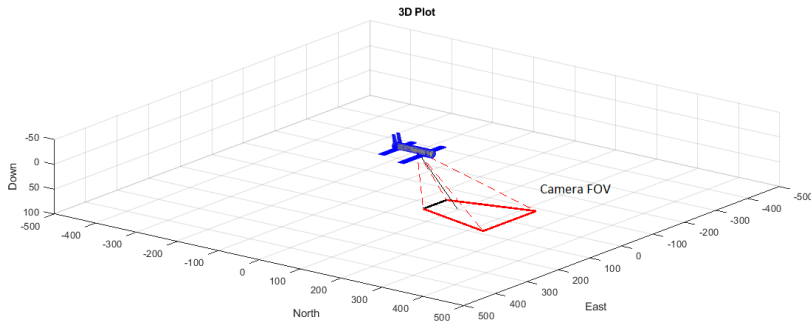
Figure 1-17: Top diagonal view of UAV with a -45-degrees gimbal elevation angle

Camera Coordinate Frame

As shown in Figure 1-18, the camera coordinate frame ($\mathcal{F}^C$) is right-handed cartesian coordinate frame where its origin is located at the optical center. Z axis is in the direction of the camera lens, X is in the right direction and the Y axis is downward direction.
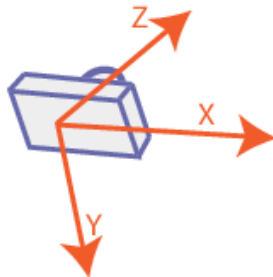
Figure 1-18: Camera coordinate frame [17]

Image Coordinate Frame

Image coordinate frame is a 2D cartesian coordinate frame that is used for representing pixel positions (ϵ_x, ϵ_y) of an object in image. The origin of this frame is on the center of the image, +X axis is in the right direction, and +Y axis is downward. For example, Figure 1-19 shows the positions of UAV, target, and camera in NED frame. Figure 1-20 shows the image plane that is captured target by the camera in Figure 1-19.
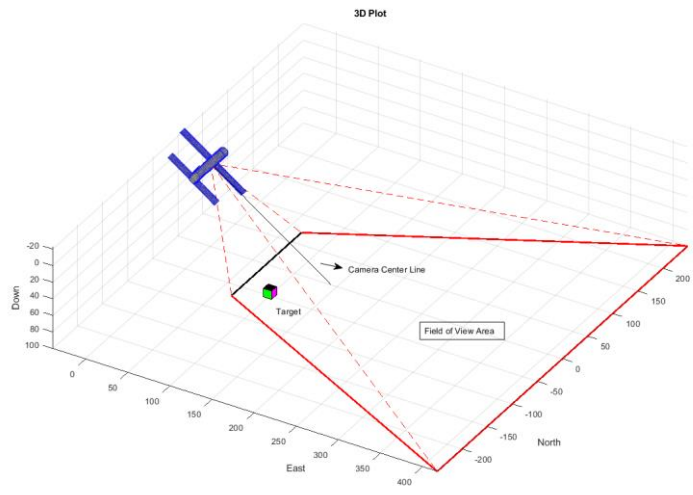
Figure 1-19: World position of UAV, target, and camera
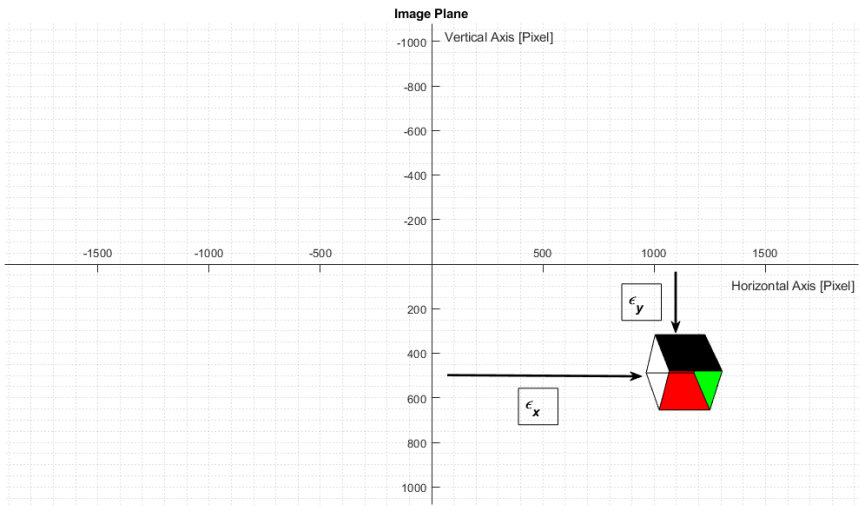
Figure 1-20: Image plane in pixels

However, in general, target location in pixels in the image frame is normalized to eliminate differences depend on image sensor sizes. In this work, as shown in Figure 1-21, the image frame is normalized such that the origin is center of the frame, and both maximum X-Y coordinates are +0.5, and minimum coordinates are -0.5.

13
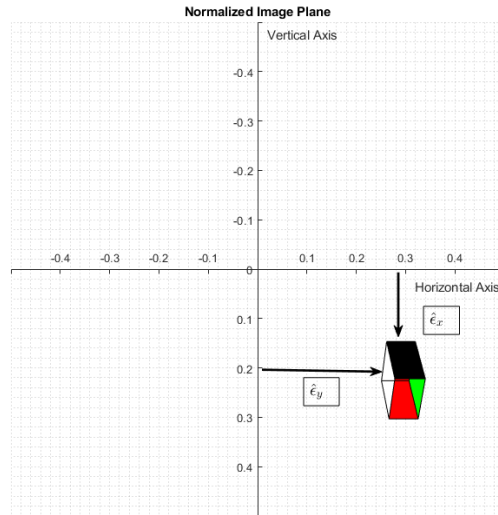
Figure 1-21: Normalized image frame

1.4.3 Coordinate Transformations

As mentioned before, different coordinate frames can be used. Sometimes it is necessary to change a vector coordinate frame to simplify equations.

Rotation Matrix

Rotation matrices are used to transfer a vector into a new coordinate frame. Rotation matrices are formed by applying three sequential rotations. After each rotation, a new coordinate frame is formed, and a new rotation is done by using this new frame coordinate axis. These rotation angles are called Euler angles [19], and they describe the orientation of coordinate frame with respect to another one. In this work, 3-2-1 rotation is used for rotation matrices. Consider frame a with XYZ axes, frame b with xyz axes and three rotation steps are:

1. Rotation around Z axis forms a' frame with X'Y'Z' axes.
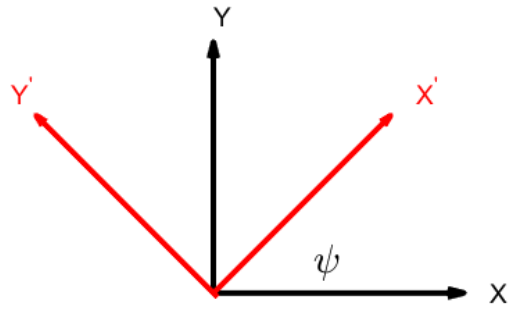
Figure 1-22: Z axis rotation of frame a

$$
\begin{bmatrix} X' \\ Y' \\ Z' \end{bmatrix} = \begin{bmatrix} \cos\psi & \sin\psi & 0 \\ -\sin\psi & \cos\psi & 0 \\ 0 & 0 & 1 \end{bmatrix} \begin{bmatrix} X \\ Y \\ Z \end{bmatrix}
\tag{1.1}
$$

2. Rotation around Y' axis forms a'' frame with X''Y''Z'' axes.
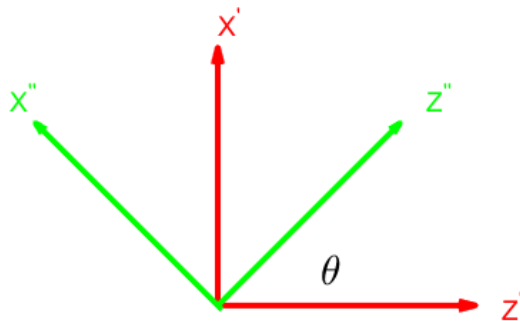
Figure 1-23: Y' axis rotation of frame a'

$$
\begin{bmatrix} X'' \\ Y'' \\ Z'' \end{bmatrix} = \begin{bmatrix} \cos\theta & 0 & -\sin\theta \\ 0 & 1 & 0 \\ \sin\theta & 0 & \cos\theta \end{bmatrix} \begin{bmatrix} X \\ Y \\ Z \end{bmatrix}
\tag{1.2}
$$

3. Rotation around X'' axis forms b frame with xyz axes.
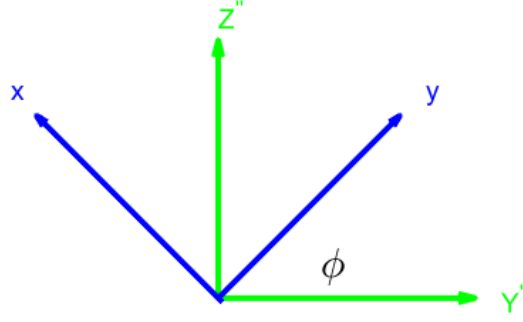
Figure 1-24: X'' axis rotation of frame a''

$$\begin{bmatrix} x \\ y \\ z \end{bmatrix} = \begin{bmatrix} 1 & 0 & 0 \\ 0 & \cos\phi & \sin\phi \\ 0 & -\sin\phi & \cos\phi \end{bmatrix} \begin{bmatrix} X'' \\ Y'' \\ Z'' \end{bmatrix} \tag{1.3}$$

Hence rotation from frame a to frame b becomes:

$$\begin{bmatrix} x \\ y \\ z \end{bmatrix} = \begin{bmatrix} 1 & 0 & 0 \\ 0 & \cos\phi & \sin\phi \\ 0 & -\sin\phi & \cos\phi \end{bmatrix} \begin{bmatrix} \cos\theta & 0 & -\sin\theta \\ 0 & 1 & 0 \\ \sin\theta & 0 & \cos\theta \end{bmatrix} \begin{bmatrix} \cos\psi & \sin\psi & 0 \\ -\sin\psi & \cos\psi & 0 \\ 0 & 0 & 1 \end{bmatrix} \begin{bmatrix} X \\ Y \\ Z \end{bmatrix} \tag{1.4}$$

Rotation matrix (R_a^b) from frame a to frame b is:

$$R_a^b = R_{a''}^b(\phi) R_{a'}^{a''}(\theta) R_a^{a'}(\psi) \tag{1.5}$$

$$R_a^b = \begin{bmatrix} c\theta c\psi & c\theta s\psi & -s\theta \\ s\phi s\theta c\psi - c\phi s\psi & s\phi s\theta s\psi + c\phi c\psi & s\phi c\theta \\ c\phi s\theta c\psi + s\phi s\psi & c\phi s\theta s\psi - s\phi c\psi & c\phi c\theta \end{bmatrix} \tag{1.6}$$

where $c\theta = \cos(\theta)$ and $s\theta = \sin(\theta)$ and ϕ, θ, ψ are the Euler angles. Using rotation matrix, any vector in a frame (P^a) can be described in b frame (P^b).

$$P^b = R_a^b * P^a \tag{1.7}$$

Since rotation matrices are orthogonal matrices [19], inverses of them are equal to their transpose.

$$R_b^a = (R_a^b)^{-1} = (R_a^b)^T \tag{1.8}$$

Vehicle Carried Frame to Body Frame Transformation

Using equation (1.6), rotation matrix from vehicle to body coordinate frame with roll, pitch, and heading Euler angles becomes:

$$R_V^B = \begin{bmatrix} c\theta c\psi & c\theta s\psi & -s\theta \\ s\phi s\theta c\psi - c\phi s\psi & s\phi s\theta s\psi + c\phi c\psi & s\phi c\theta \\ c\phi s\theta c\psi + s\phi s\psi & c\phi s\theta s\psi - s\phi c\psi & c\phi c\theta \end{bmatrix} \tag{1.9}$$

Body to vehicle coordinate frame rotation matrix from equation (1.8):

$$R_B^V = \begin{bmatrix} c\theta c\psi & s\phi s\theta c\psi - c\phi s\psi & c\phi s\theta c\psi + s\phi s\psi \\ c\theta s\psi & s\phi s\theta s\psi + c\phi c\psi & c\phi s\theta s\psi - s\phi c\psi \\ -s\theta & s\phi c\theta & c\phi c\theta \end{bmatrix} \tag{1.10}$$

Body Frame to Gimbal Frame Transformation

In the case of a three-degree rotation gimbal, transformation matrix from the body frame to the gimbal frame is similar to rotation matrix from vehicle to body coordinate frame.

$$R_B^G = \begin{bmatrix} c\theta_g c\psi_g & c\theta_g s\psi_g & -s\theta_g \\ s\phi_g s\theta_g c\psi_g - c\phi_g s\psi_g & s\phi_g s\theta_g s\psi_g + c\phi_g c\psi_g & s\phi_g c\theta_g \\ c\phi_g s\theta_g c\psi_g + s\phi_g s\psi_g & c\phi_g s\theta_g s\psi_g - s\phi_g c\psi_g & c\phi_g c\theta_g \end{bmatrix} \tag{1.11}$$

For two-degree rotation gimbal ($\phi_g = 0$) rotation matrix becomes:

$$R_B^G = \begin{bmatrix} c\theta_g c\psi_g & c\theta_g s\psi_g & -s\theta_g \\ -s\psi_g & c\psi_g & 0 \\ s\theta_g c\psi_g & s\theta_g s\psi_g & c\theta_g \end{bmatrix} \tag{1.12}$$

And rotation from gimbal to body frame:

$$R_G^B = \begin{bmatrix} c\theta_g c\psi_g & -s\psi_g & s\theta_g c\psi_g \\ c\theta_g s\psi_g & c\psi_g & s\theta_g s\psi_g \\ -s\theta_g & 0 & c\theta_g \end{bmatrix} \tag{1.13}$$

Gimbal Frame to Camera Frame Transformation

The camera frame is a rotated form of the gimbal frame with right Euler angles. Figure 1-25 shows both coordinate frames.
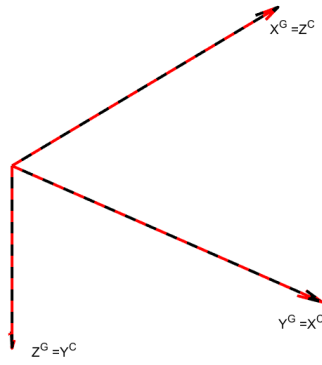
Figure 1-25: Camera and gimbal frames

As seen from Figure 1-25 camera frame is rotated form of gimbal frame with $\psi = 90, \theta = 0$ and $\phi = 90$. Hence rotation from gimbal to camera frame and inverse rotations are:

$$R_G^C = \begin{bmatrix} 0 & 1 & 0 \\ 0 & 0 & 1 \\ 1 & 0 & 0 \end{bmatrix} \tag{1.14}$$

$$R_C^G = \begin{bmatrix} 0 & 0 & 1 \\ 1 & 0 & 0 \\ 0 & 1 & 0 \end{bmatrix} \tag{1.15}$$

1.4.4   Camera Calibration

Camera calibration is a process that estimates the parameters of an image sensor. Extrinsic and intrinsic parameters are the main two groups of these camera parameters. While intrinsic parameters define sensor's inertial characteristics, extrinsic parameters are used to transform sensor's position into 3D world coordinates [20]. Intrinsic parameters are [21]:

- Focal length is the distance between the image sensor and the optical center.

- Principal point is the point where the principal axis is perpendicular to the image sensor. The principal axis is a line that passes through the optical center.

- Skew coefficient defines the angle between pixels x and y axes.

- Distortions are divided into two groups such as radial and tangential distortions. Figure 1-26 shows the effect of radial distortion on images. Tangential distortion represents parallelism between image sensor and lens, as shown in Figure 1-27.

Figure 1-26: Radial distortion effect on image, left with radial distortion [21].
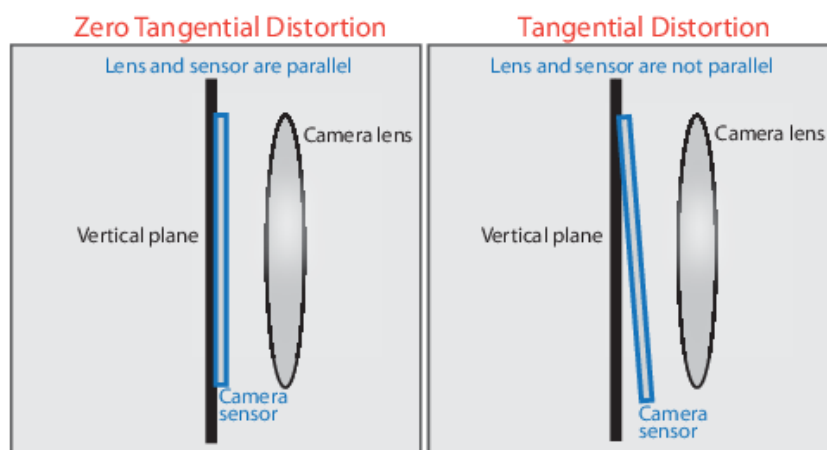
Figure 1-27: Tangential distortion [22]

Estimated parameters can be used for [23]:

- Lens distortion correction,

- Estimation size of an object in world coordinates,

- Estimation position of camera or object in the real world,

- 3D scene reconstruction.

In this work, camera parameters by using Camera Calibration Toolbox of MATLAB [22]. Then, these parameters are used to estimate the target LOS vector from the pixel location of the target in the camera frame.

The first step of camera calibration is taking several images of the checkerboard at different locations and orientations. An example image is shown in Figure 1-28.
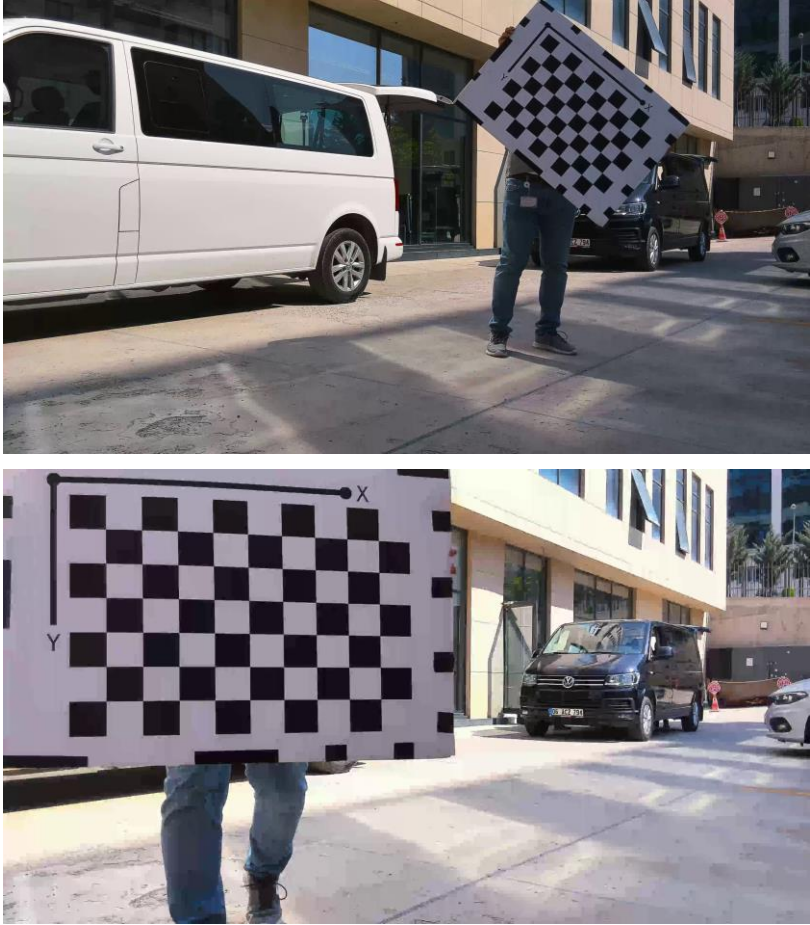
Figure 1-28: Example images for camera calibration

After corners in the checkerboard are detected, an optimization algorithm is used to determine intrinsic camera parameters. The optimization algorithm minimizes the error between detected corners and reprojected corners by using camera parameters [20], [23], [24]. Figure 1-29 and Figure 1-30 shows detected corners and reprojected corners.
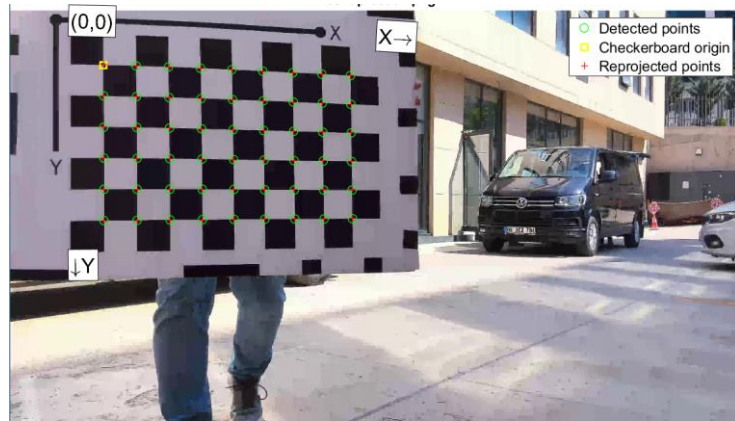
Figure 1-29: Detected and reprojected points
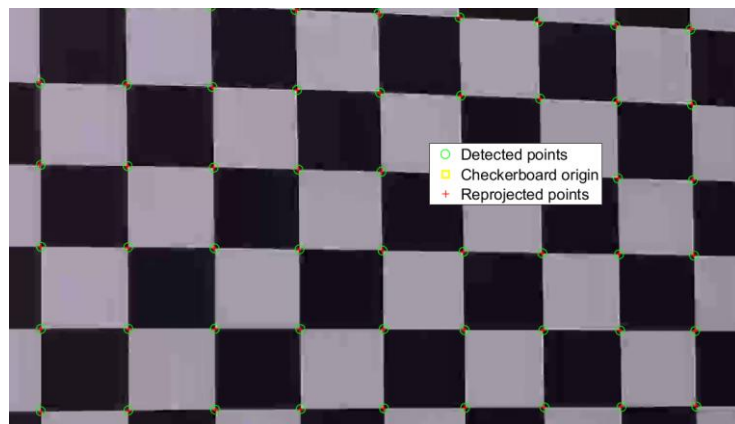
Figure 1-30: Detected and reprojected points-zoomed

Here, in Table 1.1, camera parameters are tabulated.

Table 1.1: Econ camera parameters

Image Size [pixels]	[3840, 2160]
Focal Length [pixels]	[3083.94, 3169.55]
Principal Points [pixels]	[1896, 1096]
Radial Distortion	[0.0346, -0.3734, -0.26933]
Tangential Distortion	[-0.018, -0.0235]
Skew	0

Using horizontal and vertical pixel sizes (M_H, M_V) and focal lengths (f_H, f_V) in pixels, horizontal (fov_H) and vertical (fov_V) field of view angles of the image sensor is estimated as:

$$fov_H = 2 \operatorname{atan}\left(\frac{M_H}{2 * f_H}\right) \tag{1.16}$$

$$fov_V = 2 \operatorname{atan}\left(\frac{M_V}{2 * f_V}\right) \tag{1.17}$$

The estimated field of view angles of the image sensor is tabulated in Table 1.2.

Table 1.2: Econ camera estimated field of view angles

Vertical Field of View Angle [deg]	37.63
Horizontal Field of View Angle [deg]	63.81

1.5 Layout of Thesis

Section 1 is the introduction section. In this section, definitions about the study, objective of the study, necessary systems for study, and background mathematical materials are introduced.

Section 2 is the literature review. In this section, previous works are explained.

Section 3 describes test environments such as flight and simulation test environments. In this section, how the simulation environment is developed is explained.

Section 4 describes LOS vector and LOS angles estimation. Also, how to improve this estimation is explained.

Section 5 describes image based loitering maneuver around the target. Improvements and flight and simulation results are shown in this chapter.

Section 6 describes the stationary targets position estimation method. Flight test results and comparisons between other methods are shown.

Section 7 is the conclusion section and summarizes the results that are obtained in this thesis.

2. LITERATURE SURVEY

This section summarizes the studies in the literature on target position estimation and vision-based target tracking.

2.1 Target Geolocation

Target geolocation in UAV can be divided into two sub-categories, such as target geolocation from a single UAV and a group of UAVs [25]. Moreover, these categories can be divided into two subgroups depending on the sensor used [26]. The first group is passive methods which use target image from the camera to localize the target, and the other one is subjective methods use active sensors such as laser to estimate the distance to the target.

In [27], Cazaurag, et al. develop a triangulation method for target geolocation from a single multirotor UAV with a passive camera sensor. The developed method is that the UAV first centers target in the camera image and record its own position and bearing angle (angle between UAV and target) then moves new location re-align itself to target and record new position and new bearing angle. These two positions and bearing angle measurements are used to estimate target location by using triangulation method. Figure 2-1 shows triangulation method. Even if this method is simple, however, triangulation method suffers from measurement errors [28] and this method measures only 2D position of the target.
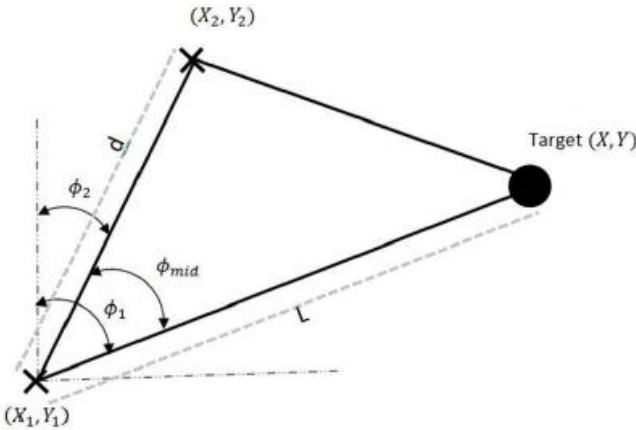
Figure 2-1: Object triangulation [27]

Sohn, et al. improved this triangulation method by converting it into a minimization problem [29]. In his work, he used a single-antenna GPS receiver with no IMU and gimballed camera. Camera gimbal is controlled by a proportional integral controller to center the target in camera image. LOS vector is calculated from pixel location of the target in image axis by using pin hole camera model. To locate the target, LOS vectors and UAV position vectors are transferred into ECEF (Earth centered Earth fixed) coordinates then nonlinear optimization method is used to estimate the distance to the target. Minimization algorithm minimizes measurement errors. To improve estimation, wind estimation and compensation for attitude from measurements are used since UAV attitude are not measured directly (due to UAV not being equipped with IMU). However, as mentioned by himself, the suggested localization algorithm is not implemented in real time estimation. This is due to the optimization algorithm which is not proper for real time estimation since it requires storing almost all LOS and position data. Also, today's IMU is a standard sensor for all UAVs and a considerably cheap sensor.

To estimate target location in real time, other works convert the triangulation method to single shot estimation method by combining LOS vector estimation with DTED (Digital Terrain Elevation Data) or flat earth assumption. Sensor measurement errors are reduced by using RLS (Recursive Least Squares) filter [30] [31] or EKF (Extended Kalman filter) [32] [33] [34] [35] [36]. Redding, et al. in their work [30], present single shot geolocation method with RLS filter to reduce errors. Also, they investigate error sources and estimation sensitivities to each source. After, Barber, et al. enhance geolocation accuracy with bias estimation, flight path selection, and wind estimation [31]. In bias estimation, online minimization method is proposed such that LOS angle biases which make the positioning variances minimum, are calculated by the quasi-Newton method while UAV loitering around the target. However, in this bias, estimation errors due to image depth will be calculated as elevation angle bias because of terrain model errors (level 2 DTED has a 30-meter resolution [37]). Also, quasi-Newton methods are not proper for real time applications. Flight path selection finds optimal altitude and loiter radius which decreases errors in attitude and position errors. Heading angle of UAV is measured with wind calculation and course angle but they assume that "*MAV is not equipped with magnetometer*" so that wind calculation is applicable. However, this assumption is extremely poor assumption because most UAVs have a magnetometer sensor. Even if

UAV does not have magnetometer, heading angle can be estimated by GPS and gyroscope sensors [38]. Therefore, wind estimation is not necessary to increase geolocation accuracy.

In EKF methods same procedure is applied as in RLS such that LOS vector is converted to the target location by using flat earth or DTED for just only initial guess of EKF. After that, target location measurements are combined with model equation and are filtered by EKF. Beard and McLain [33] suggest EKF filter with state vector as target position vector and distance between UAV and target. UAV position vector is used as a measurement vector. Hosseinpoor, et al. uses same filter with RTK GPS (Real time kinematics) to increase geolocation accuracy based on thermal video images [32]. Monda localizes riverine environment targets so that altitude of the target becomes known [34]. In EKF, 2D position and velocity vector of the target is used as state vector and 2D pixel locations of the target in the image are used as measurement vector. Also, he develops a gimbal control algorithm to maintain the target in the center of the camera. Dobrokhodov, et al. instead of using target position estimate and range to target as an EKF state, uses angle between ground speed vector, the vector perpendicular to the LOS, range to target, and LOS angle rate. [35]. Velocity tangent to LOS and Angle between ground speed vector and the vector perpendicular to the LOS is used as measurement vector.

Another target geolocation method that differs from the above methods is image registration. In this method, a satellite image or any reference image for flight zone is compared with an image taken from UAV camera. Since this method aims to match reference images with captured ones, there is no need for accurate additional measurements such as UAV position and attitude or DTED for range estimation [39],[40]. Even so, there are two main issues with this method. The first one is finding reference images. Reference images for flight zone may not be available or may be costly. Another issue is the change in environments. For example, snow on terrain hides all known landmarks to match the referenced image. Even if this method is perfectly accurate, it is not applicable to most of the missions.

On the other hand, calculation methods are different from subjective methods. Since these methods use active distance measurement sensors such as LASER, the geolocation problem becomes a single shot problem. There is no need for flat earth assumption or DTED for the range estimation [25]. This method aims to increase estimation accuracy by eliminating measurement errors. He [26] suggests a maximum likelihood estimation, where Wang [25] proposes RLS filter to eliminate measurement errors. Figure 2-2 shows the workflow of single eye localization [26]. However, the biggest problem here is the weight of the range sensor. Long distance measurement sensors will be heavy compared to small UAVs, weighing around 2-4 kilograms.
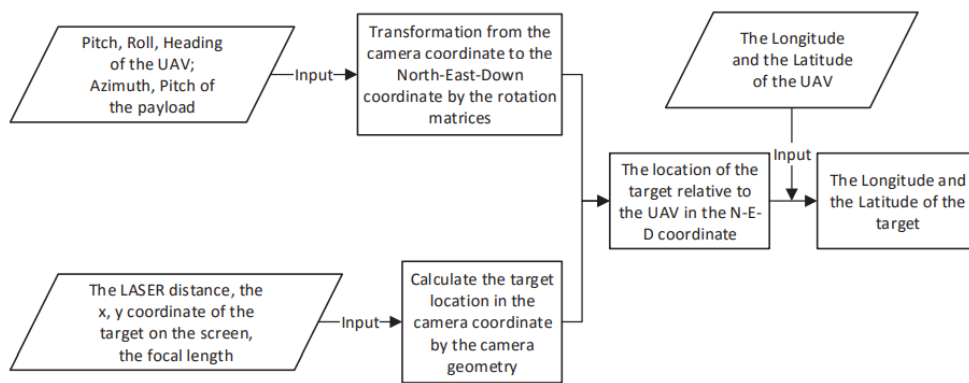
Figure 2-2: Single eye localization work flow [26]

Geolocation methods based on multiple UAVs [41],[42],[43],[44] and [45] mostly focus efficient data communication between UAVs, optimal flight plans etc. Geolocation with a group of UAVs estimates target location faster than a single UAV because of the number of measurements. However, this thesis focuses on geolocation with a single UAV.

2.2 Flight Path Design

Ross uses down looking camera and develops a path planning algorithm based on "*Direct Collocation with Nonlinear Programing*" [46] in his research [40]. UAV roll angle and longitudinal acceleration are control inputs. The cost function is defined as ensuring maximum target observation. Cost function minimizes control efforts, the distance between target and UAV, and time when the target is not centered in the camera image. This down looking camera concept is not proper for reconnaissance and surveillance

missions. Since fixed wing UAV continuously moves, target loss event occurs. In addition, for targets in motion, this system fails.

Dobrokhodov, et al. developed an exceptionally good tracking algorithm based on camera images of the target [35], [36]. The algorithm loiters around the target by keeping the ground velocity perpendicular to the LOS vector. For this loiter motion heading rate is used as a control command. For gimbal control, the gimbal angle is controlled to keep the target in the camera center. The only deficiency of this algorithm is the GPS dependence for the tracking. Since the algorithm uses the ground velocity, it fails during GPS loss.

3. TEST ENVIRONMENTS

3.1 Introduction

To design and analyze performance of estimation methods, it is necessary to have a test environment. A real flight test is the final test result to validate and show the performances of designed or investigated algorithms. However, due to the cost of the flight test, a simulation test environment is developed for pre-analysis. After all pre-design and analyses are finished, flight tests are done.

3.2 Flight Test Environment

For flight tests, FX79 flying wing UAV is used. It is equipped with right looking camera, GPS, IMU, INS, air data system, and vision tracker system. As a system, it consists of a launcher and ground control unit. It has a unique autopilot ability.

Figure 3-1: Flight test setup, UAV and the launcher

Table 3-1: Properties of test UAV

Wingspan	2000 m
Length	862 mm
Total weight	2.2 kg

3.3 Simulation Environment

3.3.1   UAV Simulation

UAV Model is used by target tracking controls. Generally, dynamic modeling of UAVs focuses on open loop modeling where control surface deflections and throttle are input, position and velocities are output. However, the control loop designed in this work for the flight path in Section 5 outputs reference roll angle (ϕ_{ref}). Hence, there is no need for a fully dynamic model of UAV. Closed loop form of the model where only reference angles are taken as input is sufficient. Moreover, the control loop for flight path design focuses on lateral dynamics so that longitudinal motion can be considered as a constant.

The first step of building a dynamic lateral model of a UAV is representing roll dynamics. The reference roll angle (ϕ_{ref}) is taken as input, whereas roll angle is an output (ϕ) in the model. To represent the closed loop dynamics, a transfer function model with three poles and two zeros is used, and transfer function parameters are found by using MATLAB System Identification Toolbox [47]. Flight data, which is used for system identification, is shown in Figure 3-2 and Figure 3-3.
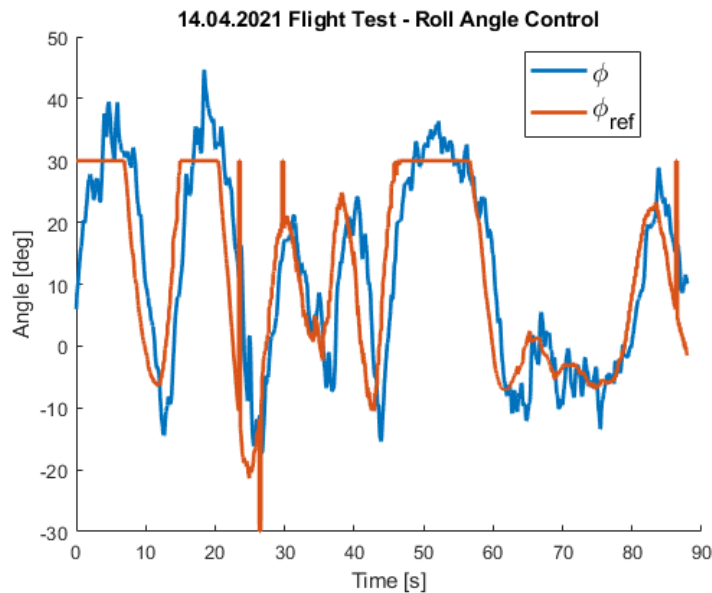
Figure 3-2: 14.04.2021 flight log data – Reference roll and roll angles
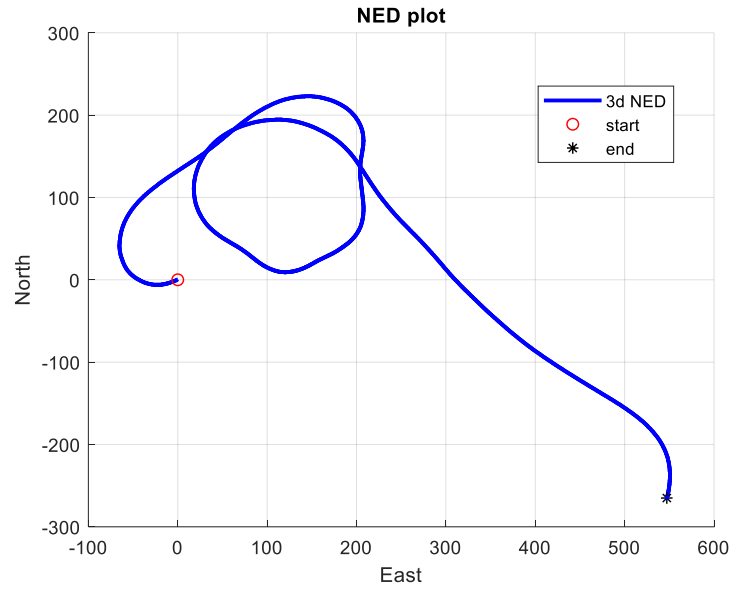
Figure 3-3: 14.04.2021 flight log data – 2D position

The estimated parameters of closed loop roll transfer function are given as follows:

$$\frac{\phi}{\phi_{ref}} = \frac{0.4229s^2 + 0.6845s + 0.01389}{s^3 + 1.149s^2 + 0.6803s + 0.01491} \tag{3.1}$$

Figure 3-4 shows model roll outputs and flight data roll angle. The root mean square error is around 3.8 degrees which can be considered as an accurate model.
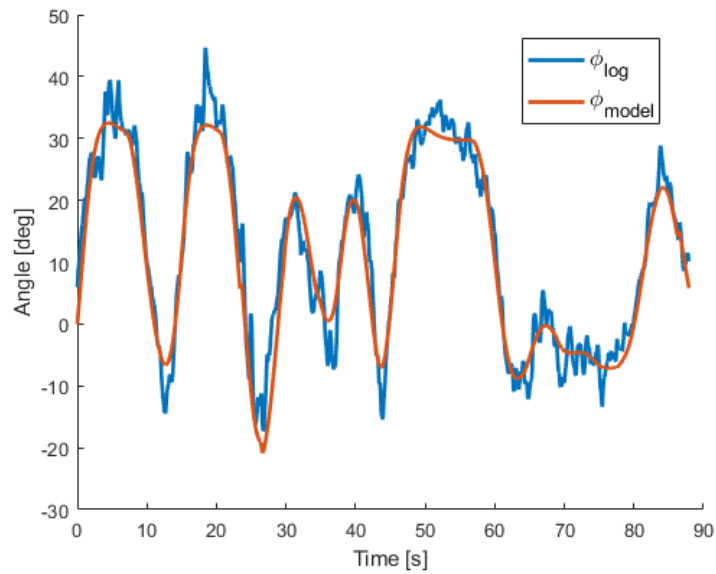
Figure 3-4: Model and flight roll angles

The next step is the estimation of heading rate ($\dot{\psi}$) and track rate ($\dot{\chi}$). Heading and track dynamics are modeled to consider wind effects. Model is developed based on works done by Rysdyk [48], Osborne, and Rysdyk [49]. Track rate is approximately modeled as a function of ground speed (V_g), gravitational acceleration (g) and roll angle (ϕ) [50],[33].

$$\dot{\chi} = \frac{g}{V_g} \tan(\phi)$$

$$\chi = \int \dot{\chi} dt \tag{3.2}$$

Heading angle depends on ground speed, track angle, wind speed (V_w) and direction (ψ_w).

$$\psi = \text{atan} \left(\frac{V_g \sin(\chi) + V_w \sin(\psi_w)}{V_g \cos(\chi) + V_w \cos(\psi_w)} \right) \tag{3.3}$$

The final step is the estimation of ground speed and position. Relation between ground speed, airspeed, and wind speed is given in Equation (3.4) which is commonly called wind triangulation.

$$\vec{V_g} = \vec{V_a} + \vec{V_w} \tag{3.4}$$

Using Equation (3.4) and cosine law, ground speed is estimated as:

$$V_g = \sqrt{V_a^2 + V_w^2 - 2 V_a V_w \cos(\psi - \psi_w + \pi)} \tag{3.5}$$

Hence position in the NED frame XY plane is:

$$\dot{X}_N = V_g \cos(\chi), \qquad \dot{Y}_E = V_g \sin(\chi)$$

$$X_N = \int \dot{X}_N dt, \qquad Y_E = \int \dot{Y}_E dt, \tag{3.6}$$

Figure 3-5 shows the flow chart of lateral dynamics simulation. In this work, longitudinal autopilot holds altitude and airspeed, so that airspeed is considered as input. Simulation step per tick time:

- Take inputs: Airspeed, reference roll, wind speed, and direction,

- Estimate roll angle using equation (3.1)

- Estimate track rate and track angle using equation (3.2),

- Estimate heading angle using equation (3.3),

- Estimate ground speed using equation (3.5),

- Convert ground speed NED speeds and positions using equation (3.6).
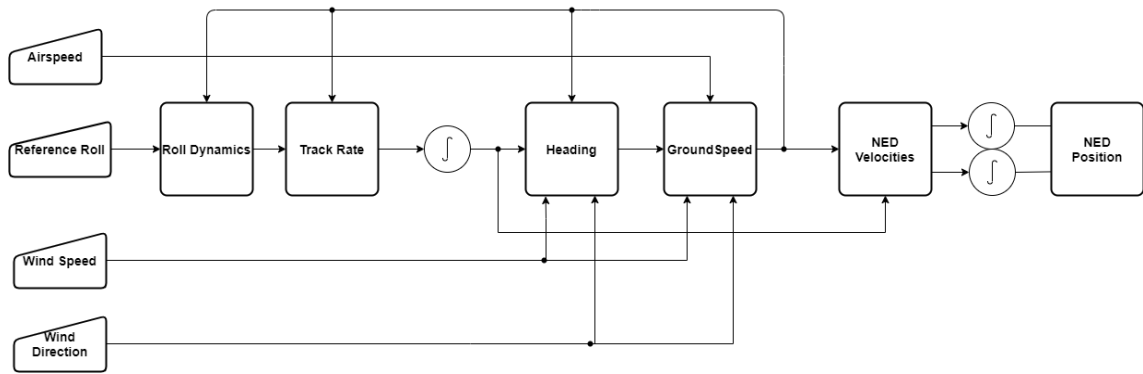
Figure 3-5: Flowchart of UAV lateral dynamics simulation

3.3.2   Camera Simulation

The aim of camera simulation is to map a 3D target position into a 2D image frame with pixel locations. Figure 3-6 shows the relation between world and pixel coordinates. Converting world coordinates to pixel coordinates is generally modeled by using pin hole [21], [23], [51] or classical polynomial distortion camera model [52]. In this work, the classical polynomial distortion camera model and estimated camera parameters are used to simulate the camera. The camera parameter estimation is detailed in the Camera Calibration section.
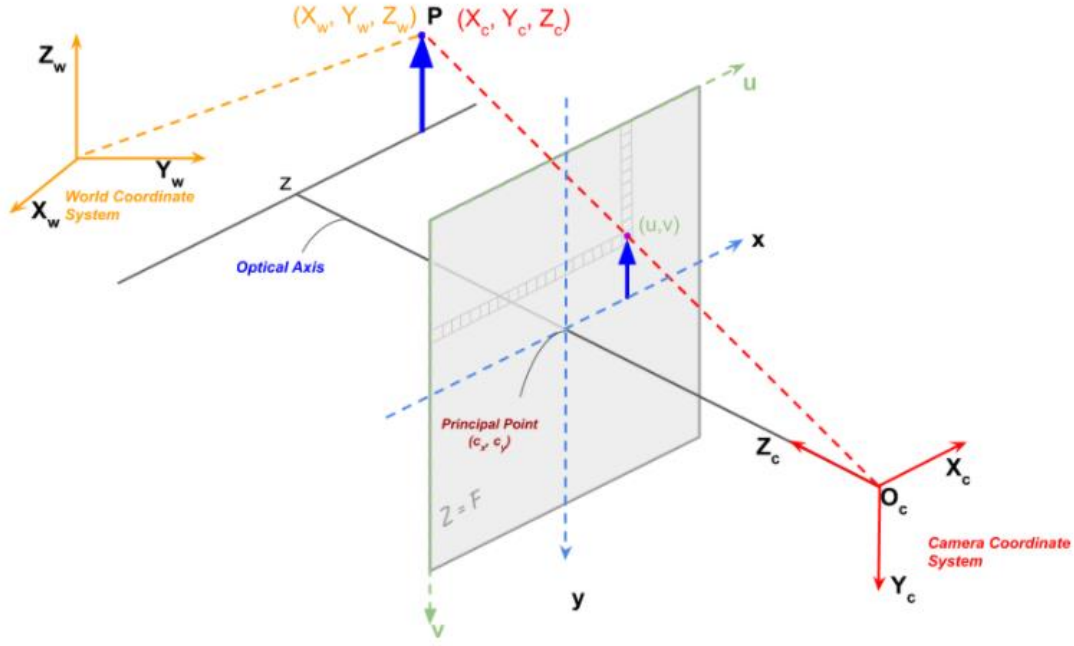
Figure 3-6: Object in world and pixel coordinates [53]

This mapping starts with estimation target vector from camera position ($\vec{r}^V_{target}$). UAV position can be used as the camera position.

$$\vec{r}^V_{target} = \vec{P}^V_{target} - \vec{P}^V_{UAV} \tag{3.7}$$

The target vector is transferred to camera coordinate frame by using rotation matrices in equations (1.9), (1.12), and (1.14).

$$\vec{r}^C_{target} = R^C_G R^G_B R^B_V \vec{r}^V_{target} \tag{3.8}$$

Normalized x_n and y_n vectors and normalized distance to center vector (r) are calculated as:

$$x_n = \frac{\vec{r}^C_{target_x}}{\vec{r}^C_{target_z}}, \qquad y_n = \frac{\vec{r}^C_{target_y}}{\vec{r}^C_{target_z}}$$
$$r^2 = x_n^2 + y_n^2 \tag{3.9}$$

Using radial distortion (k_1, k_2, k_3) and tangential distortion (p_1, p_2) parameters both distortions are calculated and added to x_n and y_n.

$$dx_r = x(k_1 r^2 + k_2 r^4 + k_3 r^6)$$
$$dy_r = y(k_1 r^2 + k_2 r^4 + k_3 r^6)$$

(3.10)

$$dx_t = 2p_1 xy + p_2(r^2 + 2x^2)$$
$$dy_t = p_1(r^2 + 2y^2) + 2p_2 xy$$

(3.11)

$$x_d = x_n + dx_r + dx_t$$
$$y_d = y_n + dy_r + dy_t$$

(3.12)

After distortions are added, the relation between final pixel locations in image frame and distorted (normalized) vectors is:

$$\epsilon_x = f_H(x_d + s * y_d) + c_x - 0.5 M_H$$
$$\epsilon_y = f_V y_d + c_y - 0.5 M_V$$

(3.13)

Finally, pixel locations can be normalized by using pixel sizes:

$$\hat{\epsilon}_x = \frac{\epsilon_x}{M_h}$$
$$\hat{\epsilon}_y = \frac{\epsilon_y}{M_v}$$

(3.14)

3.4 Simulation Environment Results

3.4.1   UAV Simulation Results

UAV Model Validation

Flight tests have been done to measure the performance of the model. The first flight results are shown in Figure 3-10, Figure 3-9, and Figure 3-10.
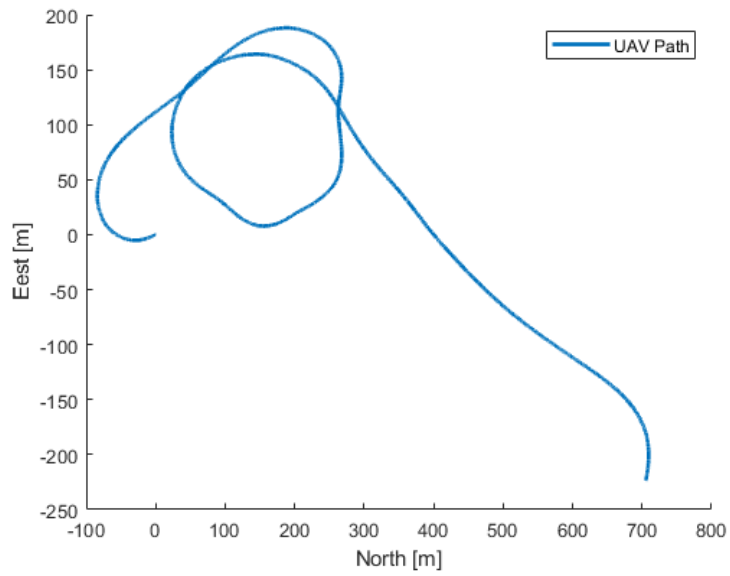
Figure 3-7: UAV flight path
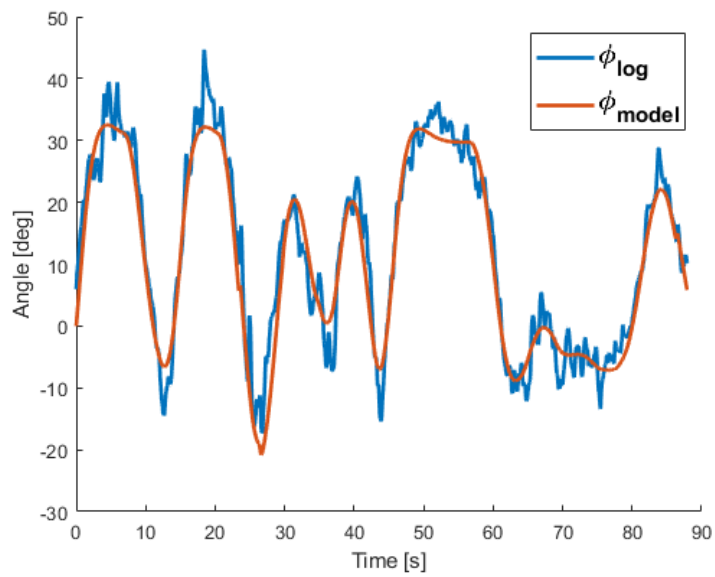
Figure 3-8: Model and flight roll angles
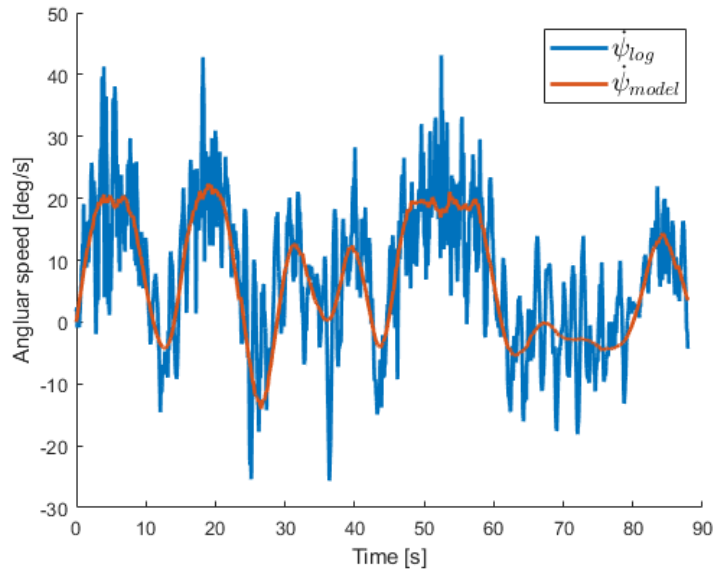
Figure 3-9: Model and flight heading angle rates
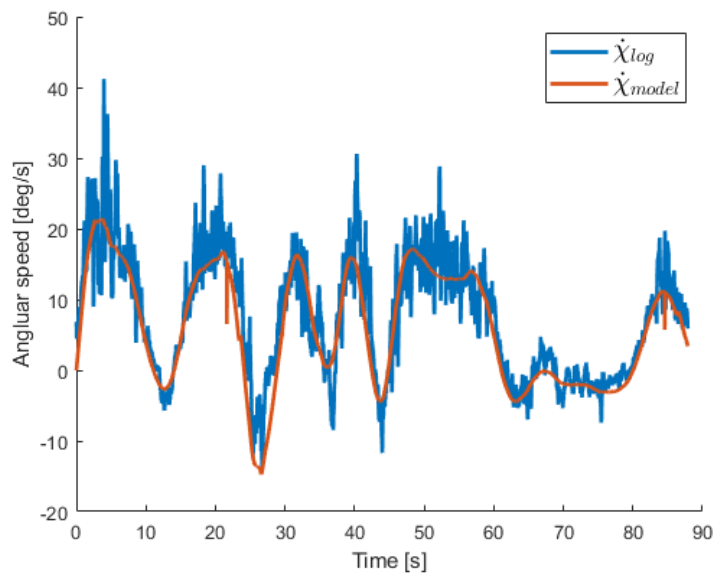
Figure 3-10: Model and flight track angle rates

Other tests are given in UAV Model Validation Flight Test section. Mean error and standard deviation between flight and model data are estimated. Results are shown in Table 3.1.

Table 3.1: UAV model mean error and standard deviations

	Roll Angle [deg]		Heading Rate [deg/s]		Track Rate [deg/s]	
Flight NO	Mean	Std	Mean	Std	Mean	Std
V1	1.03	3.71	0.84	7.01	1.32	3.72
V2	0.39	3.5	0.87	6.75	1.03	2.70
V3	2.00	3.63	1.76	6.21	1.61	2.56

UAV Model at Different Wind Conditions

UAV model performance at wind conditions is investigated model 2D position at different wind conditions are shown in Figure 3-11, Figure 3-12.
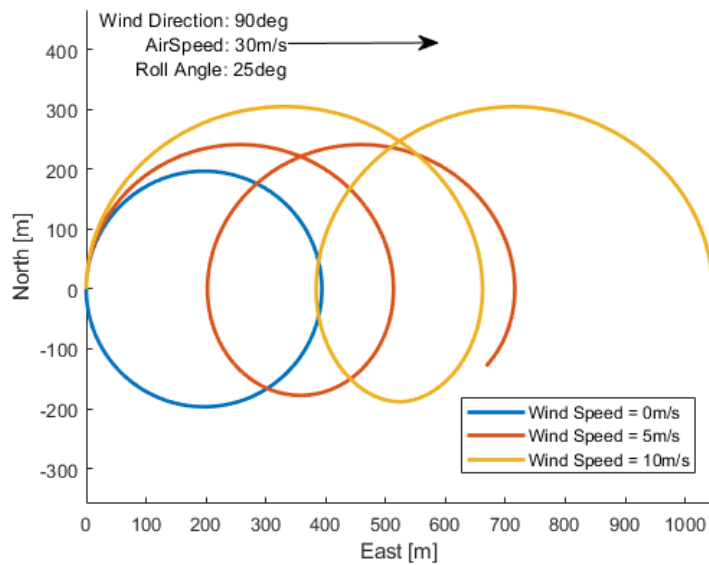
Figure 3-11: UAV 2D position at different wind speeds
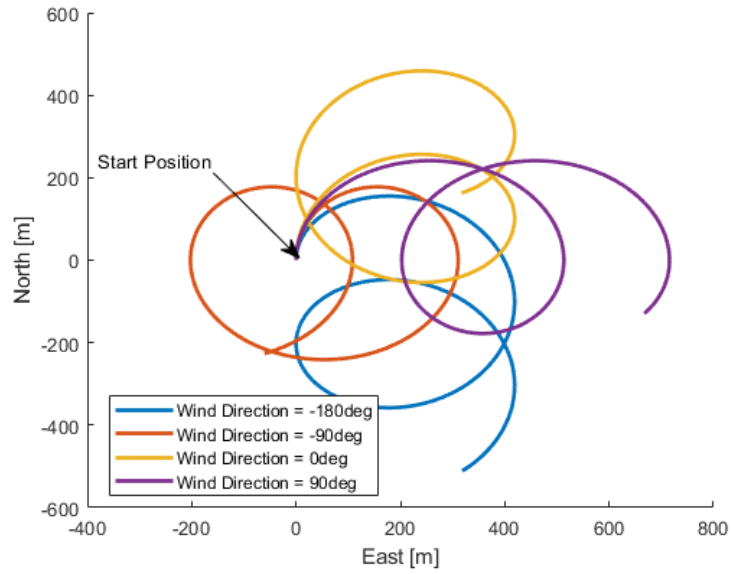
Figure 3-12: UAV 2D position at different wind directions

The relation between heading angle and difference between ground speed and airspeed at different wind speeds is shown in Figure 3-13. The same relation but at different wind directions is shown in Figure 3-14.
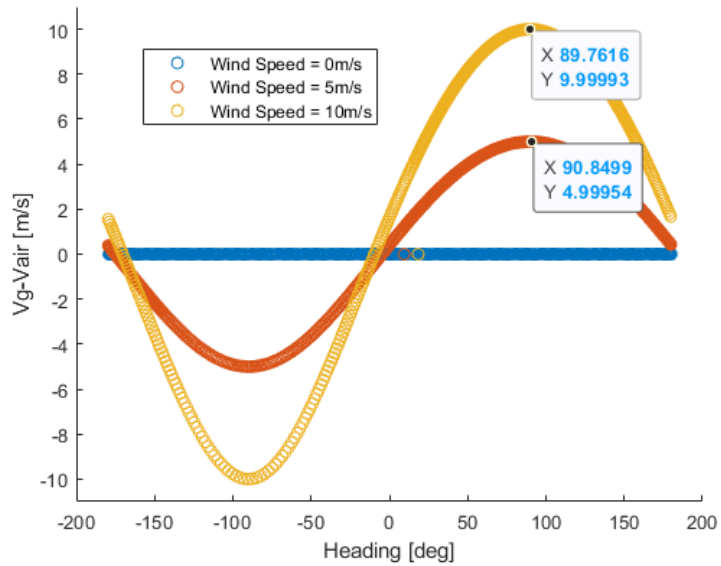
Figure 3-13: UAV model speed difference versus heading angle at different wind speeds
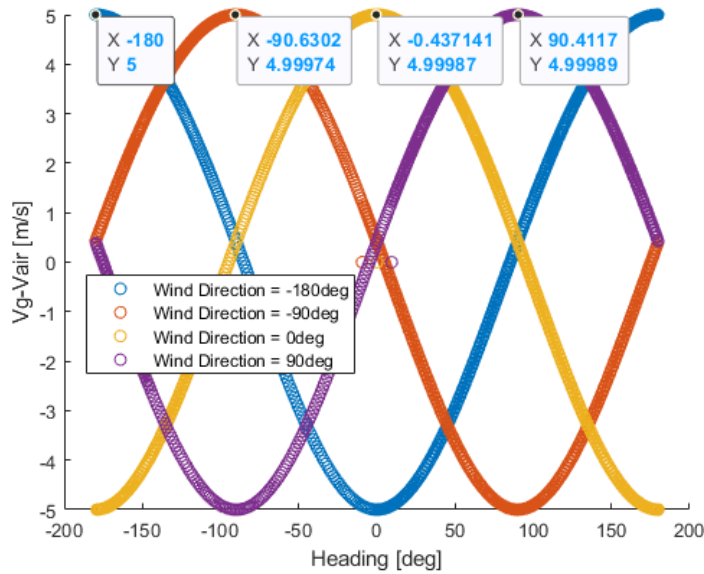
Figure 3-14: UAV model speed difference versus heading angle at different wind directions

3.4.2 Camera Simulation Results

The performance of the camera model is analyzed by using flight tests. In flight tests, the target is tracked and its pixel location is estimated by the vision system and UAV flight data and vision system data are recorded. In these tests, the camera is fixed with 0 degrees azimuth and -13 degrees elevation angle with respect to the body frame. Figure 3-15 shows target and UAV positions, respectively. Target position is measured with the same grade GNSS system.
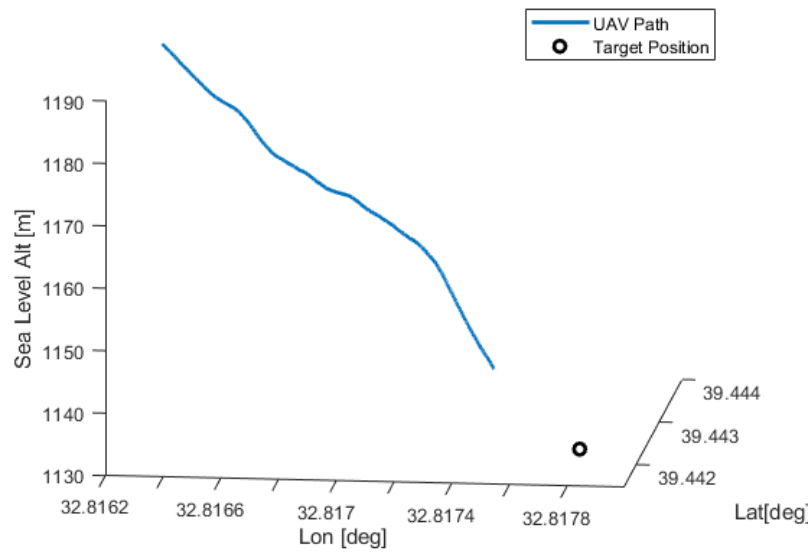
Figure 3-15: Target and UAV positions

Next, using the equations given in Camera Simulation, pixel locations of the target in the image frame are re-calculated by using flight data. Figure 3-16 and Figure 3-17 shows absolute errors in pixels for x and y axis. Figure 3-18 percentage absolute error.
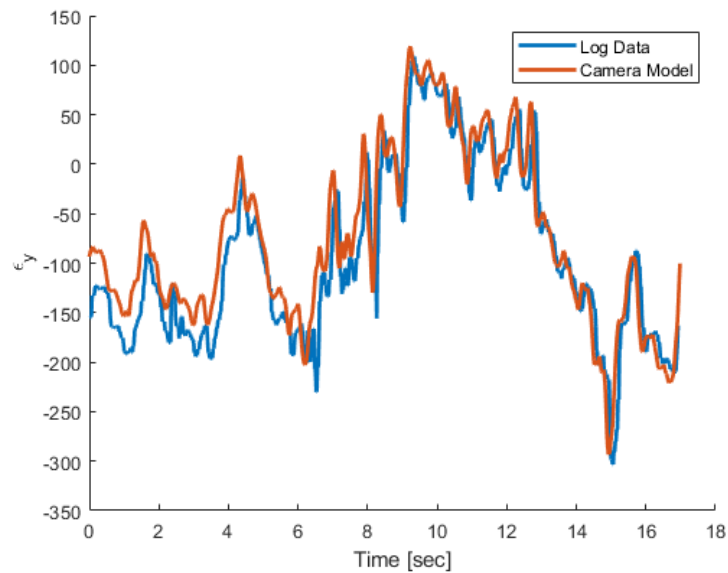
Figure 3-16: Flight and re-estimated pixel locations of the target in y-axis of camera frame
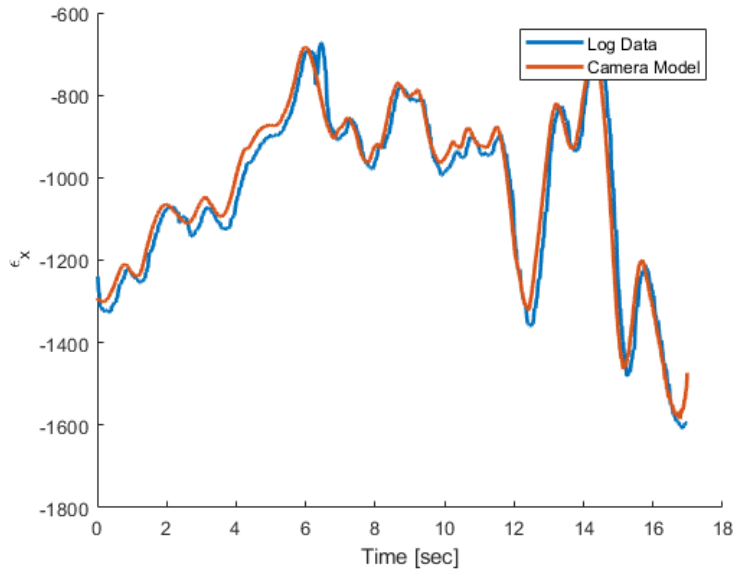
Figure 3-17: Flight and re-estimated pixel locations of the target in x-axis of camera frame
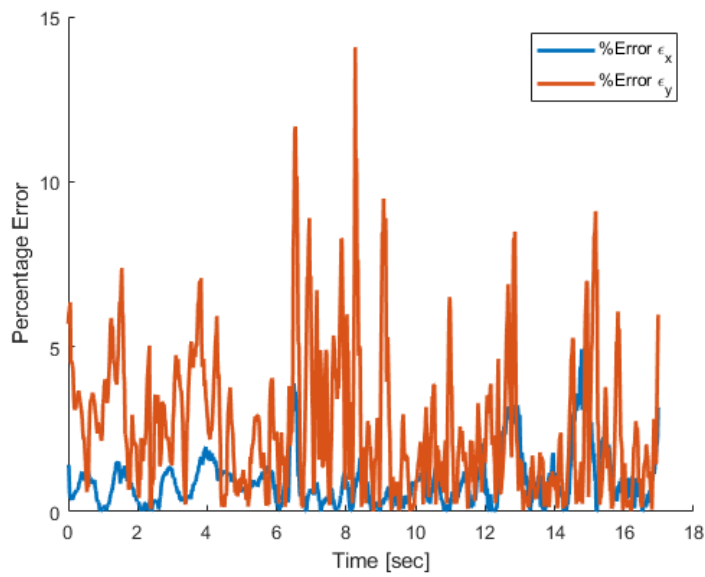
Figure 3-18: Percentage absolute errors

Other test results are given in Camera Model Validation Test section. Estimated mean and percentage mean absolute errors are tabulated in Table 3.2.

Table 3.2: Camera model absolute and % absolute errors

	Mean Absolute Error		% Mean Absolute Error	
Flight Test No	ϵ_x	ϵ_y	ϵ_x	ϵ_y
1	35.8	27.6	0.9	2.6
2	41.3	19.2	1.0	1.8
3	66.3	46.0	1.7	4.3
4	54.0	26.2	1.4	2.4

3.5 Conclusion

The primary purpose of this chapter is to develop a mathematical model of both UAV and camera system. These mathematical models are used in the upcoming chapters. To that purpose, a simple UAV model is developed that satisfies the requirements of flight path design control algorithms. Same as, camera model is developed, which maps 3D world positions to camera frame pixel locations. To validate models, flight tests are done. Both models' accuracies are estimated.

4. LOS VECTOR ESTIMATION

4.1 Introduction

The aim of this chapter is that converting the pixel location of the target in image plane to inertial frame coordinates. The LOS vector is used in FLIGHT PATH PLANNING and TARGET POSITION ESTIMATION sections. Principally, this estimation process is inverse of mapping 3D position to 2D pixel location that is mentioned in section Camera Simulation.

4.2 Estimation LOS Vector in Camera Frame from Pixel Locations

The first step of estimating the LOS vector is converting the pixel location of the target in the image plane to the camera frame. Figure 4-1 shows the camera and image frame and target positions on these frames. Where ℓ^C is target vector in camera frame (LOS vector) and $\ell_x^C, \ell_y^C, \ell_z^C$ are components. $\mathbb{L}$ is distance of target to camera frame origin. These target positions and distances are in metric units. $\epsilon, \epsilon_x, \epsilon_y$ are projected target position image frame in units of pixels and f, F are focal length and distance from camera frame to the target position in image frame in pixels. P conversation unit that converts pixel units to metrics.
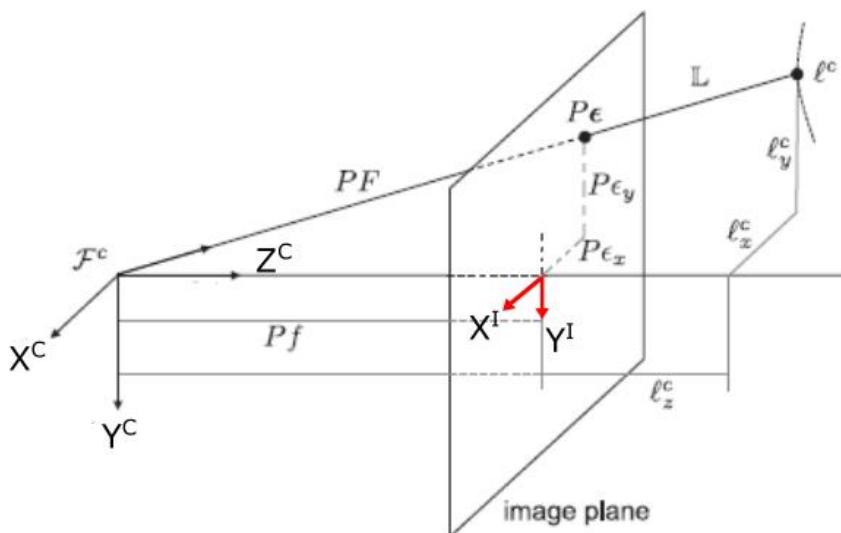
Figure 4-1: Camera and image frame [33]

44

The vision system, while tracking the target, returns its pixel locations. Hence, using both camera parameters and target pixel locations, ℓ^C is estimated. For this transformation, pinhole and polynomial distortion camera models are investigated.

4.2.1   Pinhole Camera Model

Pinhole, which is also called perspective projection, is the simplest camera model. In this model, light arrays that are emitted from objects pass through aperture (pin hole) and collide with the image sensor [52]. This model ignores distortion effects that are mentioned in the Camera Calibration section. Hence, governing equations are formed based on triangular similarities [52], [54], [55].
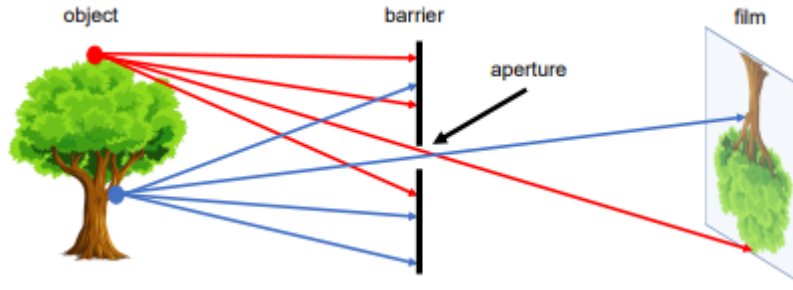
Figure 4-2: Pinhole camera model representation [54]

Referring to Figure 4-1, using Hypotenuse of triangle:

$$F = \sqrt{\epsilon_x^2 + \epsilon_y^2 + f^2} \tag{4.1}$$

$$\mathbb{L} = \sqrt{\ell_x^{C^2} + \ell_y^{C^2} + \ell_z^{C^2}} \tag{4.2}$$

And using triangular similarities, equalities in 4.3 are found:

$$\frac{\ell_x^C}{\mathbb{L}} = \frac{\epsilon_x}{F}, \qquad \frac{\ell_y^C}{\mathbb{L}} = \frac{\epsilon_y}{F}, \qquad \frac{\ell_z^C}{\mathbb{L}} = \frac{\epsilon_z}{F} \tag{4.3}$$

Then, ℓ^C in matrix form becomes:

$$\ell^C = \frac{\mathbb{L}}{F} \begin{bmatrix} \epsilon_x \\ \epsilon_y \\ f \end{bmatrix} \qquad (4.4)$$

As seen from Equation (4.4), the target vector in the camera frame depends on the distance to the target, which is unknown. This is the reason of that camera does not contain depth information so that unit target vector (LOS^C) is used.

$$LOS^C = \frac{\ell^C}{\mathbb{L}} = \frac{1}{F} \begin{bmatrix} \epsilon_x \\ \epsilon_y \\ f \end{bmatrix} \qquad (4.5)$$

4.2.2 Classical Polynomial Distortion Model

The main improvement of this method compared to the pinhole model is that this method considers distortions. Basically, this method is inversion of the model described in section Camera Simulation. This method is generally used for removing distortion effects in images [56]–[58].

Normalized pixel locations are converted such that:

$$\begin{aligned} \epsilon_x &= \hat{\epsilon}_x * M_h \\ \epsilon_y &= \hat{\epsilon}_y * M_v \end{aligned} \qquad (4.6)$$

By taking the inverse of equation (3.13), distorted target vectors in the camera frame are found.

$$\begin{aligned} y_d &= \frac{\epsilon_y - c_y + 0.5 M_V}{f_V} \\ x_d &= \frac{\epsilon_x - c_x + 0.5 M_H}{f_H} - s * y_d \end{aligned} \qquad (4.7)$$

Now distortion values should be removed from x_d and y_d to estimate normalized target vectors. However, distortion values in Equations (3.10) and (3.11) depend on x_n and y_n. It means that there is no analytical solution to this problem. Equation (3.10), (3.11), and (3.12) can be rewritten as:

$$\begin{bmatrix} x_d \\ y_d \end{bmatrix} = \begin{bmatrix} x_n \\ y_n \end{bmatrix} + f(x_n, y_n) \tag{4.8}$$

where f is a function that represents distortions both radial and tangential.

$$f(x_n, y_n) = \begin{bmatrix} dx_r + dx_t \\ dy_r + dy_t \end{bmatrix} \tag{4.9}$$

Even if there is no analytical solution for Equation (4.8), it can be solved numerically. To do this, fixed-point iteration method is used [56], [59]. Due to iterations, this method is considered slow [56]. However, in this work, fixed-point iteration is done for only one pixel location, not for the whole image.

$$\begin{bmatrix} x_{n_{i+1}} \\ y_{n_{i+1}} \end{bmatrix} = \begin{bmatrix} x_d \\ y_d \end{bmatrix} - f(x_{n_i}, y_{n_i}) \tag{4.10}$$

Now using undistorted normalized vectors, the LOS vector in the camera frame can be found using equalities in Equation (4.11).

$$\frac{LOS_x^C}{LOS_z^C} = x_n$$

$$\frac{LOS_y^C}{LOS_z^C} = y_n \tag{4.11}$$

$$LOS_x^{C^2} + LOS_y^{C^2} + LOS_z^{C^2} = 1$$

4.3 Converting LOS Vector into Vehicle Frame

LOS vector in the camera frame is not practical, so it should be transferred into a proper one. In this case vehicle frame is the best one for the LOS vector. LOS vector in the vehicle frame represents the target direction vector with respect to UAV. This rotation can be done by using Equations (1.15), (1.13), and (1.10).

$$LOS^V = R_B^V * R_G^B * R_C^G * LOS^C \tag{4.12}$$

Instead of direction vector, LOS vector can be represented in circular form, such as azimuth (ψ_{LOS}) and elevation (θ_{LOS}) angles as shown in Figure 4-3.
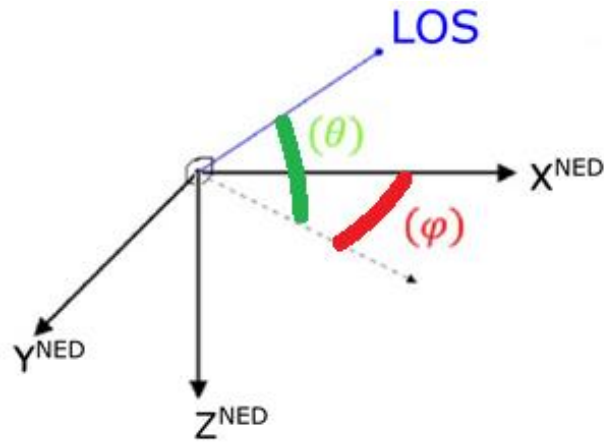
Figure 4-3: Azimuth and elevation angles

$$\psi_{LOS} = \text{atan}\left(\frac{LOS_y^V}{LOS_x^V}\right)$$

$$\theta_{LOS} = -\text{asin}\left(LOS_z^V\right)$$

(4.13)

4.4 Estimation Errors and Improvements

4.4.1 Vision System Lag

One of the error sources in the estimation is the time differences between data. In other words, delays in systems cause estimation errors. The main delay source is the vision system. The first camera captures an image, then the vision system reads the image and then processes the image. This sequence falls vision system data behind the other sensors data. A chronometer is placed in front of the camera and the vision system image is shown in the ground control station. Then with an external camera, a photo that captures both chronometer and vision system is taken. Vision system lag is measured around 200-300 ms by taking a photo of the chronometer with an external camera (Figure 4-4). The delay is not growing in time leads to a constant value which allows a simple compensation algorithm.
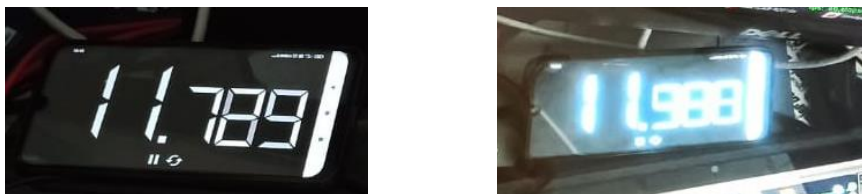
Figure 4-4: Time difference between vision system (right) and real (left)

This lag effect can be removed by arranging data. As described in the above section, LOS angle is the function of UAV attitude angles and target pixel locations in the camera frame. This delay affects target pixel locations, so that pixel location lags the attitude angles. Future pixel data are not used, but previous attitude values are used to synchronize both data. Hence, the solution to this problem is that previous attitude angles corresponding to the delay are utilized in the model.

4.4.2   Measurement Errors

The main error source is the measurement errors and LOS estimation depends on attitude angles, gimbal angles, and pixel locations. Since pixel locations are measured by the vision system, errors in these measurements are not further decreased. Attitude angles and gimbal angles are aligned with each other and errors in these angles are not distinguishable [30],[31]. Therefore, Barber suggests an optimization method for gimbal angles such that bias in gimbal angles that cause minimum variance in position estimation is found by an online quasi-Newton method [31]. However, these methods are not proper for the real time applications.

In this work, an offline gimbal bias angles estimation method for a stationary camera (non-gimballed) is used. In this method, after flight tests are done, bias angles in camera placement are estimated, such as minimizing error in LOS angle estimations between using positions and using camera models. Hence, cost function (J) is defined sum of square errors between LOS estimation from position ($\psi_{LOS,pos}, \theta_{LOS,pos}$) and LOS estimation from camera ($\psi_{LOS,cam}, \theta_{LOS,cam}$)

$$J = \left(\theta_{LOS,pos} - \theta_{LOS,cam}\right)^2 + \left(\psi_{LOS,pos} - \psi_{LOS,cam}\right)^2 \tag{4.14}$$

Estimation of bias errors is converted to the following optimization problem.

$$\min_{\psi_g,\theta_g} J(\psi_g, \theta_g) \tag{4.15}$$

4.5 Results

Flight tests, which are accomplished for camera simulation in the Camera Simulation Results section, are used to analyze the LOS estimation. Tracking target location in ECEF

frame is measured during these tests. Using target location and UAV location, LOS azimuth and elevation angles are estimated. These results are considered as ground truth and compared with the estimation method described in this section. For flight test 1, Figure 4-5 and Figure 4-6 show estimated LOS angles from both pinhole and distortion models and position data. Figure 4-7 and Figure 4-8 show LOS elevation and azimuth angles.
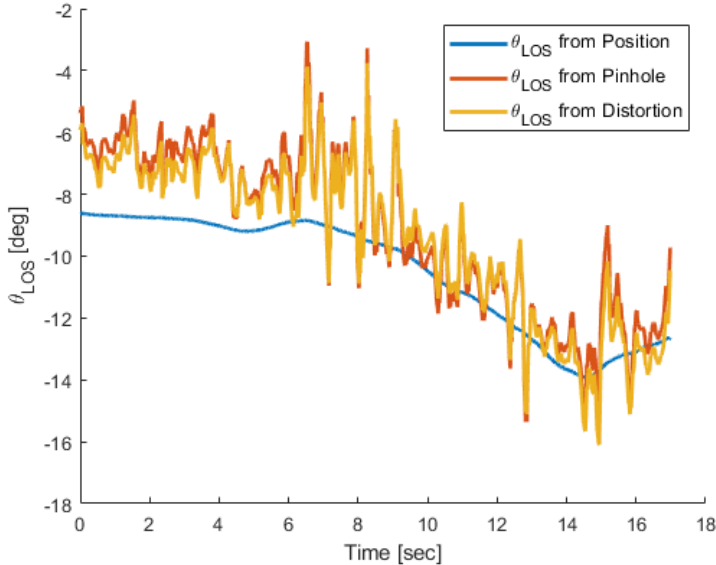
Figure 4-5: LOS elevation angles
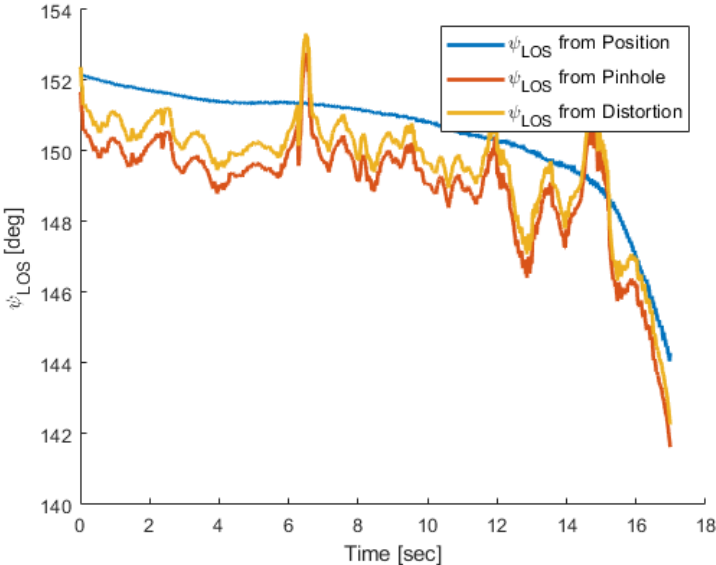
Figure 4-6: LOS azimuth angles
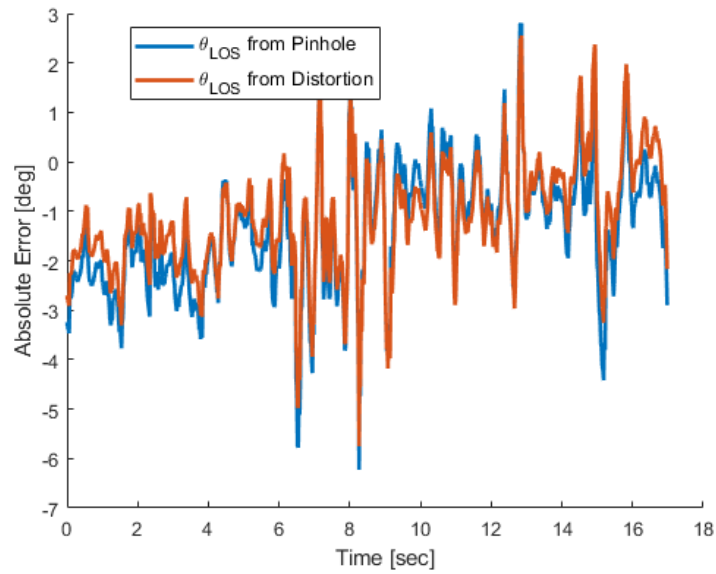
Figure 4-7: Estimated LOS elevation angle errors
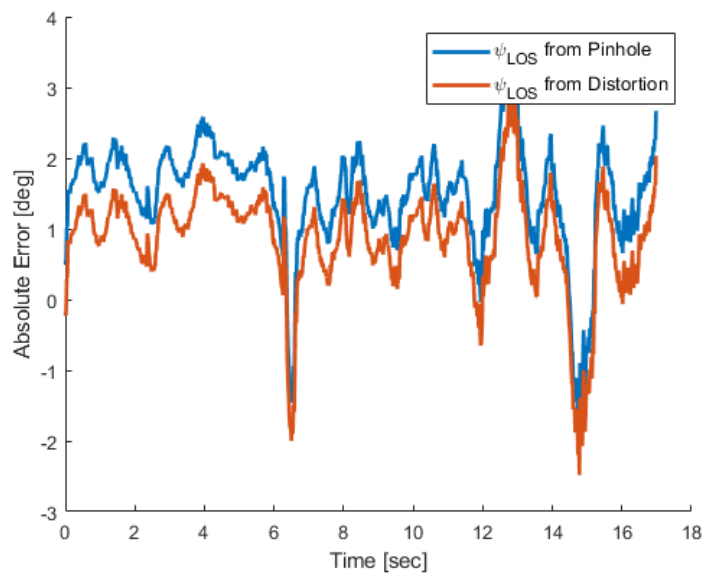
Figure 4-8: Estimated LOS azimuth errors.

Results of the other three tests are shown in LOS Estimations. Mean error and standard deviations for both models are tabulated in Table 4.1 and Table 4.2.

Table 4.1: Pinhole model LOS estimation performance

Pinhole Model	LOS Elevation Error [deg]		LOS Azimuth Error [deg]	
Flight Test	Mean	Std.	Mean	Std
1	-1.36	1.24	1.48	0.78
2	-0.65	0.89	0.75	1.03
3	-1.35	1.22	0.90	0.71
4	-1.56	1.30	1.45	1.38

Table 4.2: Distortion model LOS estimation performance

Distortion Model	LOS Elevation Error [deg]		LOS Azimuth Error [deg]	
Flight Test	Mean	Std.	Mean	Std
1	-1.11	1.12	0.86	0.75
2	-0.21	0.89	0.14	0.92
3	-0.51	1.06	0.33	0.66
4	-1.17	1.03	0.85	1.34

As seen from the above figures and tables, the distortion model performs better than the pinhole. The reason for that is distortion model uses much more parameters than the pinhole model. However, the pinhole model is used due to its simplicity.

In addition, the effect of lag in the vision system is investigated. As mentioned above, attitude angles are shifted to previous ones and the same estimated methods are applied for flight test one. For different numbers of data shifts, the standard deviation of LOS elevation and azimuth angles are shown in Figure 4-9 and Figure 4-10.
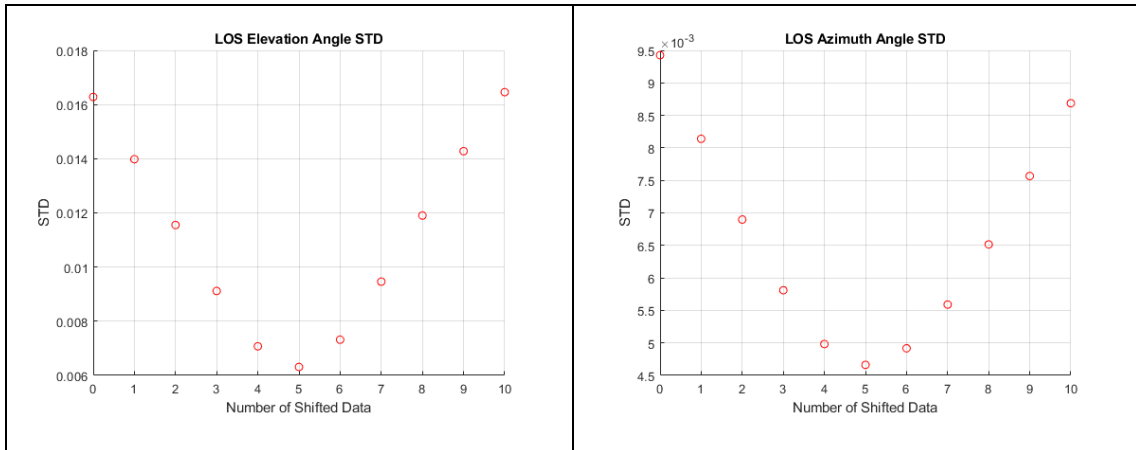
Figure 4-9: Shifted data number versus LOS elevation (left) and azimuth (right) std in radians.
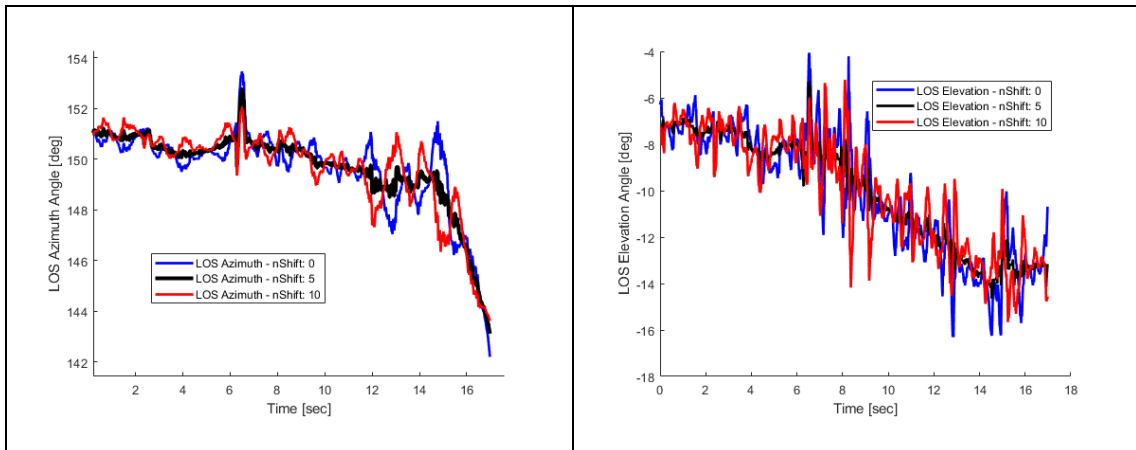
Figure 4-10: LOS azimuth (left) and elevation (right) angles estimation for 0, 5 and 10 data shifts.

Both azimuth and elevation standard variations reach their minimum value with the same number of data shifts according to the results. These test data are logged with 50 Hz and there is 250 ms time delay due to the vision system. The time delay is consistent with chronometer test measurements. For flight test one, mean and standard deviations for both LOS estimation methods are re-calculated and tabulated in Table 4.3 and Table 4.4.

Table 4.3: Pinhole model LOS estimation performance comparison with data shift

Pinhole Model	LOS Elevation Error [deg]		LOS Azimuth Error [deg]	
Flight Test	Mean	Std.	Mean	Std
1	-1.36	1.24	1.48	0.78
1 with 5 data shifts	-1.39	0.75	1.46	0.40

Table 4.4: Distortion model LOS estimation performance comparison with data shift

Distortion Model	LOS Elevation Error [deg]		LOS Azimuth Error [deg]	
Flight Test	Mean	Std	Mean	Std
1	-1.11	1.12	0.86	0.75
1 with 5data shifts	-1.14	0.65	0.84	0.36

The data shift greatly affects error standard deviations in both estimations but slightly changes the mean error. Another improvement is the estimation of bias in parameters. The minimization is solved by MATLAB "fminsearch" function [60]. Minimization is done by using all gimbal angles and camera FOV angles parameters for the pinhole model. Figure 4-11 shows the cost function value at each optimization iteration and the final values of parameters are tabulated in Table 4.5.
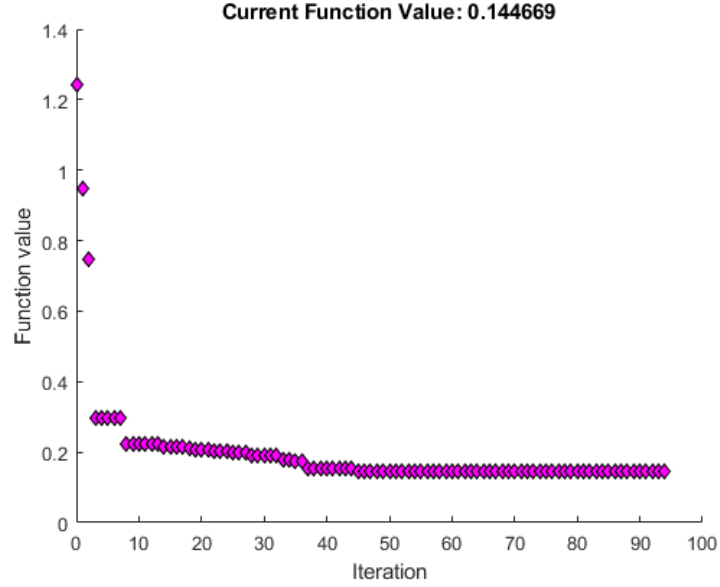
Figure 4-11: Optimization process

Table 4.5: Pinhole model parameters and gimbal angles after optimization

	ϕ_g [deg]	θ_g [deg]	ψ_g [deg]	FOV_v [deg]	FOV_h [deg]
Before	0	-13	0.0	37.6	63.6
After	0.5	-14	0.0	36.5	60.3

LOS angles are re-estimated for pinhole camera model using the analyzed parameters and data shift improvement, Flight test 1 results with and without improvements are tabulated in Table 4.6. Figure 4-12 and Figure 4-13 shows LOS angles estimation from the position, with and without improvements. From these results, obviously, it is seen that the performance of estimation is significantly increased by the improvements. Both mean error and standard deviation between estimation and measurement by using position data decreases. However, there are still exits errors and estimations are not perfect. This is due to the other errors exist in the estimations, such as pixel location and position data errors. More accurate sensors or INS system or vision system is necessary to decrease or remove these errors, but this is not the focus of this work.

Table 4.6: Pinhole model LOS estimation performance comparison with improvements

Pinhole Model	LOS Elevation Error [deg]		LOS Azimuth Error [deg]	
Flight Test 1	Mean	Std	Mean	Std
No improvement	-1.36	1.24	1.48	0.78
With Improvement	-0.12	0.64	0.52	0.31
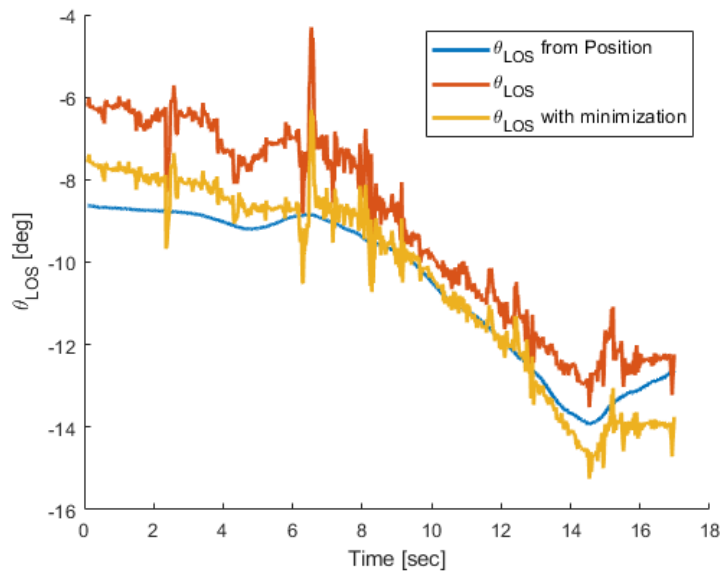
Figure 4-12: LOS elevation estimation with and without improvements
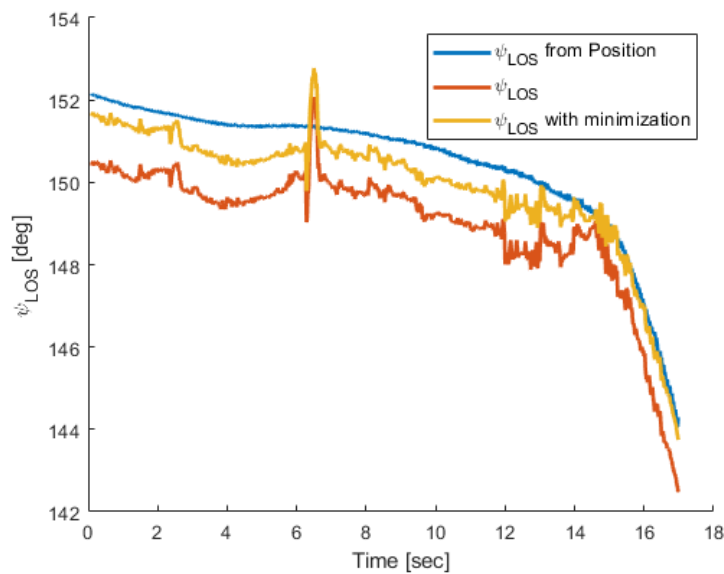
Figure 4-13: LOS azimuth estimation with and without improvements

4.6 Conclusion

As a conclusion for this chapter, two methods that are pinhole and distortion camera models, are investigated for estimation of LOS vector or angles. Both methods are described and tested with flight data. Their performances are compared with the LOS angles estimation by using position data of UAV and target. Almost similar results are obtained by both LOS estimation methods. This is due to the used image sensor which has exceptionally low distortions. Therefore, it is concluded that the pinhole model is used instead of the distortion model since it is quite a simple method in implementation and computation wise. However, it will be inevitable to use the distortion model in cases where sensor distortions are excessive.

Errors sources and improvement of these errors are described. These improvements are applied and tested with the same flight data. Results are presented and it is seen that improvements exceptionally increased LOS estimation performance.

5. FLIGHT PATH PLANNING

5.1 Introduction

Controlling UAV such that holding the target in LOS is the main purpose of this chapter. Loitering around the target is a common maneuver for fixed wing UAVs because UAV in loiter motion holds the target in a fixed position with respect to itself. It means that, for gimballed or fixed camera placed in right azimuth angles, the target is always on FOV of the camera. Therefore, continuous target tracking is the goal of this chapter.

As mentioned LITERATURE SURVEY section, the tracking algorithm, developed by Dobrokhodov, performs well. The control philosophy of that method is keeping UAV ground velocity perpendicular to the LOS vector. Therefore, perfect controls guarantee a circle (loiter) around the target. In the gimbal control gimbal continuously align itself with respect to the LOS vector. This is a virtuous method, but the ground velocity is GNSS dependent. If GNSS fails, this control system also fails. Hence, a new control philosophy that is holding the LOS vector at a right angle with respect to UAV body frame is proposed in this thesis.

5.2 Method

It is necessary that the image sensor must be placed at the right angle or rotated by a gimbal system for continuous target tracking in loitering around the target. Therefore, LOS azimuth angle is held at the right angle, simply by holding the target in the center of the camera frame. In this method, ϵ_x measured from the vision system, is used as control input for the control system. To hold the target in the image center, horizontal pixel reference value ($\epsilon_{x,ref}$) is set as zero. Output reference roll angle (ϕ_{ref}) is generated and this reference angle is executed by the attitude hold mode of the UAV autopilot. This configuration leads the control system to be modular. The control system implementation is easy to accomplish because autonomous UAVs generally have attitude control mode which is one of the main control modes. The control loop of this method is shown in Figure 5-1.
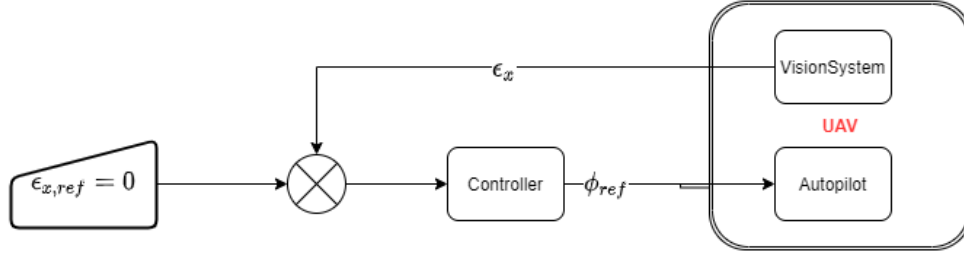
Figure 5-1: Control loop of target tracking

However, this loop does not have control over the distance to the target. Due to distributions such as wind, UAV converge or diverge to target undesirably. Moreover, the pilot/operator may desire to approach or get away from the target. Therefore, thanks to the LOS elevation angle, that is done by adding an outer loop to the controller. The schematic of control loops is shown in Figure 5-2.
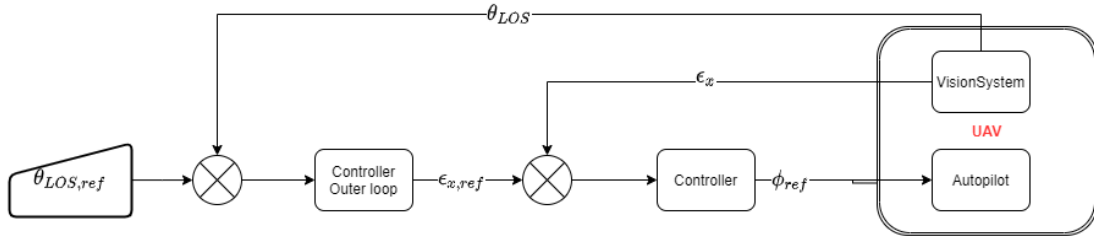
Figure 5-2: Cascade controller loop of target tracking

The horizontal distance between target and UAV (R_H) is the function of LOS elevation angle and altitude between them. Consider flat earth model where UAV altitude from ground (h_{AGL}), this altitude also becomes the height difference between UAV and target. In that case, θ_{LOS} is related with horizontal distance and h_{AGL} with trigonometric relations. Using equation (5.1), $\theta_{LOS,ref}$ is predefined depend on the UAV mission. By changing this value R_H is arranged.

$$\theta_{LOS} = \text{atan}\left(\frac{h_{AGL}}{R_H}\right) \tag{5.1}$$

Optimum altitude for minimum errors in estimation, mentioned in [31], is autonomously controlled by implementing longitudinal control loops. However, this system is not implemented because autonomously altitude change is not proper for military

applications. For that reason, for longitudinal controls, altitude hold and speed hold modes in autopilot are used and controlled remotely by the pilot.

5.3 Improvements

It is possible that the outer loop may generate $\epsilon_{x,ref}$ which is beyond the camera limits. In other words, when the target moves out of camera FOV, the target is lost. This is the most unwanted situation so $\epsilon_{x,ref}$ value must be limited to eliminate that situation. Also, this limit value works as a safety margin where the controller overshoots. Figure 5-3 visualize this limit in the image frame and Figure 5-4 shows the limited loop diagram.
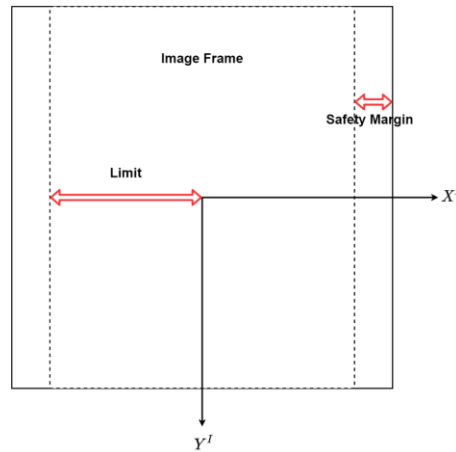
Figure 5-3: Limit and safety margin in the image frame
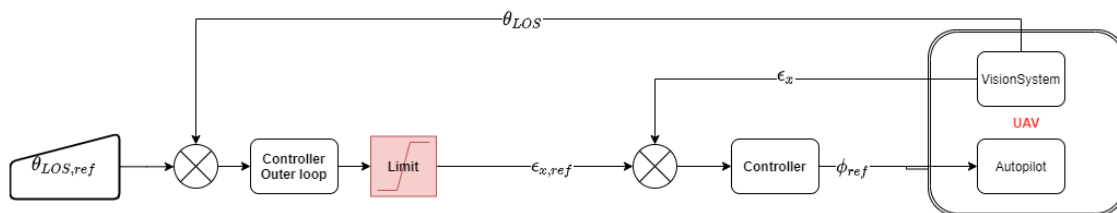
Figure 5-4: Cascade controller loop of target tracking with reference pixel limitation

The integral error may accumulate due to the limit on the outer loop. For example, when the target moves faster than UAV, the distance between them increases. The outer loop wants to hold that desired distance, but holding distance is not possible without losing the target in camera FOV. Hence, a proper integral windup method must be added [61].

Another issue is that target may be lost in camera FOV or the vision system may fail to track the target. For example, another object such as a tree or building may be block target in the image or maneuvering around a moving target may be impossible without losing it. In these situations, the maneuver should continue without target tracking. To do that, if the target position is estimated, then it is used as loiter waypoint and autopilot switches to position loiter mode. If it is not or GNSS fails, a pseudo reference roll value corresponding to the active pseudo-range is used. Pseudo reference roll value is estimated by using the coordinated turn equation. Instead of that, the last reference roll value may be used, such as:

$$\phi = \text{atan}\left(\frac{V_g^2}{gR}\right) \qquad (5.2)$$

5.4 Results

5.4.1   Simulation Results

The control loops presented in this section are added to the simulation environment that is designed in the TEST ENVIRONMENT section. The PID controller is chosen due to its simplicity and tuned using simulation for the controller [61]. Tuned PID parameters for both loops are tabulated in Table 5.1.

Table 5.1: PID parameters

	Kp	Ki	Kd
Inner loop	0.8	0.15	0.2
Outer loop	7	0.13	0.5
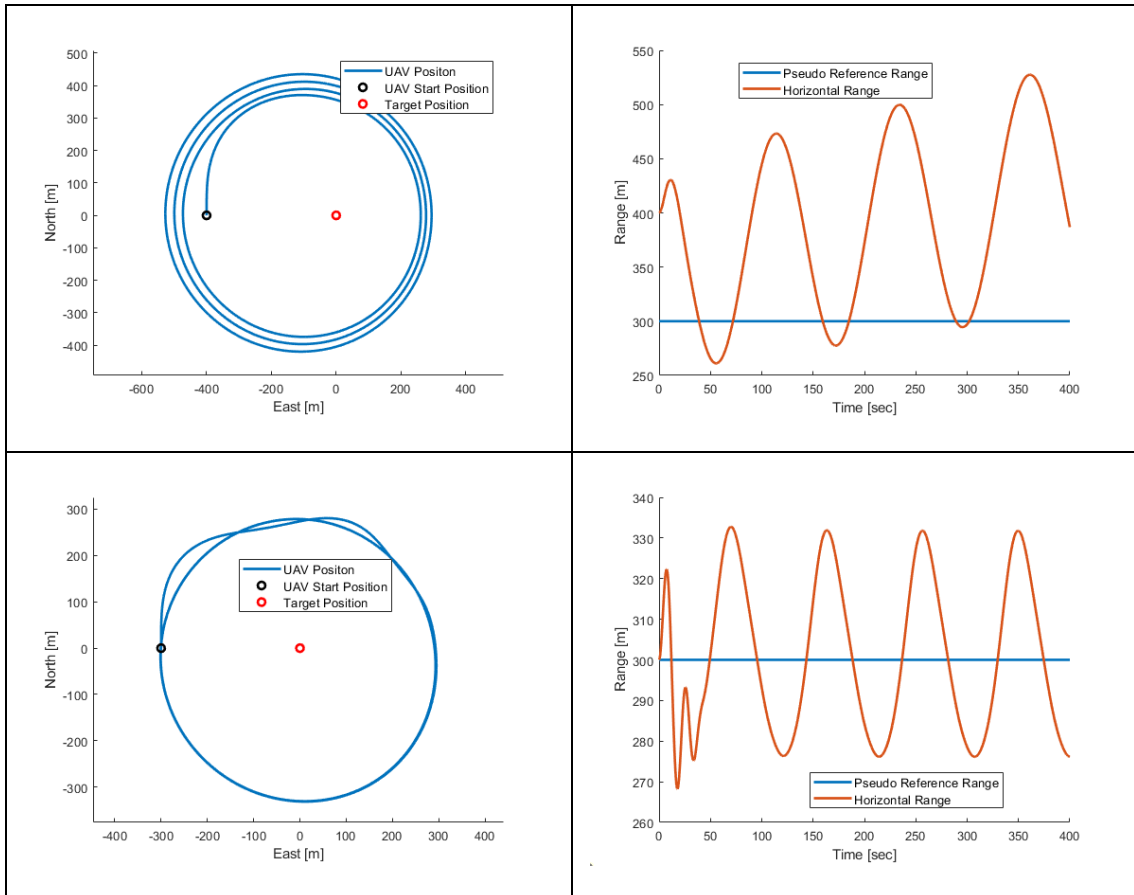
Figure 5-5: Only inner loop response (top) and cascade loop response (bottom) under 5 m/s wind conditions

Figure 5-5 shows UAV and target position for only inner loop and cascade loop implementations. Since there is no direct control on the range, UAV position slowly diverges as expected under the disturbance for only pixel location control. For the cascaded controller, UAV is able to hold the distance to the target with 10% steady state error. Figure 5-6 shows 2D positions and distance changement between target and UAV for different initial conditions and $\theta_{LOS,ref}$ values. Results show that UAV is able to diverge or converge to the target depending on the $\theta_{LOS,ref}$.
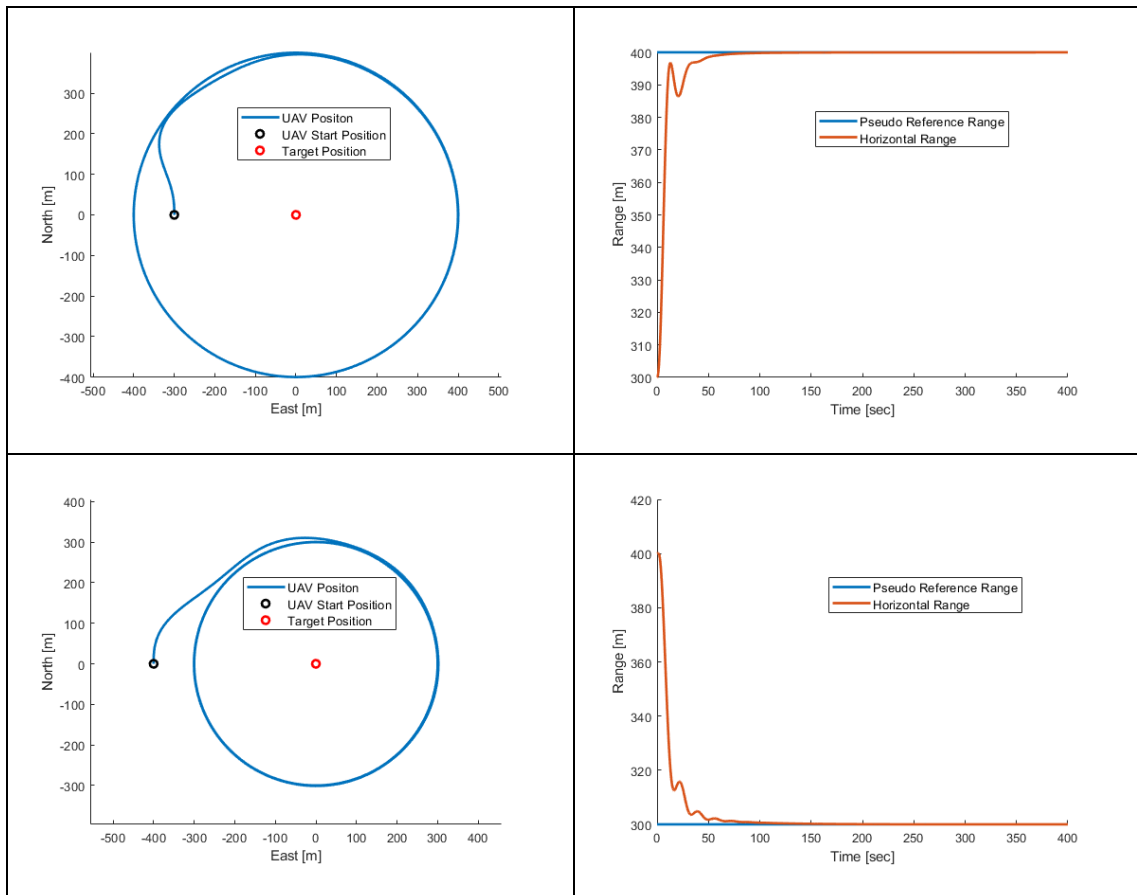
Figure 5-6: Cascade controller diverging from target (top) and converging into target (bottom) 2D position (left) and distance (right) graphs.

Figure 5-7 shows positions and distances for moving targets with 5 m/s and 25 m/s. UAV is able to hold the distance for slow moving targets but for faster targets holding the distance is not an option. Yet, UAV still tracks the targets. Figure 5-8 shows UAV and target positions for moving and turning targets with different speeds.
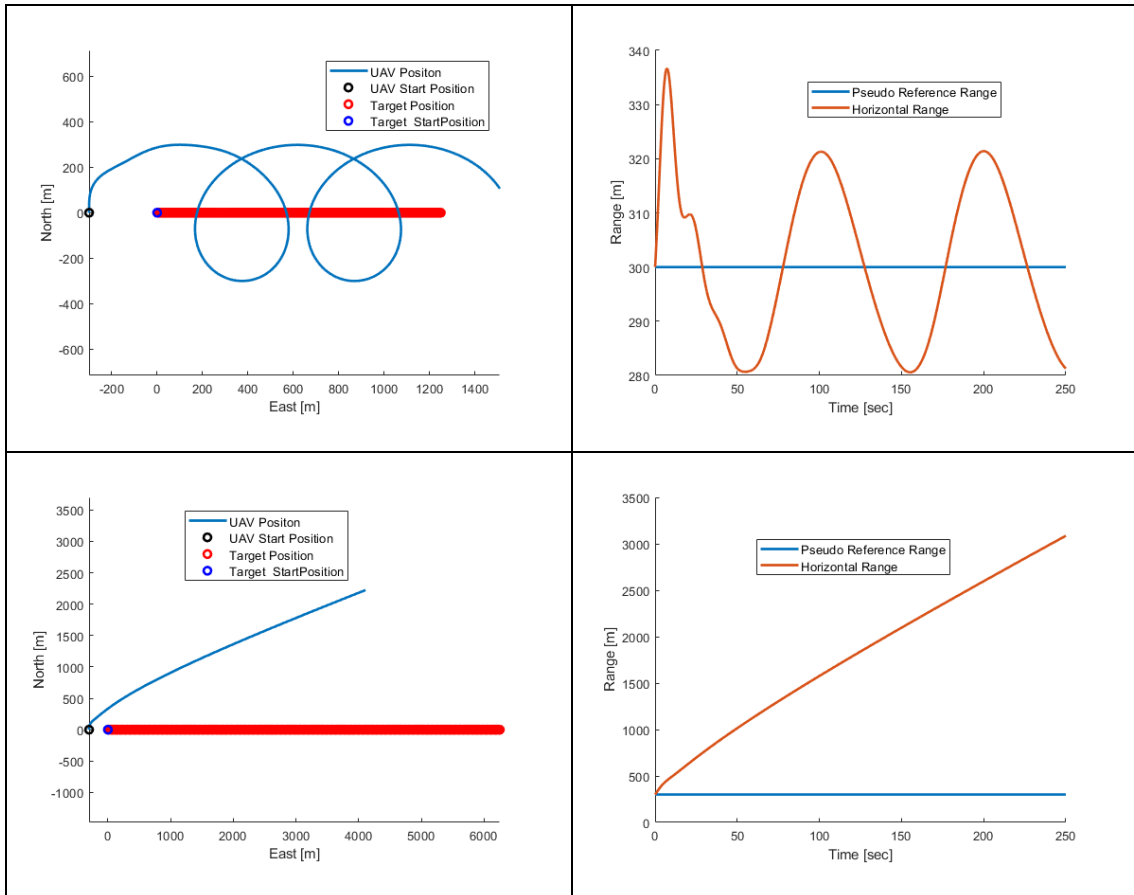
Figure 5-7: For moving targets with 5 m/s (top) and 25 m/s (bottom) towards east, 2D position (left) and distance (right) graphs.
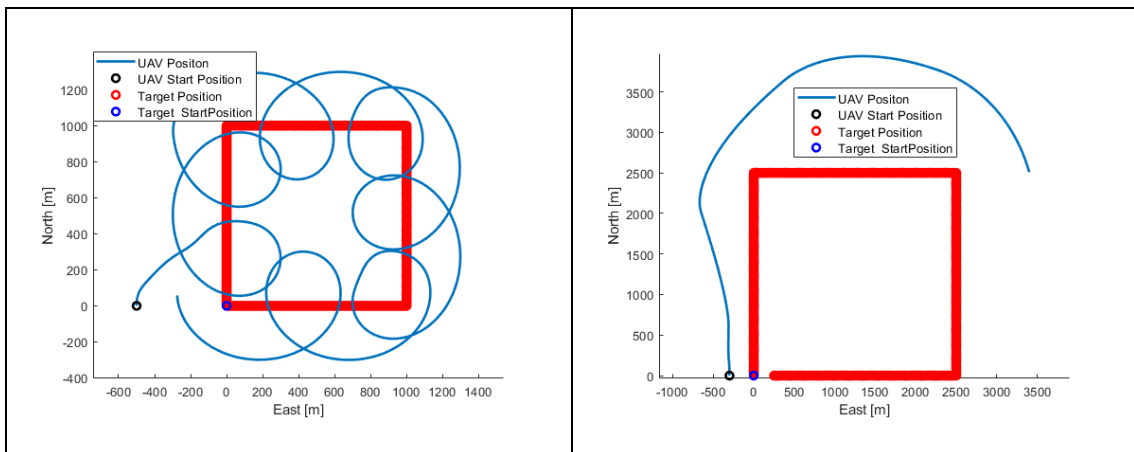
Figure 5-8: 2D position graph for moving and turning target with 5 m/s and 25 m/s speeds.

5.4.2 Flight Test Results

After promising simulation results, developed control structure is added to autopilot and four different test flights are performed. Example tracking images in these tests are shown in Figure 5-9.

Figure 5-9: Successive target tracking and image-based loitering.

In the first test flight, only the inner loop is enabled, and the outer loop is closed. Figure 5-10 shows UAV flight path with the target position and horizontal distance to the target. During this test, wind speed is estimated as 1.1 m/s. The used wind estimation method is based on wind triangle, and it is a similar method to [62]. Same as simulation results, UAV position converges to the target.
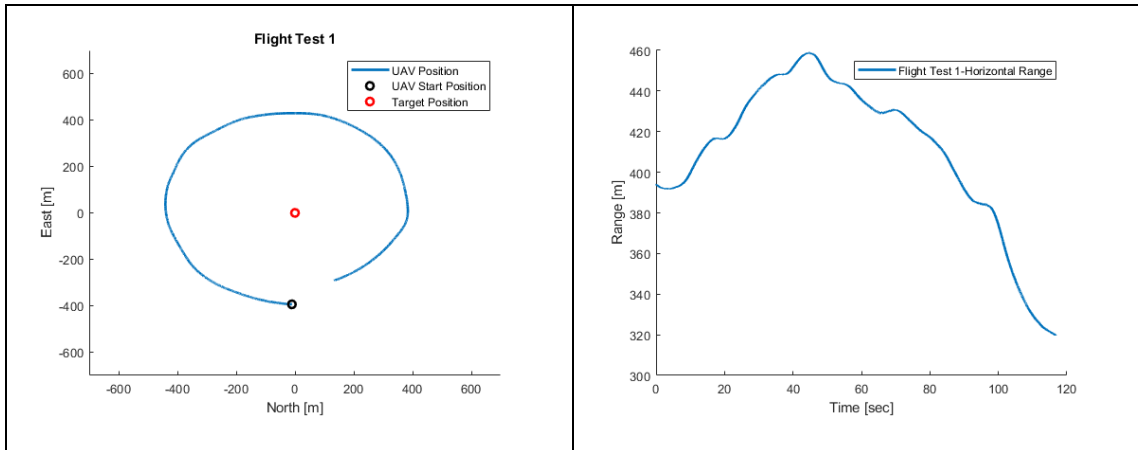
Figure 5-10: Flight Test 1 response graphs.

In flight test 2, both loops are enabled and PID parameters in Table 5.1 are used. UAV is able to loiter around the target with some oscillations. Wind speed is estimated at around 3.8 m/s. Results are shown in Figure 5-11.
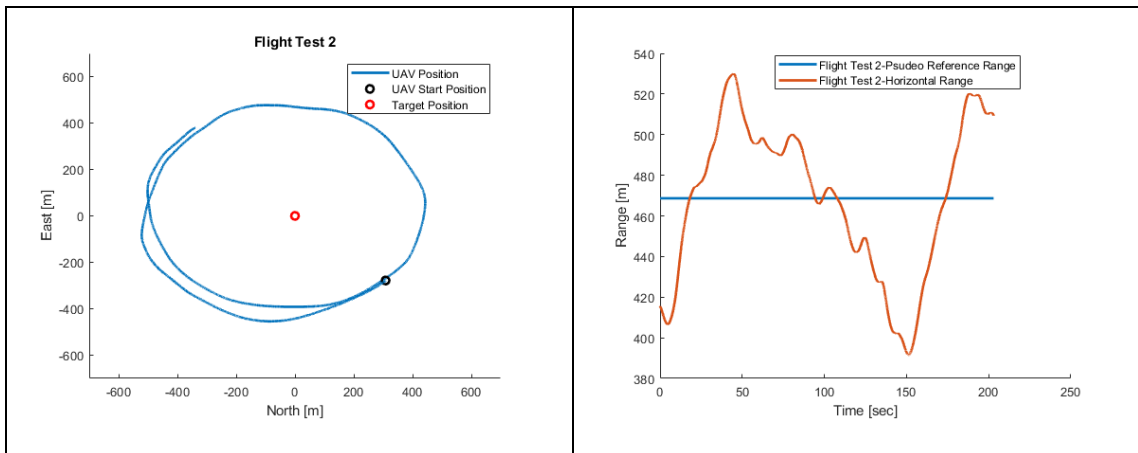
Figure 5-11: Flight Test 2 response graphs.

After Flight Test 2, it is observed that camera misalignment has a detrimental effect on the controller performance. Camera alignment angles are estimated as mentioned in LOS VECTOR ESTIMATION section and they are corrected in the software. Also, both controller loops are tuned and Flight Test 3 and 4 are performed. In these tests, UAV loiters around the target with fewer oscillations compare to Flight Test 2. In these tests, the estimated wind speed is less than 1.5 m/s. The results of both tests are shown in Figure 5-12.
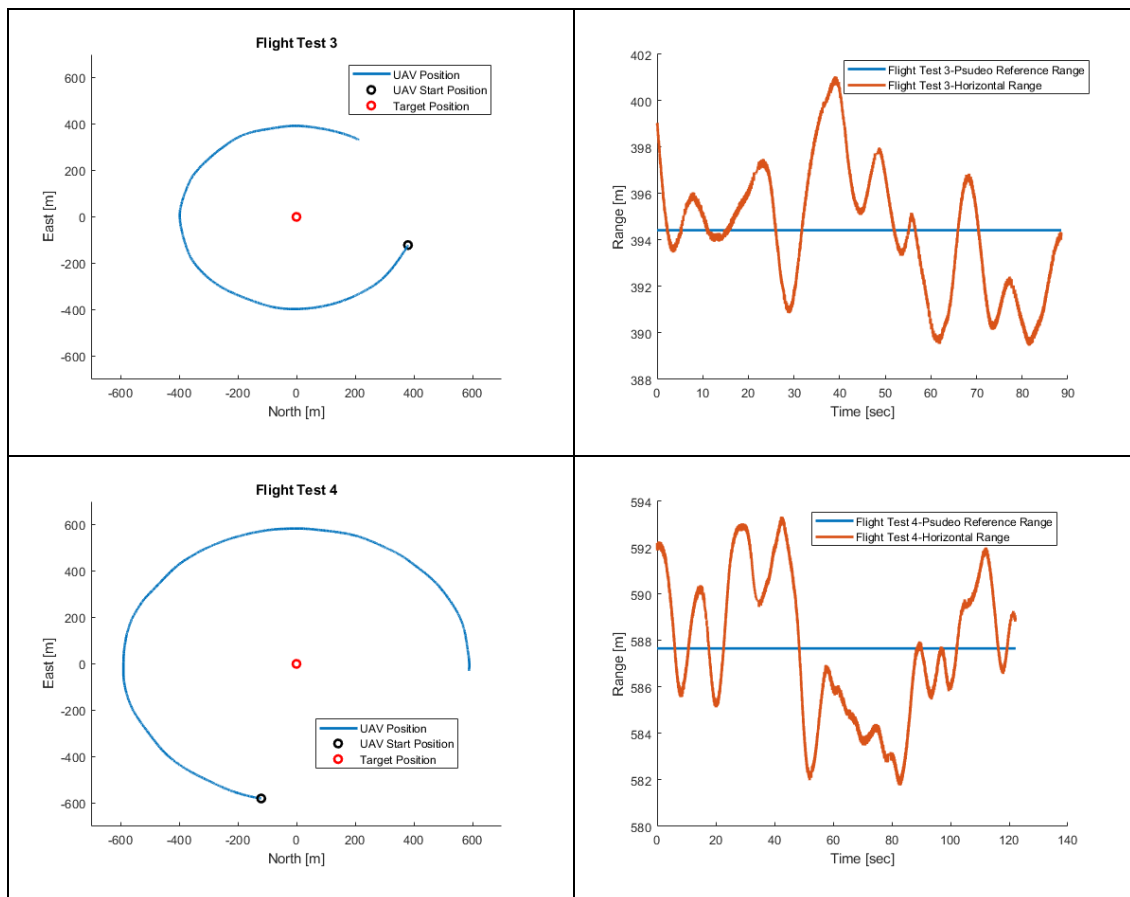
Figure 5-12: Flight Test 3 (top) and Flight Test 4 (bottom) response graphs.

5.5 Conclusion

In conclusion, the lateral controller, which tracks the target and holds the desired distance, is developed. The controller is independent of GNSS measurements such as position and velocity. Hence it works under GNSS denied environments as long as attitude measurements are satisfactory. Also, it has a modular structure, and it is effortlessly implemented.

Solutions for target lost situations due to maneuvering or vision system fails are developed. Even if the target is lost in FOV of the camera, UAV may maneuver around the target by using the estimated target location or holding the last reference roll angle.

The performance of the developed controller is tested by real flight tests. In these tests, it is observed that the controller performs better in less windy environments. Also, it is

noticed that since vertical pixel location (ϵ_y) is not taken into account when UAV reaches high roll angles, the target goes out of the camera field of views. To prevent that in future work, ϵ_y should be connected to the controller as a feedforward input

6. TARGET POSITION ESTIMATION

6.1 Introduction

This chapter aims to estimate the target location in ECEF frame. It can be accomplished by combining the UAV position with estimated LOS angles. Figure 6-1 visualizes target, UAV positions and LOS vectors at different positions with perfect measurements and measurement errors. Under perfect measurement conditions, the target position is easily estimated by using the triangulation method. However, due to measurement errors, accurate estimation is not possible just by using the simple triangulation method.
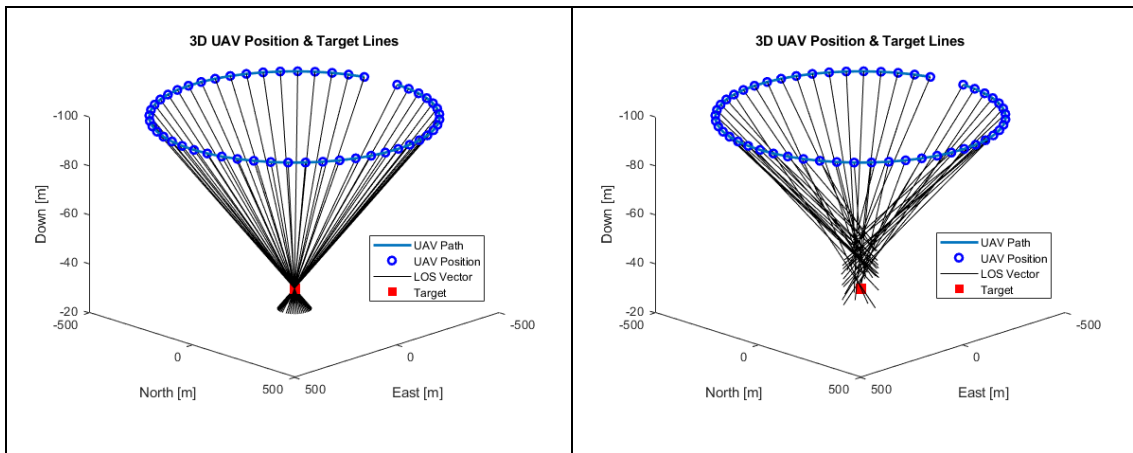
Figure 6-1: Visualization of UAV position, target position and LOS vector without (left) and with (right) LOS measurement errors.

In this work, a new EKF algorithm is developed to estimate the target position. The developed algorithm is designed based on [33] with taking consideration of camera misplacement errors. These errors are considered as bias and added as a state to EKF. The target location is measured with GPS to measure the performance of the proposed method (Figure 6-2). Here, the GPS location is considered as a ground truth. Furthermore, the proposed method is compared with the other methods such as minimization method [29], RLS method [31], EKF1 method [33], and EKF2 method [34].
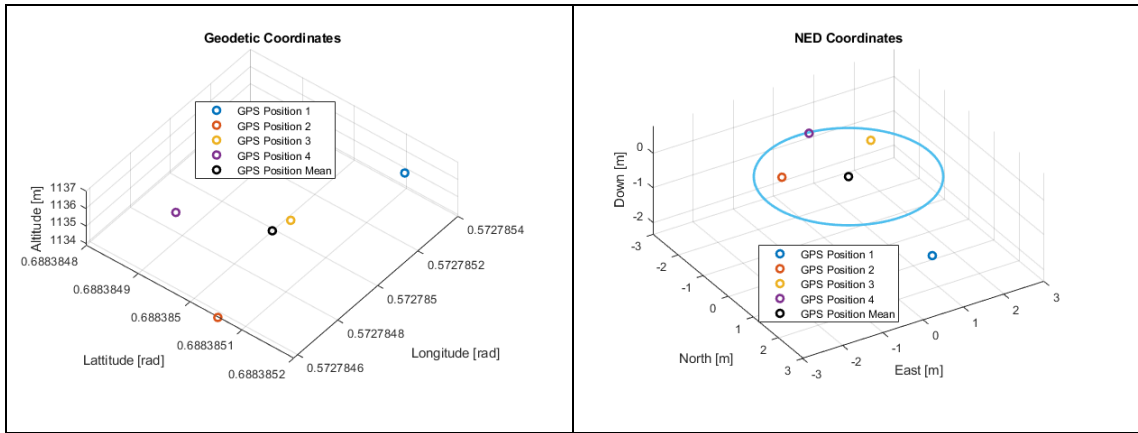
Figure 6-2: Target position measurements from GPS, left geodetic frame right NED frame

6.2 Measurement Errors

As mentioned in the Introduction section, target position estimation is a function of UAV position and LOS vector. UAV position is measured by INS system that combines GNSS and IMU measurements. Still, this INS position measurement has errors. These errors can clearly be seen from Figure 6-2. Here, four different position measurements for the same stationary target have around 2 meters standard deviation. However, these position errors have a direct effect on the position estimations. In Figure 6-3, while UAV making a perfect circle with a radius of 400 meters around the target, the LOS vector is estimated perfectly, and UAV positions are shifted 15 meters in X-direction. Therefore, LOS lines intersect at 15 meters away from the target in X-direction. It means that UAV position errors have a direct effect on the target position estimations.
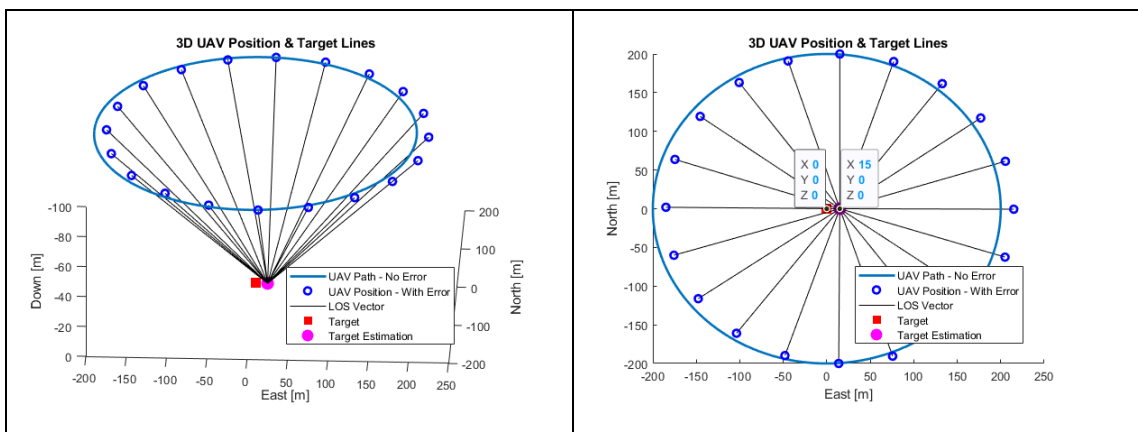
Figure 6-3: Position estimation with UAV position error (Left 3D view, right top view)

Another error is the LOS vector estimation error that depends on the camera parameters, camera alignment angles, and UAV angular position. That is the primary error source in the position estimation. As seen from Figure 6-4, 5 degrees LOS error can cause 230 meters position error at 400 meters away from the target with 100 meters altitude difference. Therefore, the LOS angle error should be taken into consideration while estimating the target position.
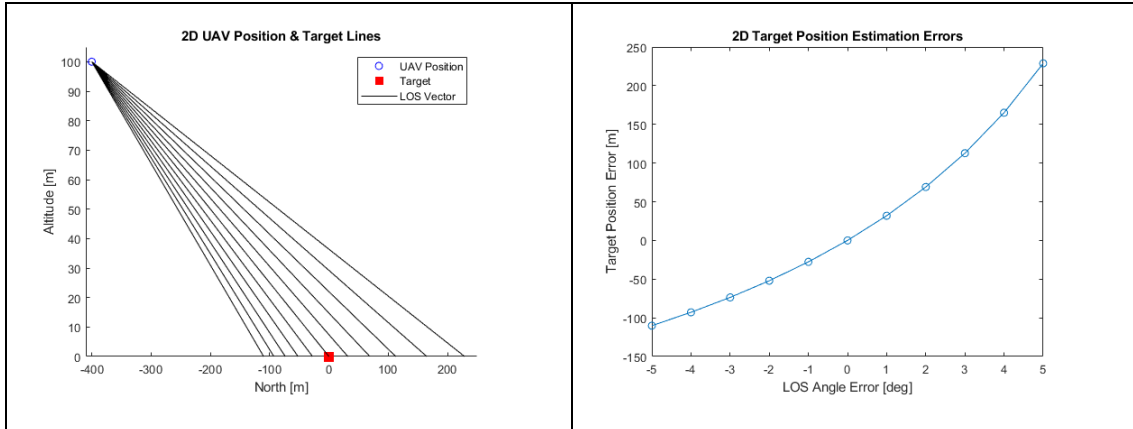
Figure 6-4: LOS angle errors (left) and effect on target position estimation (right)

6.3 Methods

6.3.1 Proposed Method

In this method, target position estimation starts whenever a target is started to track in the vision system. At the beginning of the algorithm, UAV position (θ_{lat}, θ_{lon}, h) is considered as the origin of the local NED frame. Then, at each step, UAV position at local NED frame and LOS angles are estimated. Finally, the target position is calculated in the local NED frame and then converted into the geodetic ECEF frame.

EKF filter is used to estimate stationary target position while eliminating the measurement errors. Its states are target North-East-Down positions ($P_{obj_x}, P_{obj_y}, P_{obj_z}$) in local NED frame, the distance between UAV and target ($\mathbb{L}$) and camera misalignment errors which can be considered as LOS angle biases ($\Delta\psi_{LOS}, \Delta\theta_{LOS}$). Therefore the state is given as:

$$x = \begin{bmatrix} P_{obj_x} \\ P_{obj_y} \\ P_{obj_z} \\ \mathbb{L} \\ \Delta\psi_{LOS} \\ \Delta\theta_{LOS} \end{bmatrix} \tag{6.1}$$

where

$$\mathbb{L} = \sqrt{\left(P_{uav_x} - P_{obj_x}\right)^2 + \left(P_{uav_x} - P_{obj_x}\right)^2 + \left(P_{uav_x} - P_{obj_x}\right)^2}$$

For stationary target and non-moving camera state derivatives with respect to time becomes:

$$\dot{x} = f = \begin{bmatrix} 0 \\ 0 \\ 0 \\ \dfrac{(P_{uav_x}-P_{obj_x})V_{uav_x}+(P_{uav_x}-P_{obj_x})V_{uav_y}+(P_{uav_x}-P_{obj_x})V_{uav_z}}{\mathbb{L}} \\ 0 \\ 0 \end{bmatrix} \tag{6.2}$$

And Jacobian of state equation is:

$$A = \nabla f =$$

$$\begin{bmatrix} 0 & 0 & 0 & 0 & 0 & 0 \\ 0 & 0 & 0 & 0 & 0 & 0 \\ 0 & 0 & 0 & 0 & 0 & 0 \\ -\dfrac{V_{uav_x}}{\mathbb{L}} & -\dfrac{V_{uav_y}}{\mathbb{L}} & -\dfrac{V_{uav_z}}{\mathbb{L}} & -\dfrac{\left(P_{uav_x} - P_{obj_x}\right)V_{uav_x} + \left(P_{uav_x} - P_{obj_x}\right)V_{uav_y} + \left(P_{uav_x} - P_{obj_x}\right)V_{uav_z}}{\mathbb{L}^2} & 0 & 0 \\ 0 & 0 & 0 & 0 & 0 & 0 \\ 0 & 0 & 0 & 0 & 0 & 0 \end{bmatrix} \tag{6.3}$$

For the measurements, UAV position is used:

$$z = \begin{bmatrix} P_{uav_x} \\ P_{uav_y} \\ P_{uav_z} \end{bmatrix} \tag{6.4}$$

Target position is related to UAV position, LOS vector, and distance between them.

$$\vec{P}_{obj} = \vec{P}_{uav} + \mathbb{L}\widehat{LOS} \tag{6.5}$$

For the measurement equation, UAV position is estimated from equation (6.5) by taking into account LOS angle biases:

$$h = \begin{bmatrix} P_{obj_x} - \mathbb{L}\cos(\psi_{LOS} + \Delta\psi_{LOS})\cos(\theta_{LOS} + \Delta\theta_{LOS}) \\ P_{obj_y} - \mathbb{L}\sin(\psi_{LOS} + \Delta\psi_{LOS})\cos(\theta_{LOS} + \Delta\theta_{LOS}) \\ P_{obj_z} + \mathbb{L}\sin(\theta_{LOS} + \Delta\theta_{LOS}) \end{bmatrix} \tag{6.6}$$

For initial guess of the developed EKF filter, flat earth assumption or if available DTED can be used. In the flat earth assumption, as shown in Figure 6-5, take-off altitude is considered as target altitude and altitude difference between target and UAV is found. Then using LOS angles, the target position in the local NED frame is estimated.

$$\Delta h = h_{uav} - h_{uav,home}$$

$$\mathbb{L}_0 = \frac{\Delta h}{\sin(-\theta_{LOS})}$$

$$P_{t_{x0}} = P_{uav_{x0}} + \mathbb{L}_0 \cos(\theta_{LOS})\cos(\psi_{LOS}) \tag{6.7}$$

$$P_{t_{y0}} = P_{uav_{y0}} + \mathbb{L}_0 \cos(\theta_{LOS})\cos(\psi_{LOS})$$

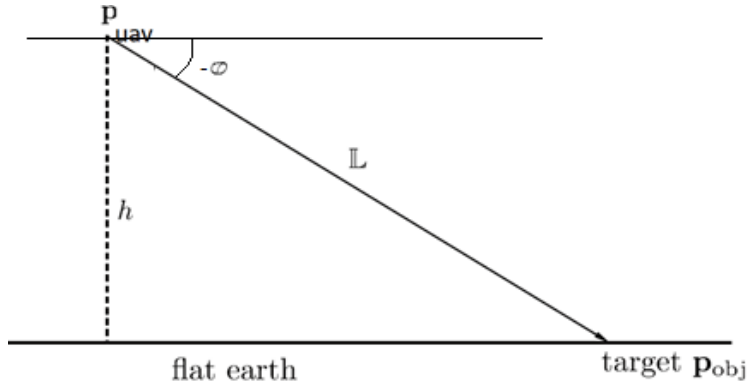$$P_{t_{z0}} = P_{uav_{z0}} + \Delta h$$

Figure 6-5: Flat earth assumption [33]

Since the ideal system should not have a bias, initial guesses for LOS angles are all set to zero values.

6.3.2   Minimization Method

This method is derived from equation (6.5) [29]. At each measurement step UAV position and LOS angles are collected. After that, a nonlinear optimization method is used for

target position estimation. In this work, a new minimization method is developed. UAV positions and LOS angles are used to form target line equations, as shown in Figure 6-6. For North-East plane, line equations are:

$$a_i x + b_i y + c_i = 0$$
$$a_i = \tan\left(\psi_{LOS_i}\right)$$
$$b_i = -1$$
$$c_i = P_{uav_{y,i}} - P_{uav_{x,i}} * \tan\left(\psi_{LOS_i}\right)$$

(6.8)
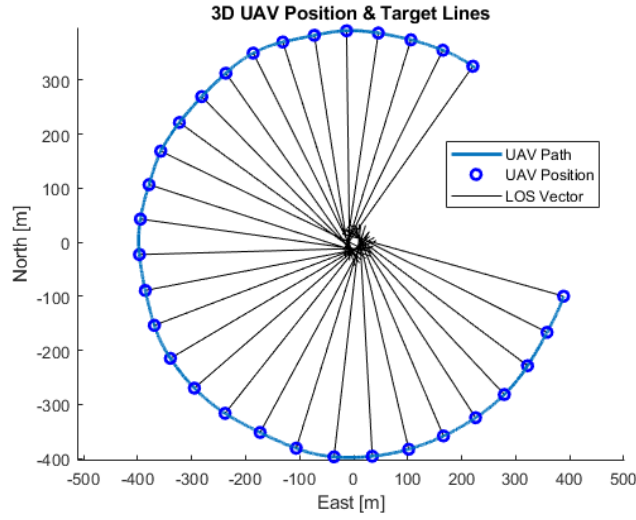
Figure 6-6: UAV positions and target lines

In an ideal case where there aren't any measurement errors, these target lines should cross each other at the target location. A point that has the smallest distance to these all lines is the target position. Hence, the cost function becomes a sum of all distances to LOS lines.

$$\left[P_{obj_x}, P_{obj_y}\right] = \min_{(x,y)} \left(\sum_{i=1}^{N} \frac{|a_i x + b_i y + c_i|}{\sqrt{a^2 + b^2}} \right)$$

(6.9)

This method has several advantages for the target position estimation since it does not need any information other than UAV position and LOS angles. However, this is not proper for real time estimations. It requires nonlinear minimization algorithms that are not proper for real time and requires storing all measurement data that is not applicable for real time systems.

6.3.3 RLS Method

RLS method is developed by using flat earth assumption or DTED information [31]. By using one of these, distance to the target is estimated and then target position is estimated with LOS angles and the distance to the target is the same as in equation (6.7). After that, measurement errors are compensated by using the RLS filter. However, it is noticed that mentioned RLS method is a simple cumulative averaging of the target position estimations as shown in Figure 6-7. Therefore, instead of RLS filter, cumulative averaging can be used.

$$P_{obj,mean_{n+1}} = \frac{(P_{obj,est_{n+1}} + n * P_{obj,mean_n})}{n+1} \tag{6.10}$$
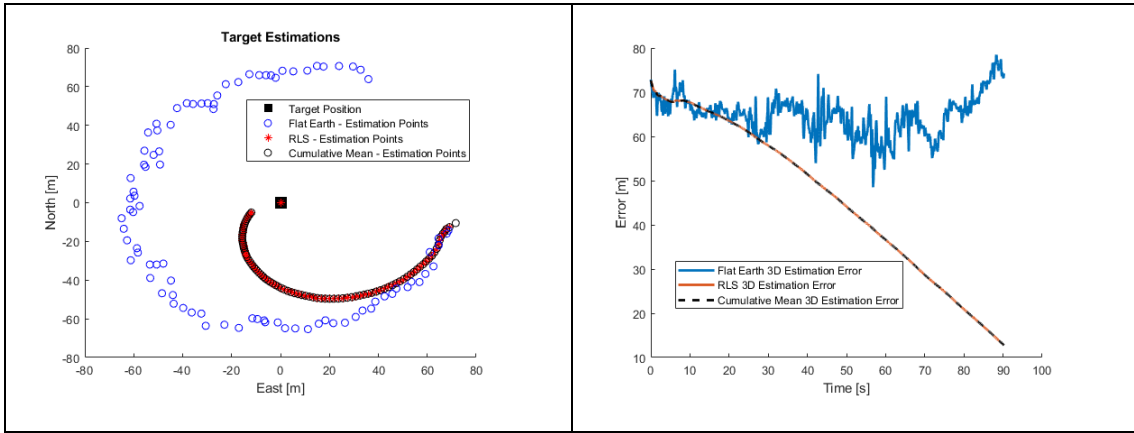
Figure 6-7: RLS and cumulative mean target position estimations

6.3.4 EKF Methods

To compare the performance, EKF1 method [33] and EKF2 method [34] are used. Both EKF methods use target position and distance to target as states.

$$x = \begin{bmatrix} P_{obj_x} \\ P_{obj_y} \\ P_{obj_z} \\ \mathbb{L} \end{bmatrix} \tag{6.11}$$

Their difference is their measurement parameters. EKF1 uses UAV position as a measurement and EKF2 uses LOS angles as a measurement.

$$z_{EKF1} = \begin{bmatrix} P_{uav_x} \\ P_{uav_y} \\ P_{uav_z} \end{bmatrix}, \qquad z_{EKF2} = \begin{bmatrix} \psi_{LOS} \\ \theta_{LOS} \end{bmatrix} \tag{6.12}$$

6.4 Flight Test Results

The first flight test in section FLIGHT PATH PLANNING is used. As mentioned earlier UAV position at estimation start is considered as local NED origin. UAV position, LOS lines and target position (GPS-measurement) are shown in Figure 6-8.

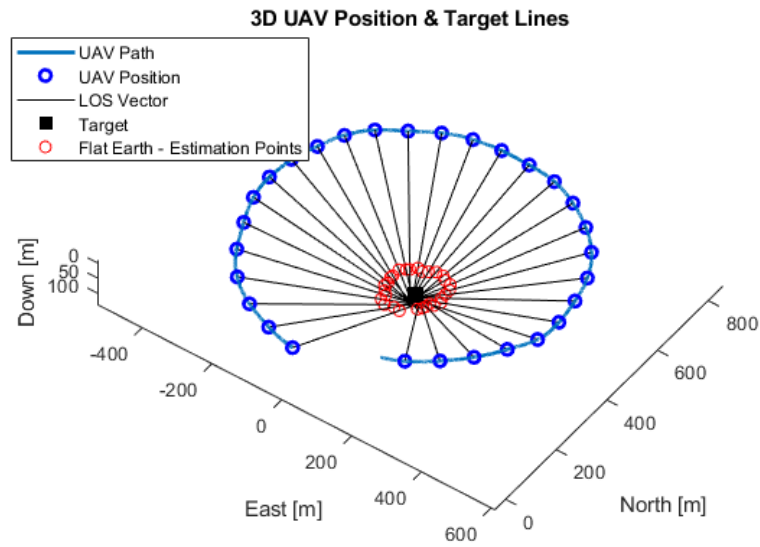Figure 6-8: Flight Test 1 UAV position, target lines, and target position.

Flat earth target estimation position in local NED frame shown in Figure 6-9. To be more clear, the target is centered in this local NED frame, as shown in Figure 6-10.
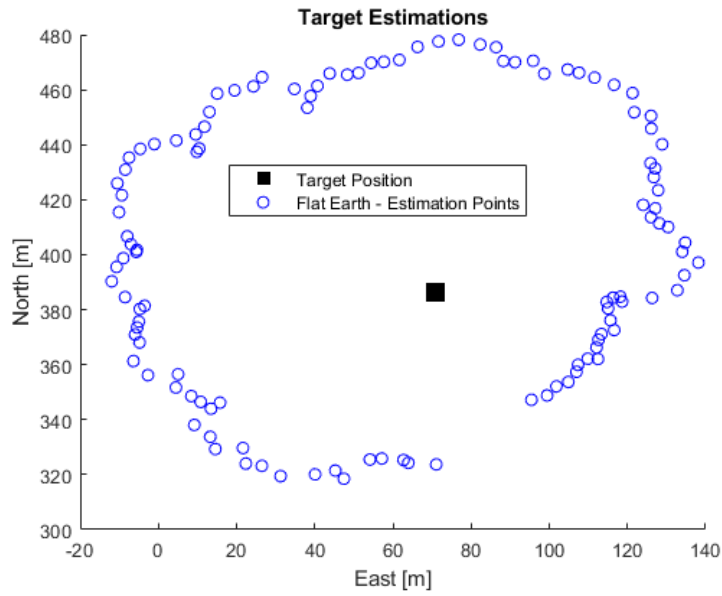
Figure 6-9: Local NED frame target position and flat Earth estimation points
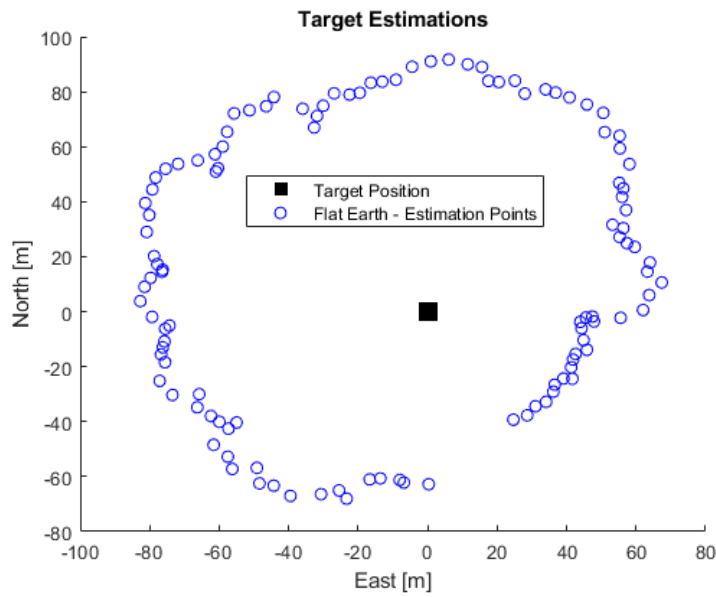
Figure 6-10: Target centered NED frame target position and flat earth estimation points

For the EKF estimations, the process (Q) and measurement (R) covariances are shown in Table 6.1.

Table 6.1: EKF process and measurement covariances

	Q	R
EKF1	diag([10^{-5} 10^{-5} 10^{-5} 10^{-5}])	diag(([5 5 5])^2)
EKF2	diag([10^{-5} 10^{-5} 10^{-5} 10^{-5}])	diag(([5π/180 5π/180])^2)
EKF proposed	diag([10^{-5} 10^{-5} 10^{-5} 10^{-5} 10^{-7} 10^{-7}])	diag(([5 5 5])^2)

Initial estimation covariance (P) is set according to the initial estimation error such as:

$$P_{EKF1} = P_{EKF2} = diag([60\ 0\ 0\ 60]^2)$$
$$P_{EKF\ our} = diag([60\ 0\ 0\ 60\ 5\pi/180\ 5\pi/180]^2)$$

(6.13)

Estimation results for test 1 with mentioned parameters are shown in Figure 6-11, Figure 6-12, Figure 6-13, Figure 6-14, and Figure 6-15.
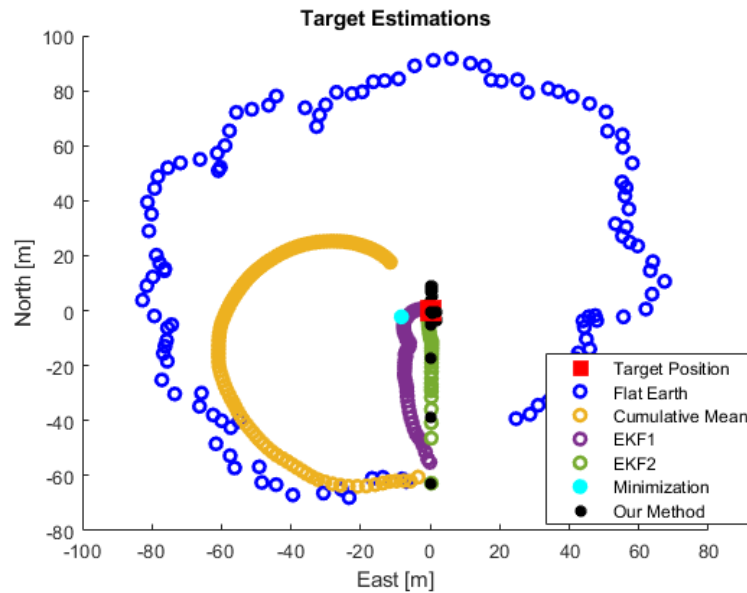
Figure 6-11: Target position estimation in North-East plane view
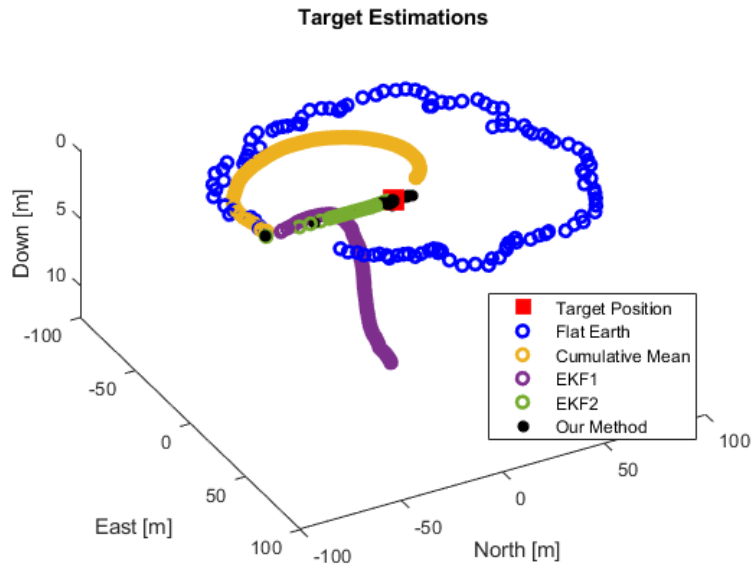
Figure 6-12: Target position estimations in NED plane view
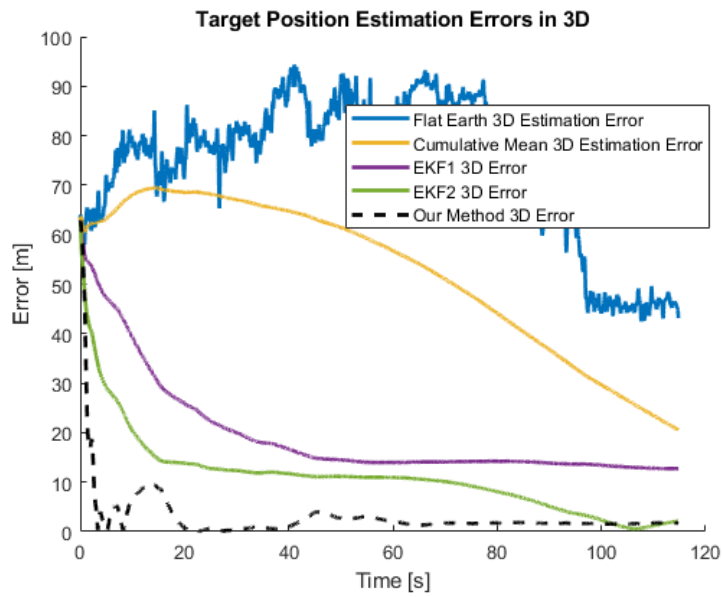
Figure 6-13: Target position estimation errors in N-E plane
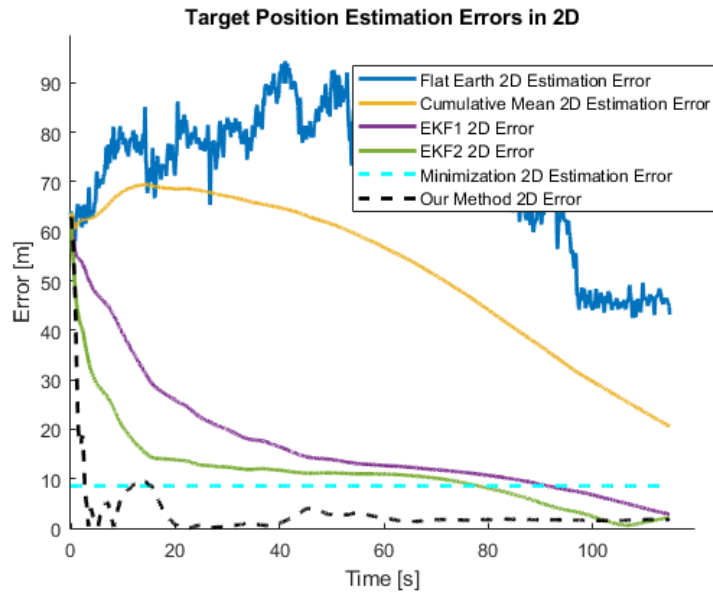
Figure 6-14: Target position estimation errors
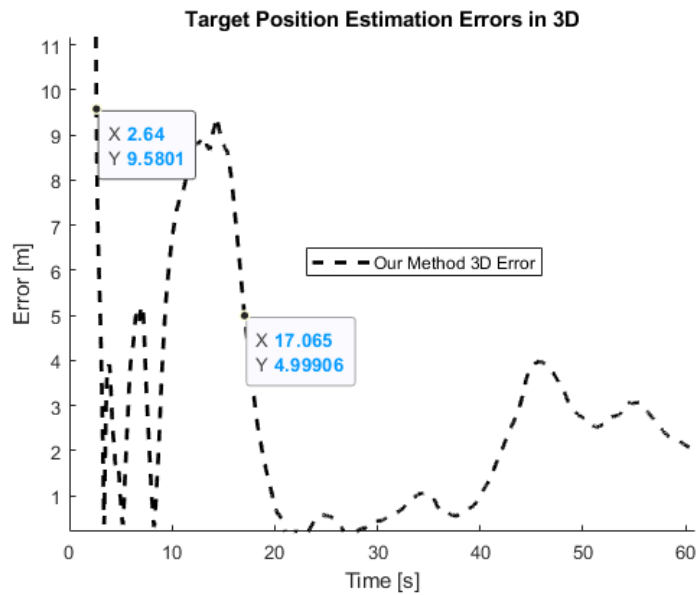
Figure 6-15: Target position estimation errors of proposed solution (Zoomed)

The Cumulative mean (or RLS) solution reaches 20 meters estimation error at the end of the test, as seen from the graphs. EKF methods reach below 15 meters error after 15 seconds and 49 seconds. The minimization method error is 8.5 meters and as mentioned earlier, it estimates target position by using all available data. On the other hand, the proposed method reaches below 10 meters error after 2.6 seconds and stays below 5

meters error after 17 seconds. Also, as shown in Figure 6-16, the proposed method estimates LOS angle biases very accurately. In Figure 6-16, blue lines are the difference between LOS angles estimation from GPS positions of target and UAV and LOS angles estimations from the camera. Red lines are the proposed method's EKF states.
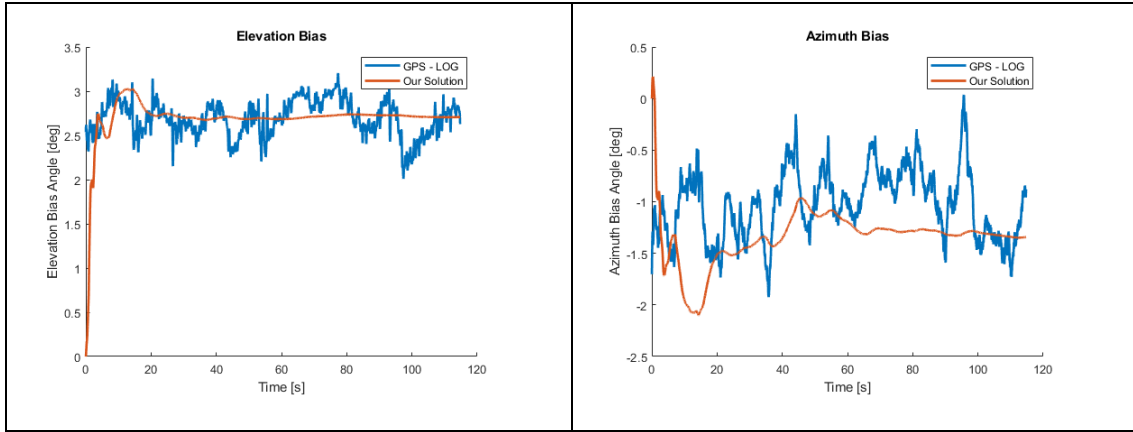
Figure 6-16: Proposed solution LOS angle bias estimations.

However, in the above estimations, initial estimation covariance (P) is set as perfectly. This is not possible without knowing the target location. Hence more generic initial estimation covariance is set as given in equation (6.14), and corresponding results are shown in Figure 6-17.

$$P_{EKF1} = P_{EKF2} = diag([100\ 100\ 20\ 200]^2)$$
$$P_{EKF\ our} = diag([100\ 100\ 20\ 200\ 5\pi/180\ 5\pi/180]^2)$$

(6.14)
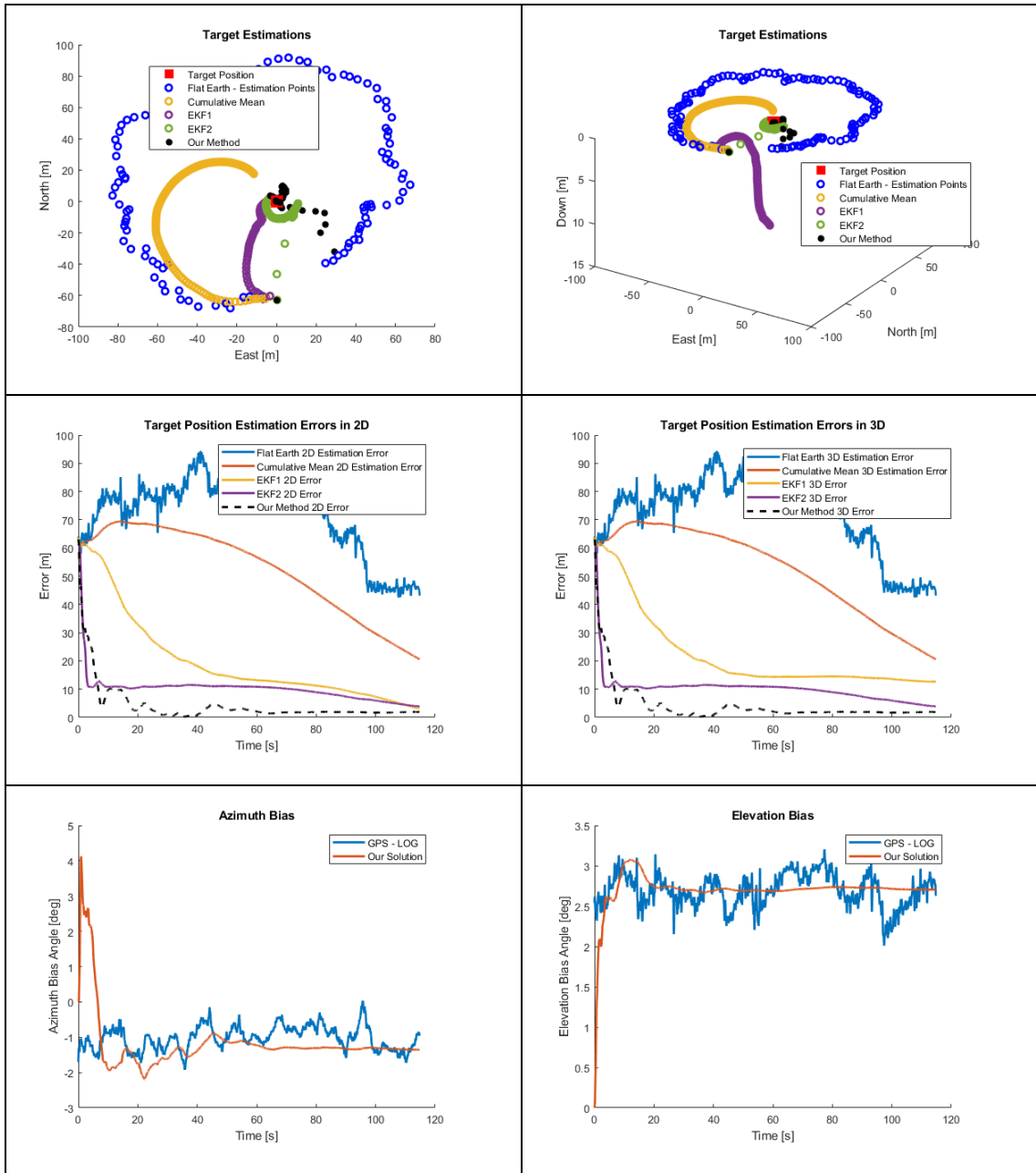
Figure 6-17: Estimation result with new initial estimation covariance, target estimation positions (top), target position estimation errors (middle) and LOS angle biases (bottom).

Here, the RLS solution is still the same, but the EKF1 method reaches 15 meters error after 51 seconds. Proposed solution goes 10 meters error after 6.7 seconds and same as before stays below 5 meters error after 17 seconds and able to estimate the LOS biases accurately. Since the minimization method is not affected by changing estimation covariance, it does not re-estimated.

All the above solutions are done by at perfect flat earth assumption. 20 meters error added to flat earth solution and results of methods are shown in Figure 6-18.
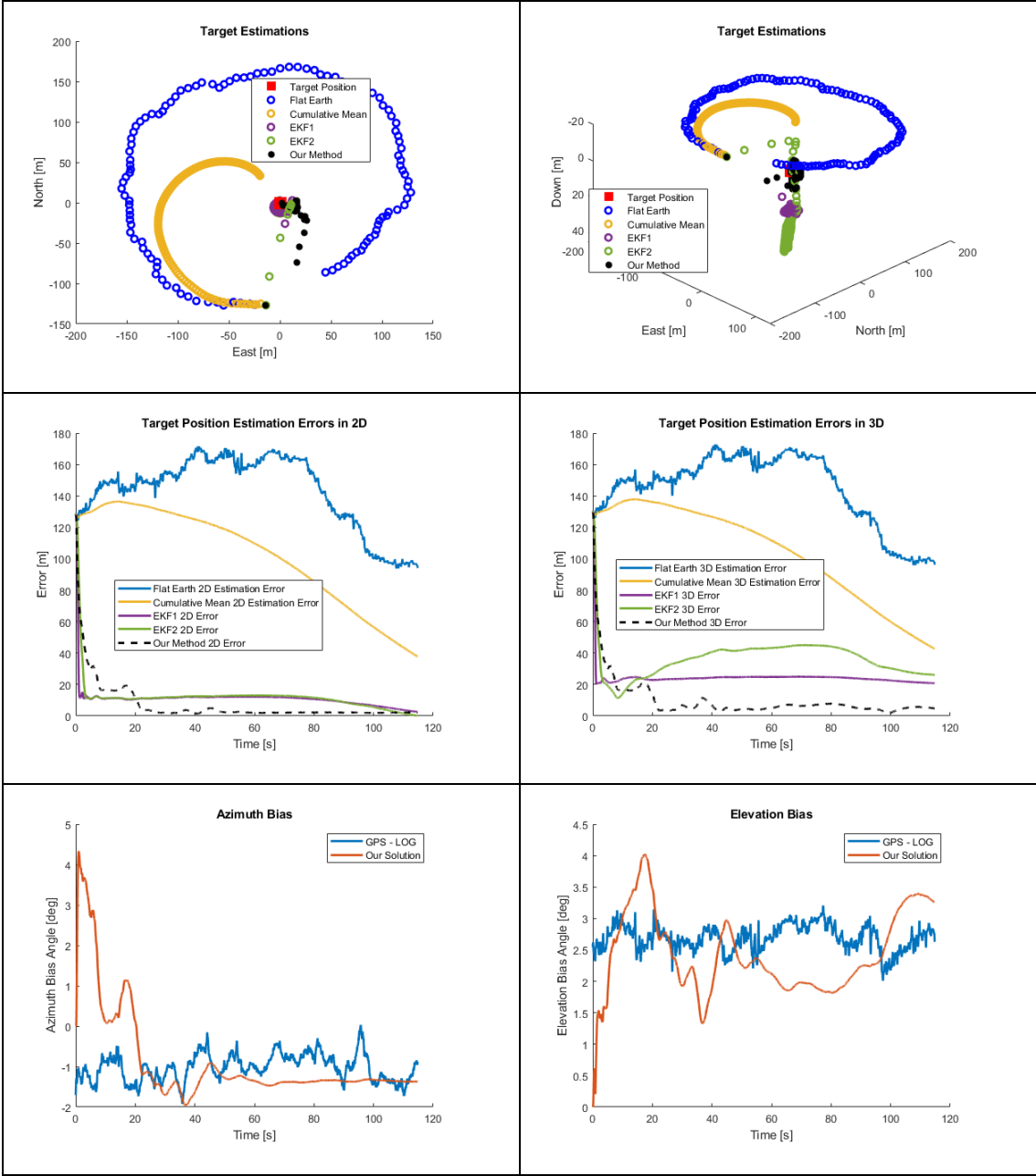
Figure 6-18: Estimation result with 20 meters altitude error at flat earth assumption, target estimation positions (top), target position estimation errors (middle), and LOS angle biases (bottom).

As seen from the given figures, flat earth estimation errors are increased to 140 meters and the cumulative mean method decreases this error to 37 meters. Both EKF1 and EKF2 reach 10 meters error almost 10 seconds faster than the proposed method in North-East

plane. However, for the total error case, the proposed method error is around 5 meters while EKF1 error is around 25 meters and EKF2 error is around 35 meters. The proposed method is still able to estimate the LOS angles biases with some oscillations. The reason for these oscillations is that the EKF algorithm does not have enough information about the sources of the error. In other words, altitude error and elevation bias have the same effect on EKF, so they are not distinguishable.

6.5 Conclusion

In conclusion, a new EKF based target position estimation method that also considers LOS angles biases is developed. The developed method performance is measured by flight test data and compared with other methods. As seen from the results, the proposed method performs much better than the others when there exist LOS angle biases such as camera misalignment. The estimation error of the proposed method is around 5 meters, while the other best estimation error is around 20 meters.

7. GENERAL CONCLUSIONS AND FUTURE WORK

In the Flight Path Planning section, a new loitering maneuver controller is designed such that it works under GNSS denied environments as long as attitude measurements are fine. In this controller, two control loops are designed which control the lateral motion of UAV. The inner loop controls the target pixel location in the image frame and the outer one controls the elevation angle that is related to the distance to the target. Longitudinal motion of UAV is controlled by desired control modes such as altitude hold and speed hold. However, the vertical pixel position of the target in the image is not considered. Hence, future research should consider the vertical pixel location. It can be used as feedforward input to the controller so that roll angle is limited and the target does not go out of the camera field of view. After the flight test, it is observed that loiter performance is affected by elevation measurement errors. This elevation measurement error mainly arises from camera misalignment. Thanks to work in target geolocation estimation, camera misalignment angles are estimated, and it can be used for correction to loiter maneuver.

In the Target Position Estimation section, a novel target position estimation algorithm based is developed. This estimation algorithm takes into consideration of the LOS angle biases. The performance of the algorithm is tested in real test flights and compared with the other methods. Target position is estimated with an accuracy of 5 meters, from a distance of approximately 400 meters, while other methods' accuracies are around 20 meters. For target position estimation, future research should consider the coordinated turn equation as an additional measurement for EKF. In a coordinated turn, turn radius is related to the roll angle and heading rate. Hence, the distance between the UAV and the target may be estimated. Therefore, it may increase the target position estimation accuracy and decrease the estimation time. Moreover, in the future, estimation biases can be expanded for the field of view parameters of the camera.

REFERENCES

[1] S. W. Walker, "Integrating Department of Defense Unmanned Aerial Systems into the National Airspace Structure."

[2] Ministry of Defence, "Joint Doctrine Note 2 / 11 the UK Approach To Unmanned Aircraft," *Jt. Doctrin. Note 2/11*, 2011.

[3] "Sınırsız Teknolojiler, Güvenli Yarınlar." https://www.stm.com.tr/tr/cozumlerimiz/otonom-sistemler/togan-2457 (accessed May 19, 2021).

[4] "Sınırsız Teknolojiler, Güvenli Yarınlar." https://www.stm.com.tr/tr/cozumlerimiz/otonom-sistemler/kargu (accessed May 19, 2021).

[5] "Sınırsız Teknolojiler, Güvenli Yarınlar." https://www.stm.com.tr/tr/cozumlerimiz/otonom-sistemler/alpagu-2459 (accessed May 19, 2021).

[6] "Switchblade® 300 - Tactical Missile System - Air, Sea, Ground | AeroVironment, Inc." https://www.avinc.com/tms/switchblade (accessed May 19, 2021).

[7] "US20170139416A1 - Unmanned aircraft turn and approach system - Google Patents." https://patents.google.com/patent/US20170139416A1 (accessed May 19, 2021).

[8] R. B. Langley, "Dilution of Precision," *GPS World*, vol. 10, no. May, 1999.

[9] R. M. Rogers, "Applied Mathematics in Integrated Navigation Systems," *Computers & Geosciences*, vol. 27, no. 7. 2001.

[10] "IMU (Inertial Measurement Unit) | Product Overview | TDK Product Center." https://product.tdk.com/en/techlibrary/productoverview/imu.html (accessed May 06, 2021).

[11] M. S. Sri, "Object Detection and Tracking Using KLT Algorithm," vol. 7, no. 2, pp. 75–86, 2019.

[12] C. Tomasi, "Detection and Tracking of Point Features Technical Report CMU-CS-91-132," *Image Rochester NY*, vol. 91, no. April, 1991.

[13] H. D. Lopes, E. Kampen, and Q. P. Chu, "UAVs with GPS / MEMS-AHRS integration," no. August, pp. 1–17, 2012.

[14] T. Duc-Tan, P. Fortier, and H.-T. Huynh, "Design, Simulation, and Performance Analysis of an INS/GPS System using Parallel Kalman Filters Structure," *REV J. Electron. Commun.*, vol. 1, no. 2, 2011, doi: 10.21553/rev-jec.15.

[15] S. Rönnbäck, "Development of a INS / GPS navigation loop for an UAV MASTER ' S THESIS Development of a INS / GPS navigation loop," *Computer (Long. Beach. Calif).*, 2000.

[16] "Reference frames and how are they used in inertial navigation." https://www.vectornav.com/resources/reference-frames (accessed May 06, 2021).

[17] "Coordinate Systems - MATLAB & Simulink." https://www.mathworks.com/help/vision/gs/coordinate-systems.html (accessed May 06, 2021).

[18] D. Koks, "Using Rotations to Build Aerospace Coordinate Systems," p. 31, 2008, [Online]. Available: http://www.dtic.mil/cgi-bin/GetTRDoc?AD =ADA484864.

[19] A. Romano, "Principles of dynamics," *Model. Simul. Sci. Eng. Technol.*, vol. 56, pp. 197–213, 2012, doi: 10.1007/978-0-8176-8352-8_13.

[20] J. Heikkila and O. Silven, "Four-step camera calibration procedure with implicit image correction," 1997, doi: 10.1109/cvpr.1997.609468.

[21] Y. Ma, S. Soatto, J. Košecká, and S. Sastry, *An Invitation to 3D Vision*, vol. 19, no. 108. 2004.

[22] "Camera Calibration - MATLAB & Simulink." https://www.mathworks.com/help/vision/camera-calibration.html (accessed May 09, 2021).

[23] "What Is Camera Calibration? - MATLAB & Simulink." https://www.mathworks.com/help/vision/ug/camera-calibration.html (accessed Apr. 23, 2021).

[24] Z. Zhang, "A flexible new technique for camera calibration," *IEEE Trans. Pattern Anal. Mach. Intell.*, vol. 22, no. 11, pp. 1330–1334, 2000, doi: 10.1109/34.888718.

[25] X. Wang, J. Liu, and Q. Zhou, "Real-time multi-target localization from unmanned aerial vehicles," *Sensors (Switzerland)*, vol. 17, no. 1, pp. 1–28, 2017, doi: 10.3390/s17010033.

[26] R. He, H. Liu, D. Li, and H. Liu, "A maximum likelihood estimation approach for image based target localization via small unmanned aerial vehicle," *CGNCC 2016 - 2016 IEEE Chinese Guid. Navig. Control Conf.*, no. 365, pp. 1186–1192, 2017, doi: 10.1109/CGNCC.2016.7828956.

[27] Franck Cazaurang, K. Cohen, and M. Kumar, *Multi-Rotor Platform-based UAV Systems*, vol. 53, no. 9. 2012.

[28] G. Dudek and M. Jenkin, *Computational Principles of Mobile Robotics*. 2010.

[29] S. Sohn, B. Lee, J. Kim, and C. Kee, "Vision-based real-time target localization for single-antenna GPS-guided UAV," *IEEE Trans. Aerosp. Electron. Syst.*, vol. 44, no. 4, pp. 1391–1401, 2008, doi: 10.1109/TAES.2008.4667717.

[30] J. D. Redding, T. W. McLain, R. W. Beard, and C. N. Taylor, "Vision-based target localization from a fixed-wing miniature air vehicle," *Proc. Am. Control Conf.*, vol. 2006, pp. 2862–2867, 2006, doi: 10.1109/acc.2006.1657153.

[31] D. B. Barber, J. D. Redding, T. W. McLain, R. W. Beard, and C. N. Taylor, "Vision-based target geo-location using a fixed-wing miniature air vehicle," *J. Intell. Robot. Syst. Theory Appl.*, vol. 47, no. 4, pp. 361–382, 2006, doi: 10.1007/s10846-006-9088-7.

[32] H. R. Hosseinpoor, F. Samadzadegan, and F. DadrasJavan, "Pricise target geolocation and tracking based on UAV video imagery," *Int. Arch. Photogramm. Remote Sens. Spat. Inf. Sci. - ISPRS Arch.*, vol. 41, no. July, pp. 243–249, 2016, doi: 10.5194/isprsarchives-XLI-B6-243-2016.

[33] R. W. Beard and T. W. McLain, *Small unmanned aircraft: Theory and practice.* 2012.

[34] M. J. Monda, C. A. Woolsey, and C. Konda Reddy, "Ground target localization and tracking in a riverine environment from a UAV with a gimbaled camera," *Collect. Tech. Pap. - AIAA Guid. Navig. Control Conf. 2007*, vol. 4, no. August, pp. 3788–3801, 2007, doi: 10.2514/6.2007-6747.

[35] I. H. Wang, V. N. Dobrokhodov, I. I. Kaminer, and K. D. Jones, "On vision-based target tracking and range estimation for small UAVs," *Collect. Tech. Pap. - AIAA Guid. Navig. Control Conf.*, vol. 7, no. August, pp. 5507–5517, 2005, doi: 10.2514/6.2005-6401.

[36] V. N. Dobrokhodov, I. I. Kaminer, K. D. Jones, and R. Ghabcheloo, "Vision-based tracking and motion estimation for moving targets using unmanned air vehicles," *J. Guid. Control. Dyn.*, vol. 31, no. 4, pp. 907–917, 2008, doi: 10.2514/1.33206.

[37] National Imagery and Mapping Agency, "Performance specification Digital Terrain Elevation Data (DTED)," *Mil-Prf-89020B*, no. May, 2000, [Online]. Available: http://dds.cr.usgs.gov/srtm/version2_1/Documentation/.

[38] K. Gade, "The Seven Ways to Find Heading," *J. Navig.*, vol. 69, no. 5, pp. 955–970, 2016, doi: 10.1017/S0373463316000096.

[39] G. Conte *et al.*, "High accuracy ground target geo-location using autonomous micro aerial vehicle platforms," *AIAA Guid. Navig. Control Conf. Exhib.*, pp. 1–14, 2008, doi: 10.2514/6.2008-6668.

[40] J. A. Ross, B. R. Geiger, G. L. Sinsley, J. F. Horn, L. N. Long, and A. F. Niessner, "Vision-based target geolocation and optimal surveillance on an Unmanned Aerial Vehicle," *AIAA Guid. Navig. Control Conf. Exhib.*, no. January 2015, 2008, doi: 10.2514/6.2008-7448.

[41] F. Morbidi and G. L. Mariottini, "Active target tracking and cooperative localization for teams of aerial vehicles," *IEEE Trans. Control Syst. Technol.*, vol. 21, no. 5, pp. 1694–1707, 2013, doi: 10.1109/TCST.2012.2221092.

[42] R. W. Deming and L. I. Perlovsky, "Concurrent multi-target localization, data association, and navigation for a swarm of flying sensors," *Inf. Fusion*, vol. 8, no. 3, p. 66, 2007, doi: 10.1016/j.inffus.2005.11.001.

[43] H. Kwon and D. J. Pack, "A robust mobile target localization method for cooperative unmanned aerial vehicles using sensor fusion quality," *J. Intell. Robot. Syst. Theory Appl.*, vol. 65, no. 1–4, pp. 479–493, 2012, doi: 10.1007/s10846-011-9581-5.

[44] S. Minaeian, J. Liu, and Y. J. Son, "Vision-Based Target Detection and Localization via a Team of Cooperative UAV and UGVs," *IEEE Trans. Syst. Man, Cybern. Syst.*, vol. 46, no. 7, pp. 1005–1016, 2016, doi: 10.1109/TSMC.2015.2491878.

[45] Y. Qu, J. Wu, and Y. Zhang, "Cooperative localization based on the azimuth angles among multiple UAVs," *2013 Int. Conf. Unmanned Aircr. Syst. ICUAS 2013 - Conf. Proc.*, pp. 818–823, 2013, doi: 10.1109/ICUAS.2013.6564765.

[46] L. Beiner and S. W. Paris, "Direct trajectory optimization using nonlinear programming and collocation," *J. Guid. Control. Dyn.*, vol. 10, no. 4, pp. 338–342, 1987, doi: 10.2514/3.20223.

[47] "System Identification Toolbox - MATLAB." https://www.mathworks.com/products/sysid.html (accessed May 15, 2021).

[48] R. Rysdyk, "Course and heading changes in significant wind," *J. Guid. Control. Dyn.*, vol. 30, no. 4, pp. 1168–1171, 2007, doi: 10.2514/1.27359.

[49] J. Osborne and R. Rysdyk, "Waypoint guidance for small UAVs in wind," *Collect. Tech. Pap. - InfoTech Aerosp. Adv. Contemp. Aerosp. Technol. Their Integr.*, vol. 1, pp. 459–470, 2005, doi: 10.2514/6.2005-6951.

[50] B. Etkin, *Dynamics of Atmospheric Flight*, vol. XXXIII, no. 2. 2005.

[51] A. Zelinsky, *Learning OpenCV---Computer Vision with the OpenCV Library (Bradski, G.R. et al.; 2008)[On the Shelf]*, vol. 16, no. 3. 2009.

[52] P. Sturm, S. Ramalingam, J. P. Tardif, S. Gasparini, and J. Barreto, "Camera models and fundamental concepts used in geometric computer vision," *Found. Trends Comput. Graph. Vis.*, vol. 6, no. 1–2, pp. 1–183, 2010, doi: 10.1561/0600000023.

[53] "Geometry of Image Formation | LearnOpenCV #." https://learnopencv.com/geometry-of-image-formation/ (accessed Jun. 03, 2021).

[54] K. Hata and S. Savarese, "CS231A Course Notes 1: Camera Models."

[55] R. Hartley and A. Zisserman, *Multiple View Geometry in Computer Vision*. 2004.

[56] J. Heikkila, "Using Circular Control Points," *IEEE Trans. Pattern Anal. Mach. Intell.*, vol. 22, no. 10, pp. 1066–1077, 2000.

[57] L. Ma, Y. Chen, and K. L. Moore, "Rational Radial Distortion Models with Analytical Undistortion Formulae," 2003, [Online]. Available: http://arxiv.org/abs/cs/0307047.

[58] J. Mallon and P. F. Whelan, "Precise radial un-distortion of images," *Proc. - Int. Conf. Pattern Recognit.*, vol. 1, pp. 18–21, 2004, doi: 10.1109/ICPR.2004.1333995.

[59] "Camera Calibration Toolbox for Matlab." http://www.vision.caltech.edu/ bouguetj/calib_doc/htmls/parameters.html (accessed May 17, 2021).

[60] "Find minimum of unconstrained multivariable function using derivative-free method - MATLAB fminsearch." https://www.mathworks.com/help/ matlab/ref/fminsearch.html (accessed May 18, 2021).

[61] K. J. Astrom and T. HÄgglund, "Advanced PID control," *IEEE Control Systems*, vol. 26, no. 1. pp. 98–101, 2006, doi: 10.1109/MCS.2006.1580160.

[62] A. Cho, J. Kim, S. Lee, and C. Kee, "Wind estimation and airspeed calibration using a UAV with a single-antenna GPS receiver and pitot tube," *IEEE Trans. Aerosp. Electron. Syst.*, vol. 47, no. 1, pp. 109–117, 2011, doi: 10.1109/TAES.2011.5705663.

APPENDICES

APPENDIX 1 -   UAV Model Validation Flight Test
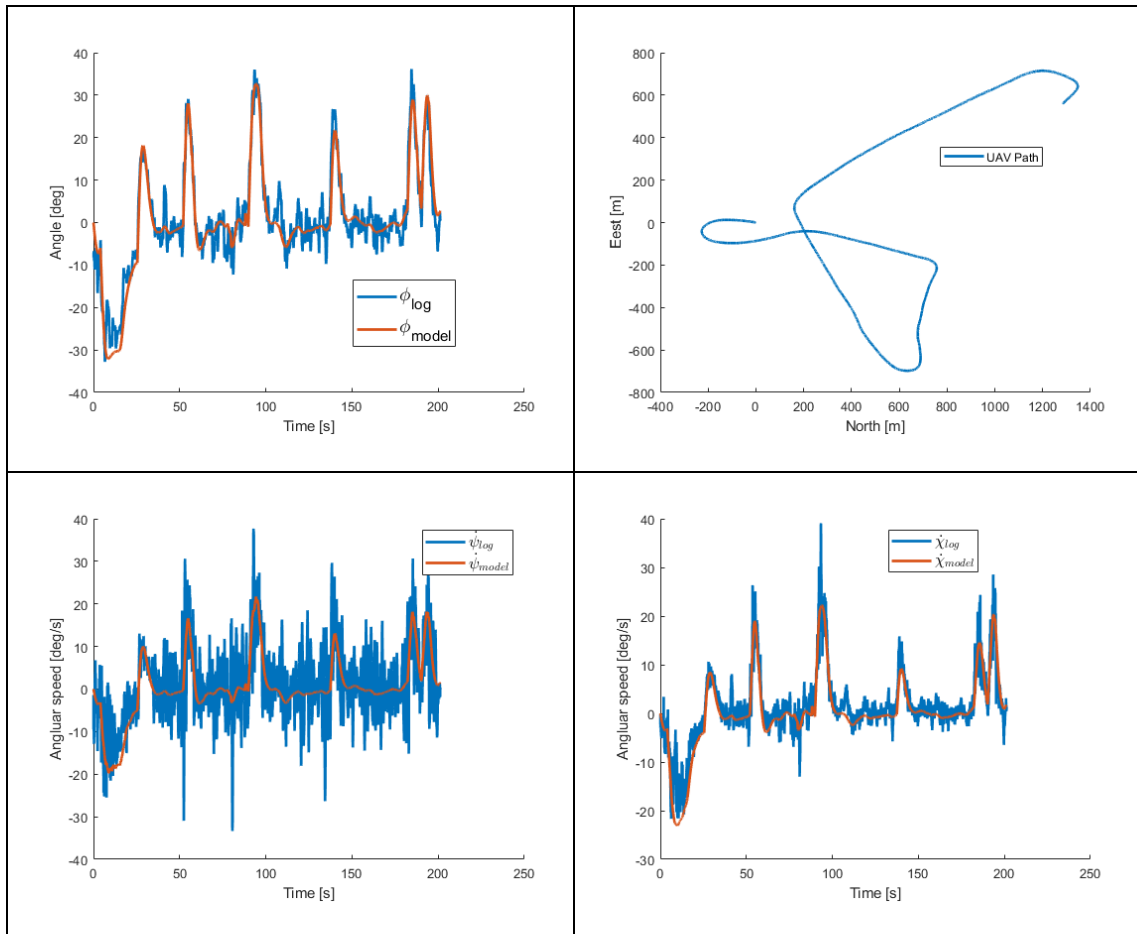

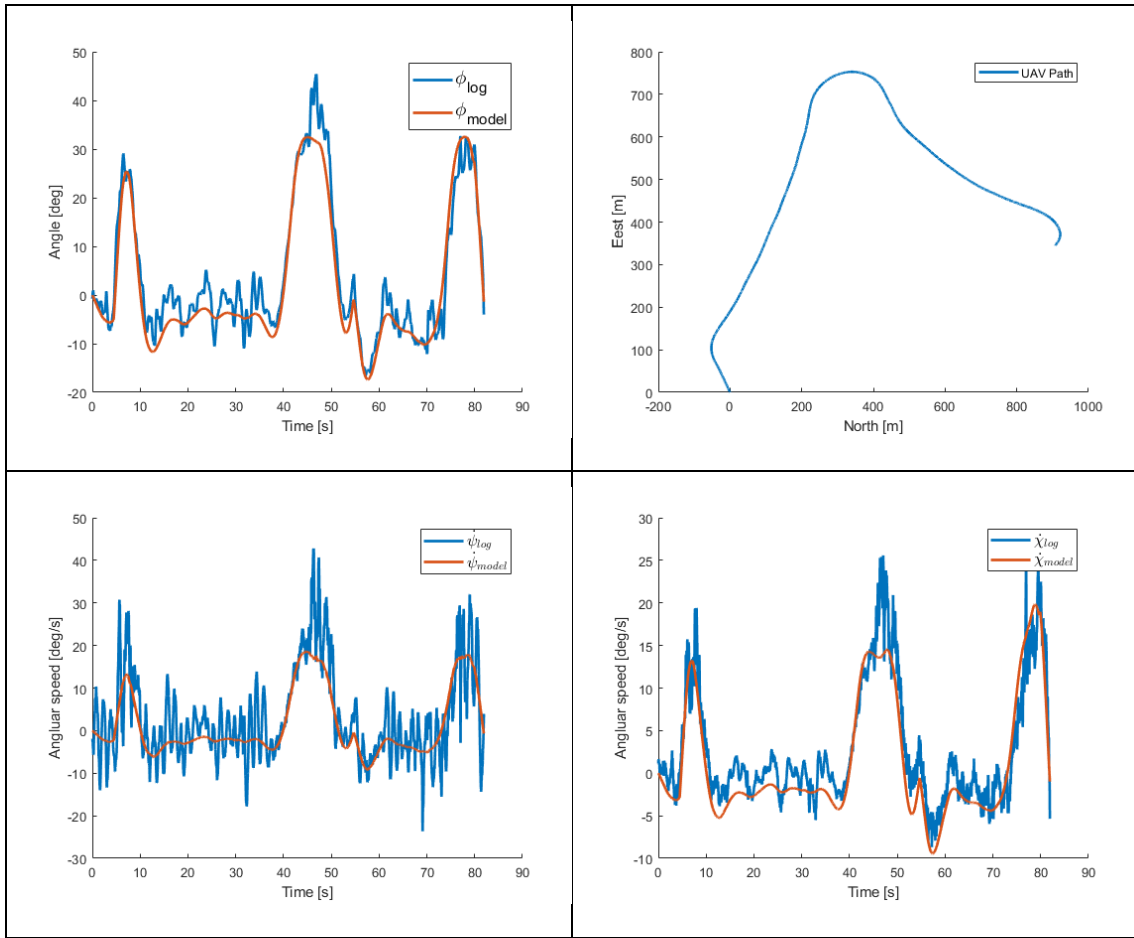Figure A1- 1: Validation flight test 2

Figure A1- 2: Validation flight test 3
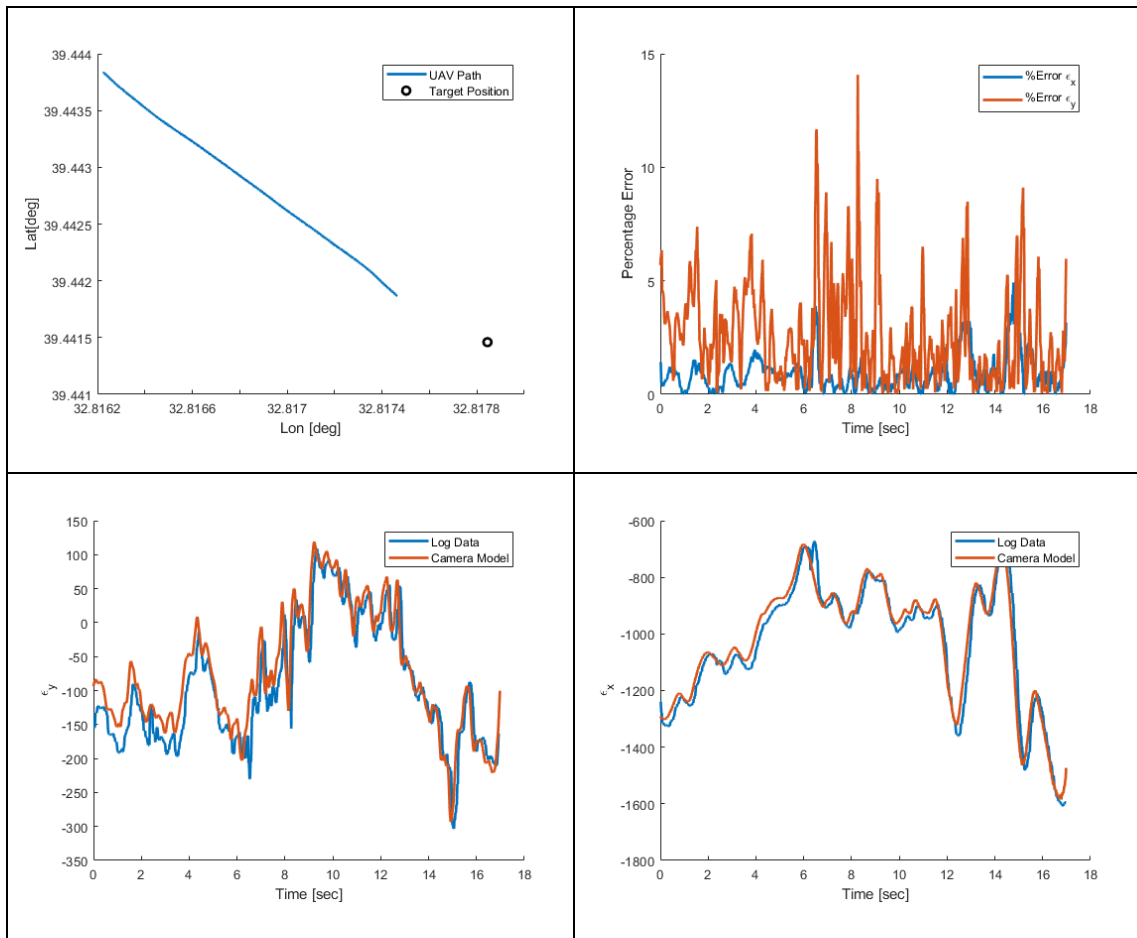
APPENDIX 2 - Camera Model Validation Test
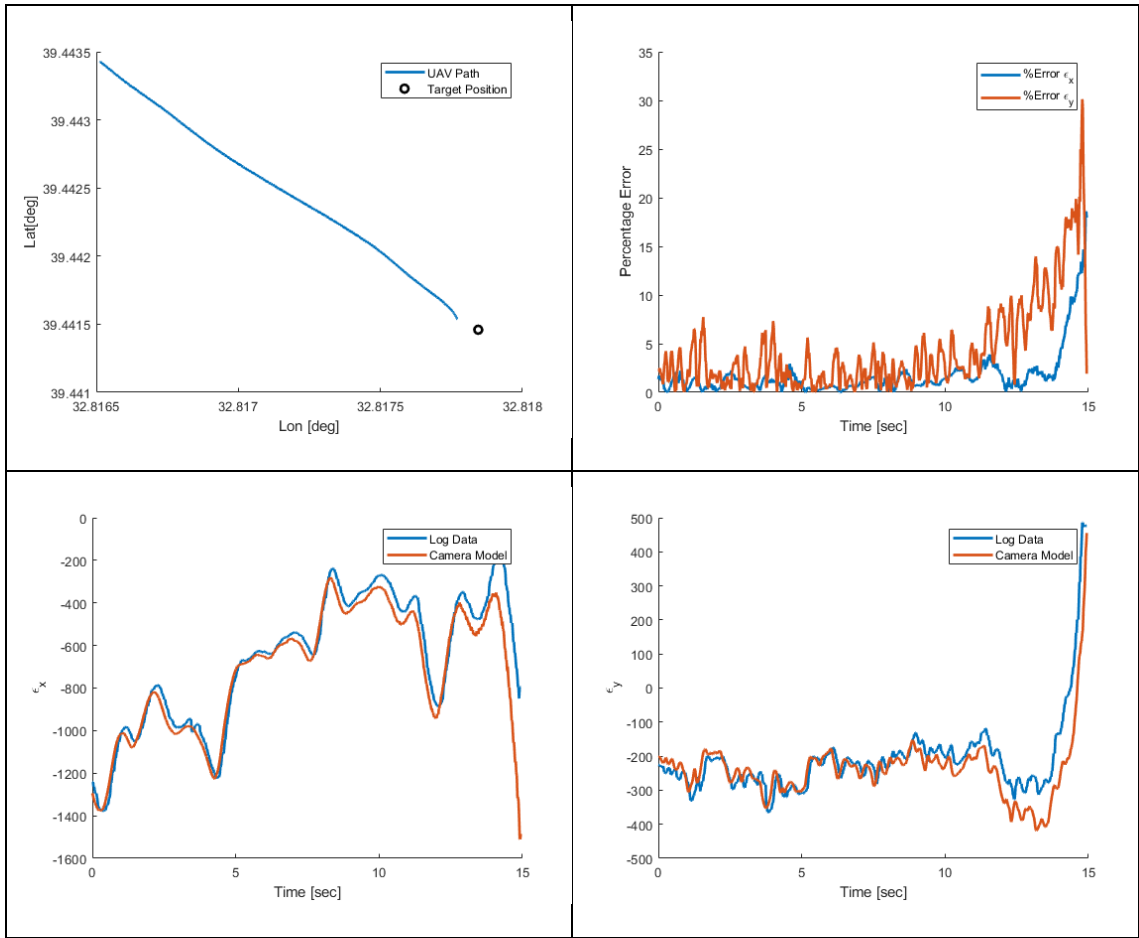

Figure A2- 1: Camera model validation test 2

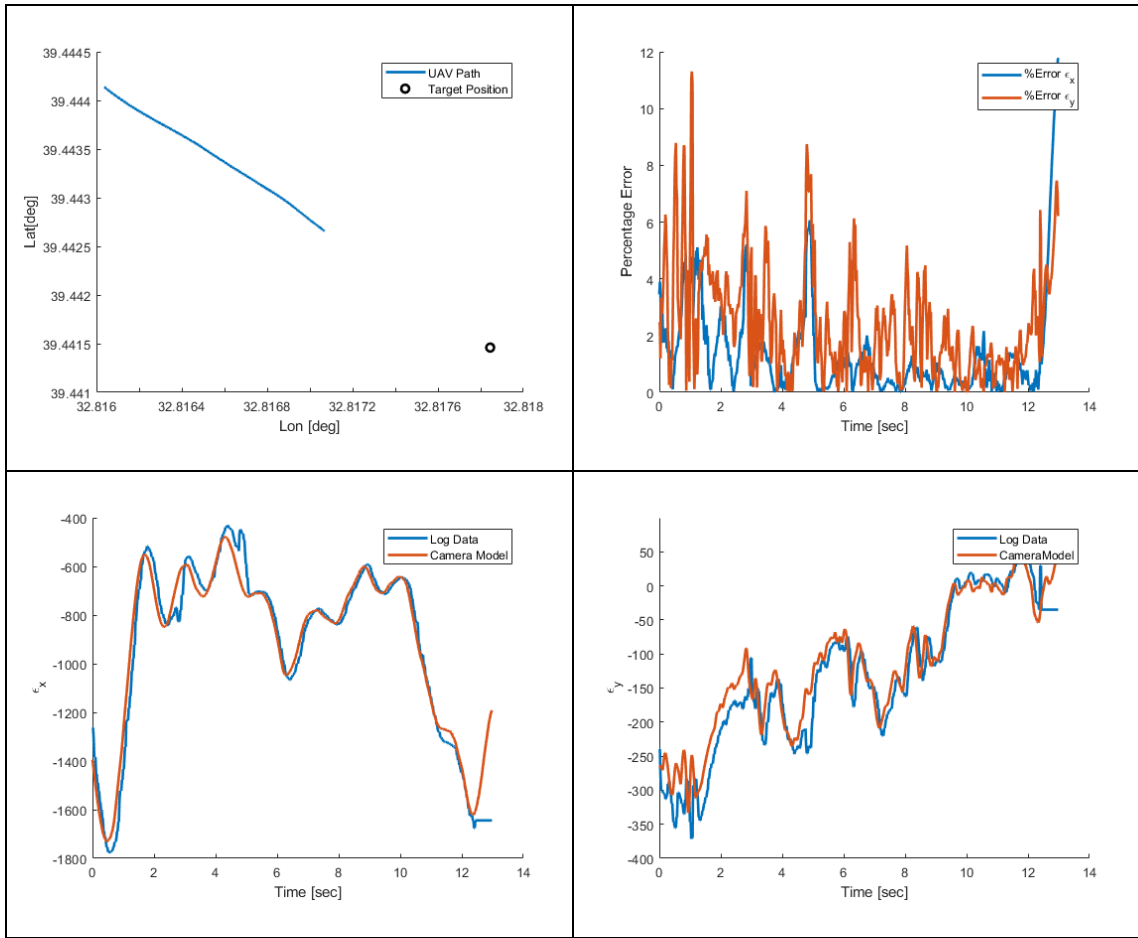Figure A2- 2: Camera model validation test 3

Figure A2- 3: Camera model validation test 4
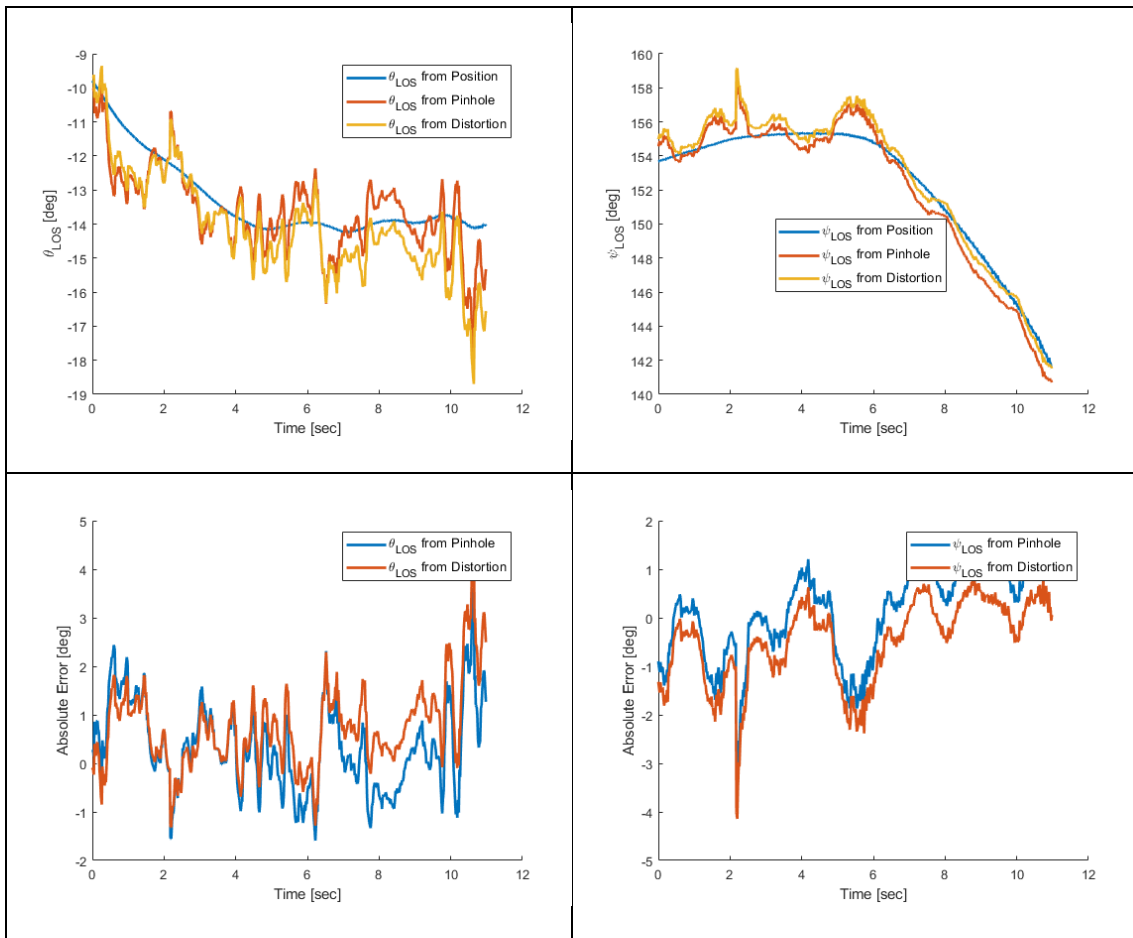
APPENDIX 3 -   LOS Estimations

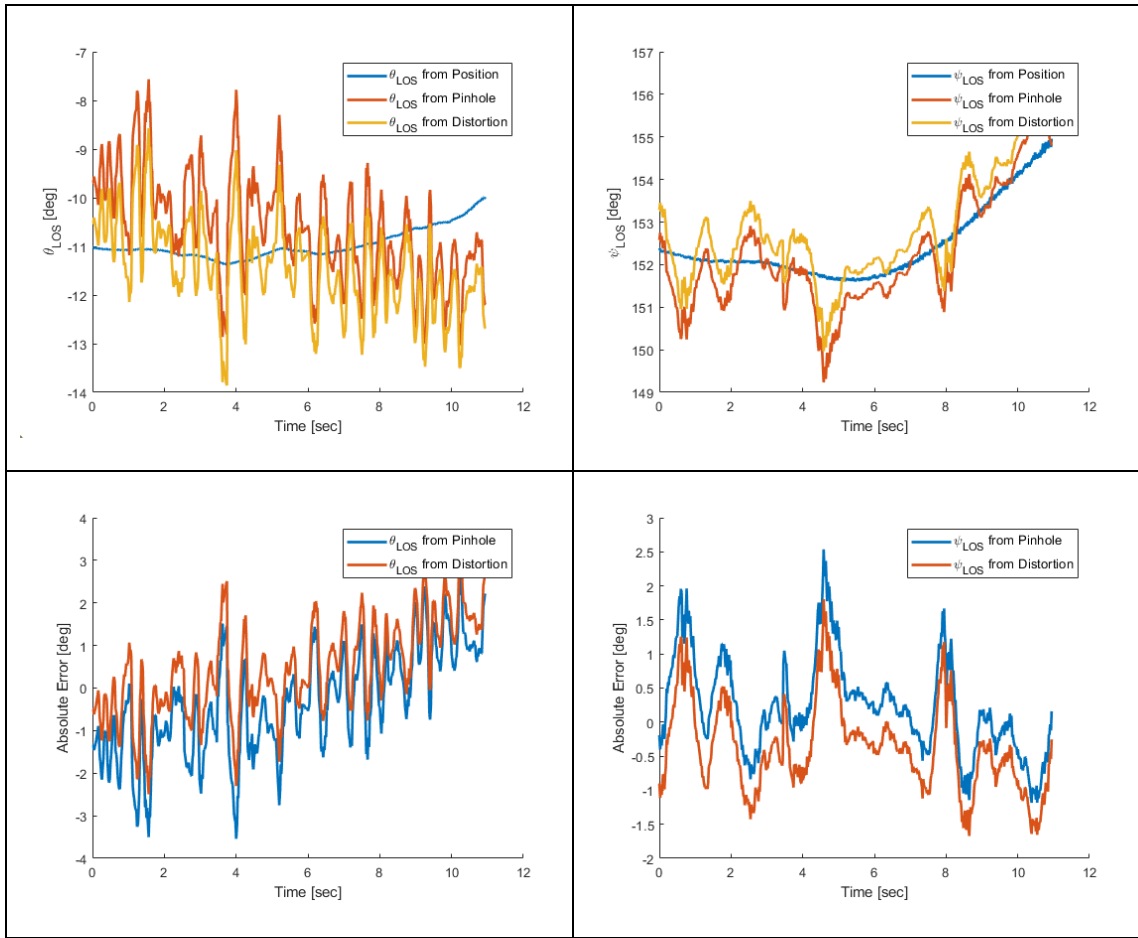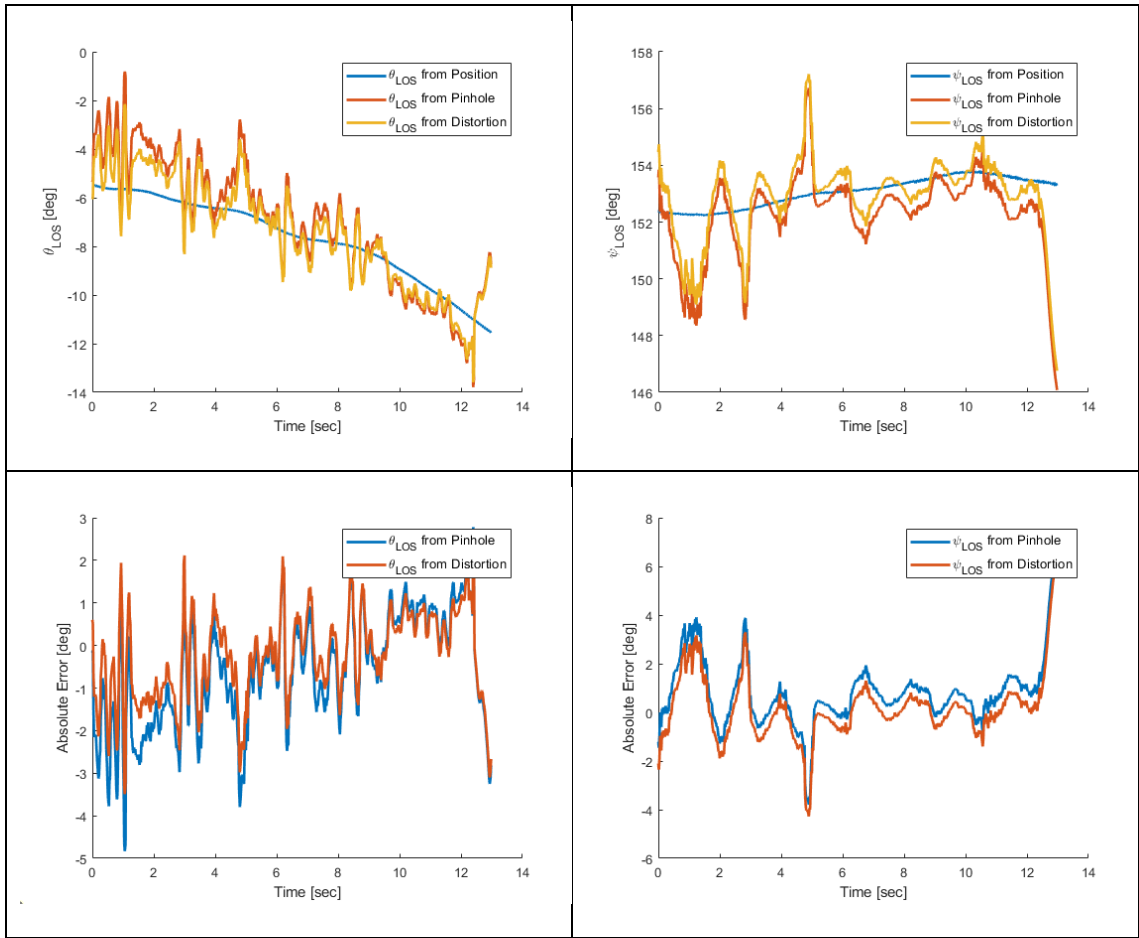

Figure A3- 1: LOS estimation test 2

Figure A3- 2: LOS estimation test 3

Figure A3- 3: LOS estimation test 4